Supporting Information

Rational design of efficient photosensitizers based on cyclometalated iridium(III) complexes with 2-arylbenzimidazole and aromatic 1,3-diketone ligands

Sergei V. Tatarin, Elisaveta A. Meshcheriakova, Sergey A. Kozyukhin, Victor V. Emets and Stanislav I. Bezzubov*

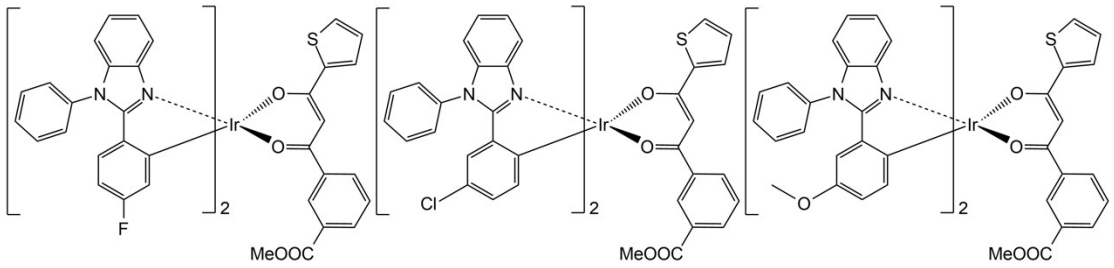

complex **1**

complex **2**

complex **3**

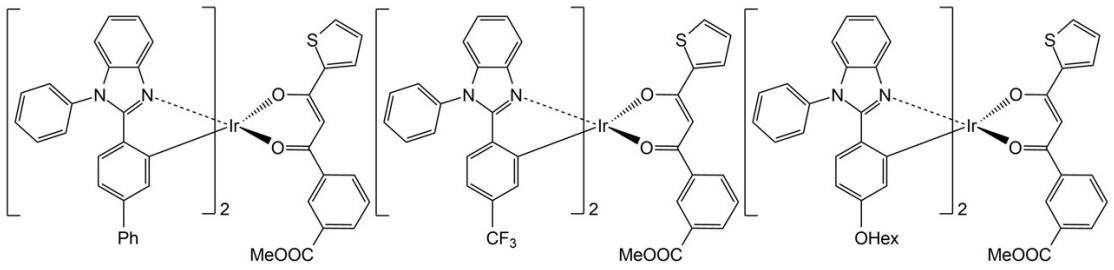

complex **4**

complex **5**

complex **6**

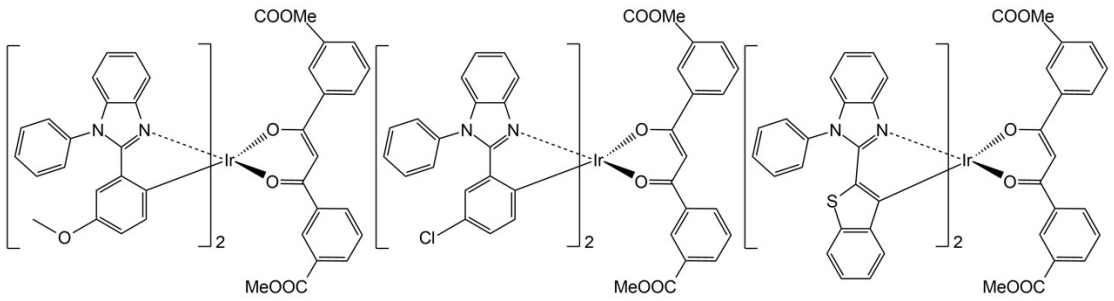

complex **7**

complex **8**

complex **9**

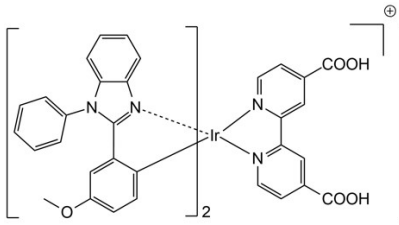

complex **10**

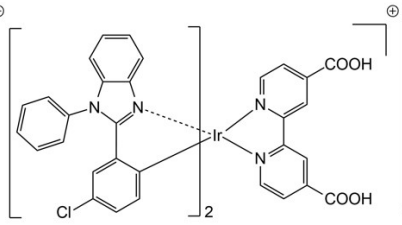

complex **11**

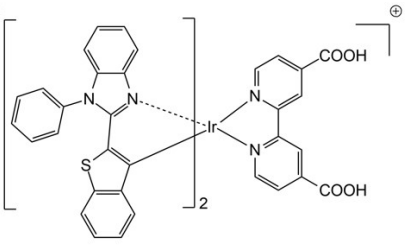

complex **12**

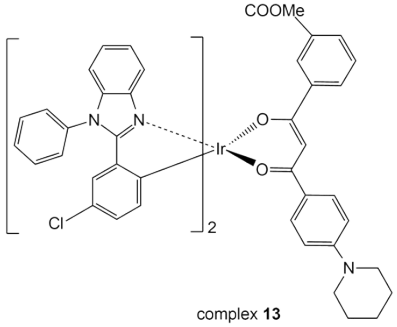

complex **13**

Figure S1. Synthesized complexes **1**–**13**

1. **NMR and mass spectra.**

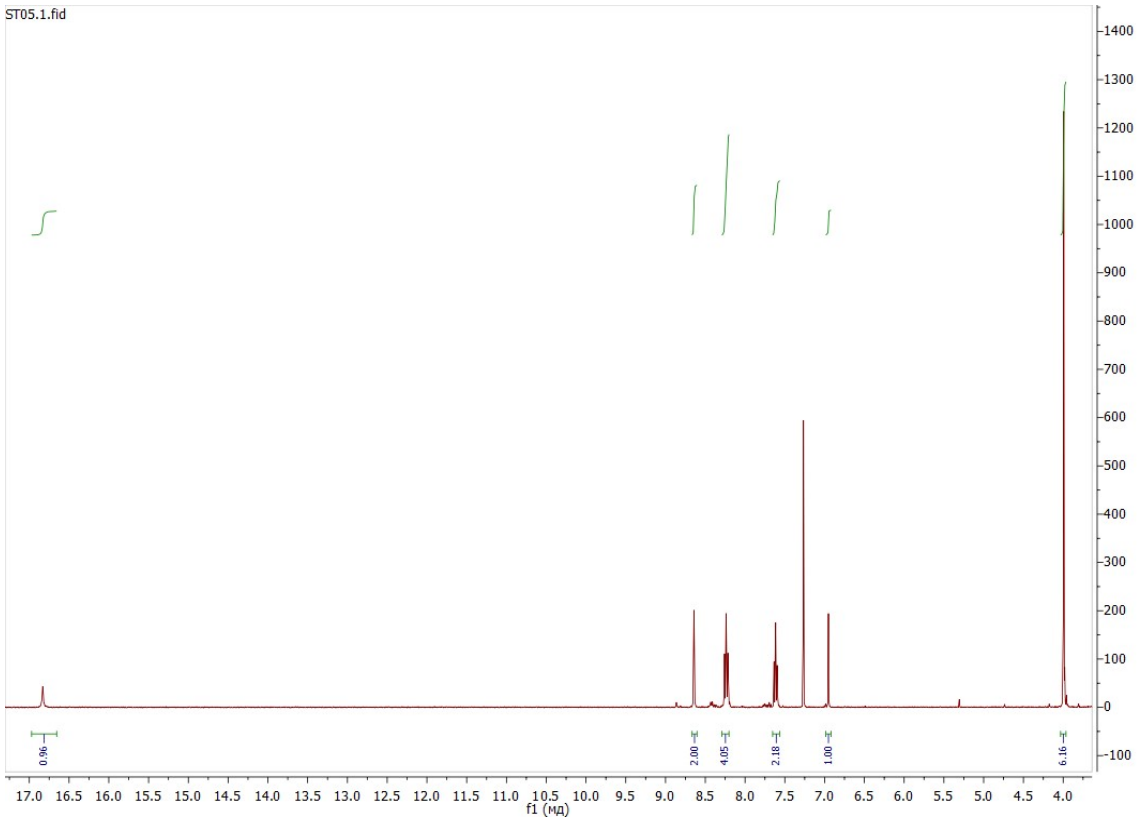

Figure S2. ^{1}H NMR spectrum of L_2 (400 MHz, 298K, $CDCl_3$).

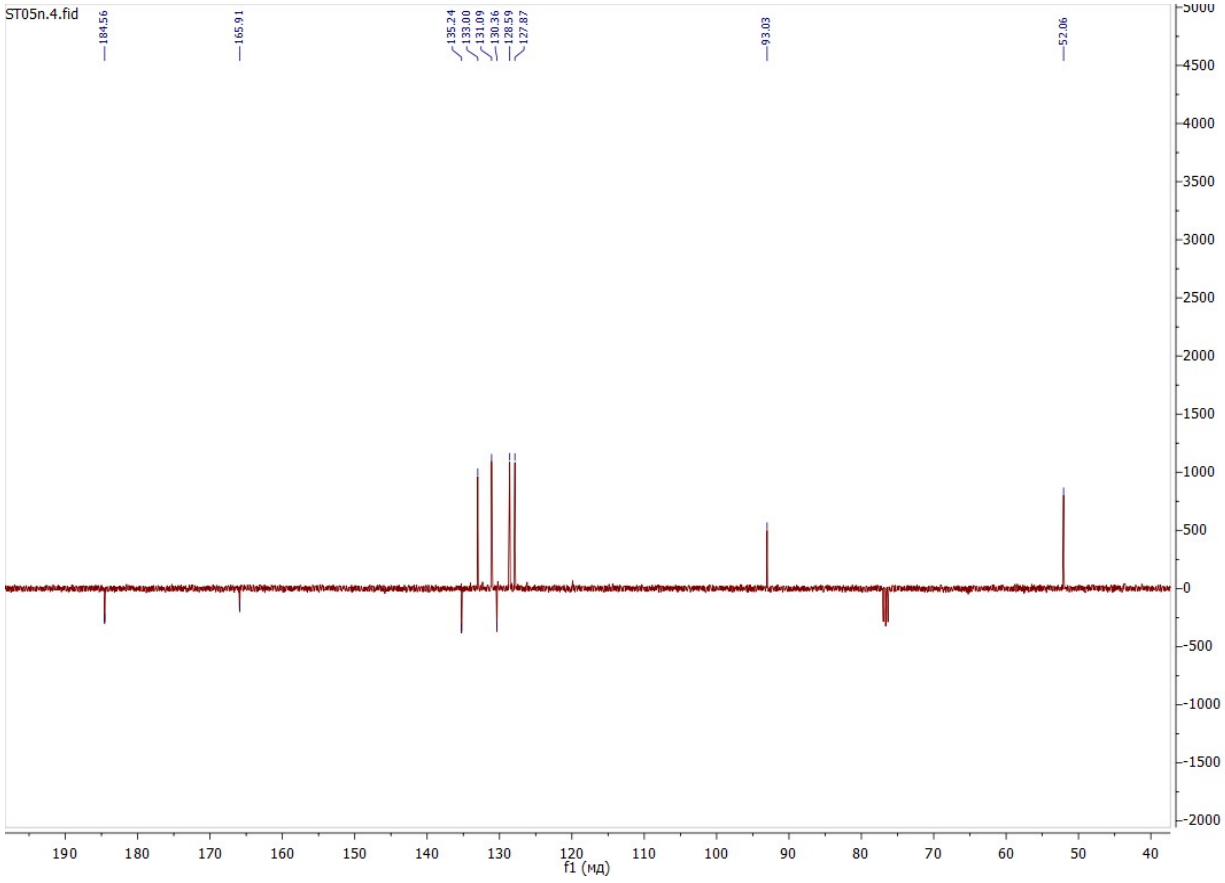

Figure S3. $^{13}C\{^{1}H\}$ NMR spectrum (APT) of L_2 (101 MHz, 298K, $CDCl_3$).

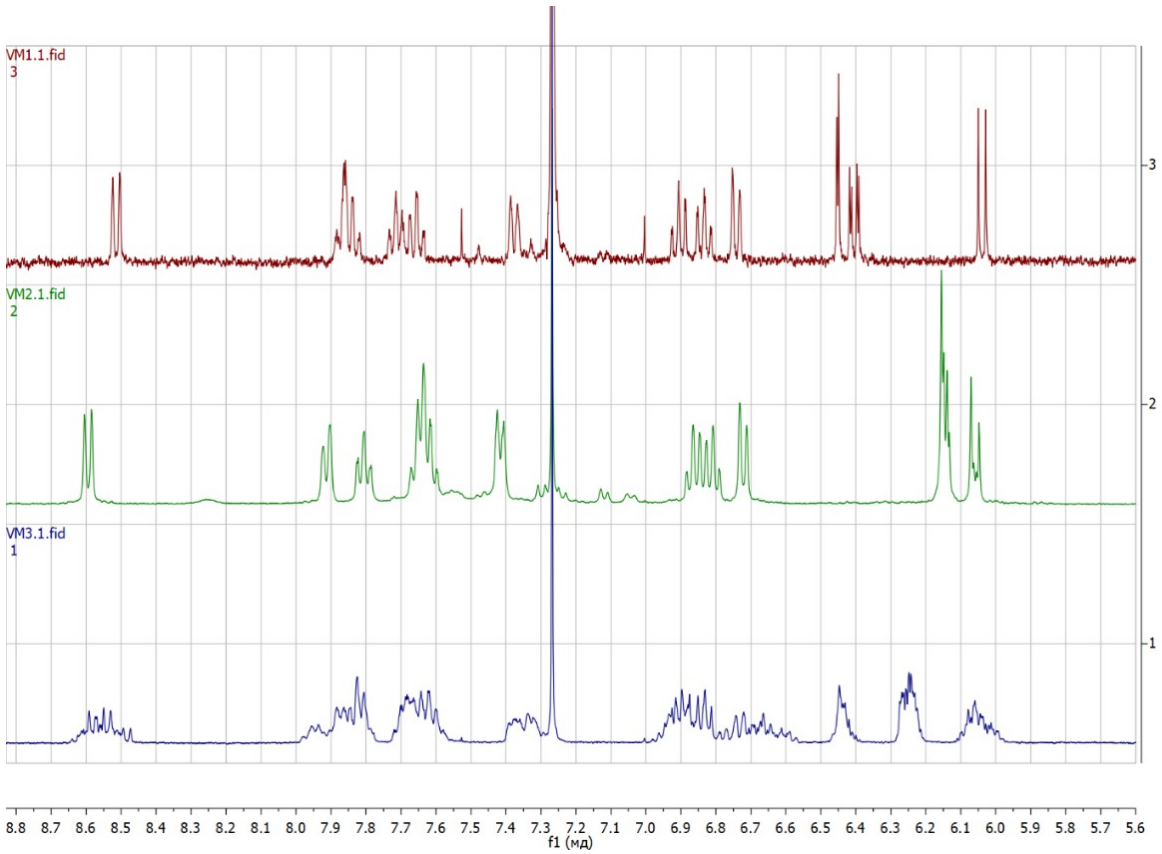

Fig.S4. ^{1}H NMR spectra of dimeric compounds with 3cbi (red), 3mbi (green) and 3fbi(blue) (400 MHz, 298K, $CDCl_3$).

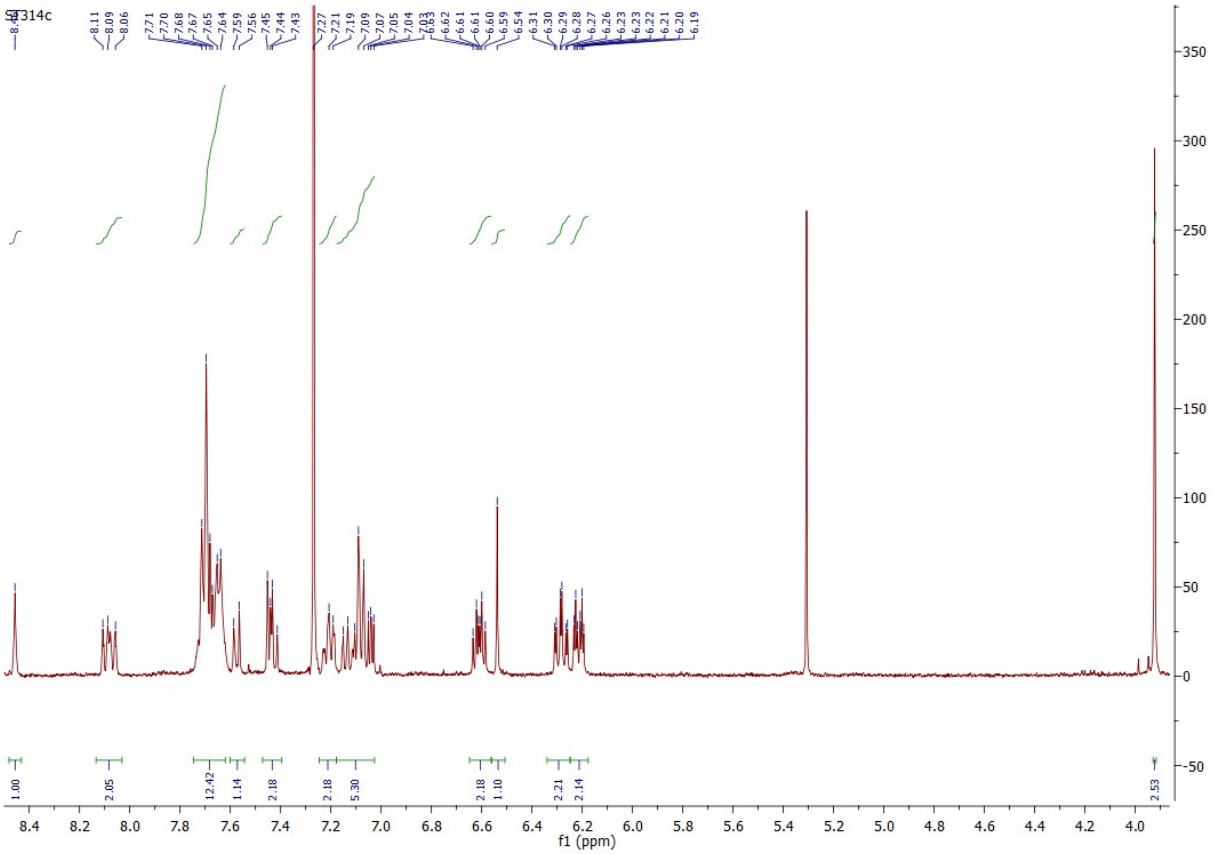

Figure S5. ^{1}H NMR spectrum of **1** (400 MHz, 298K, $CDCl_3$).

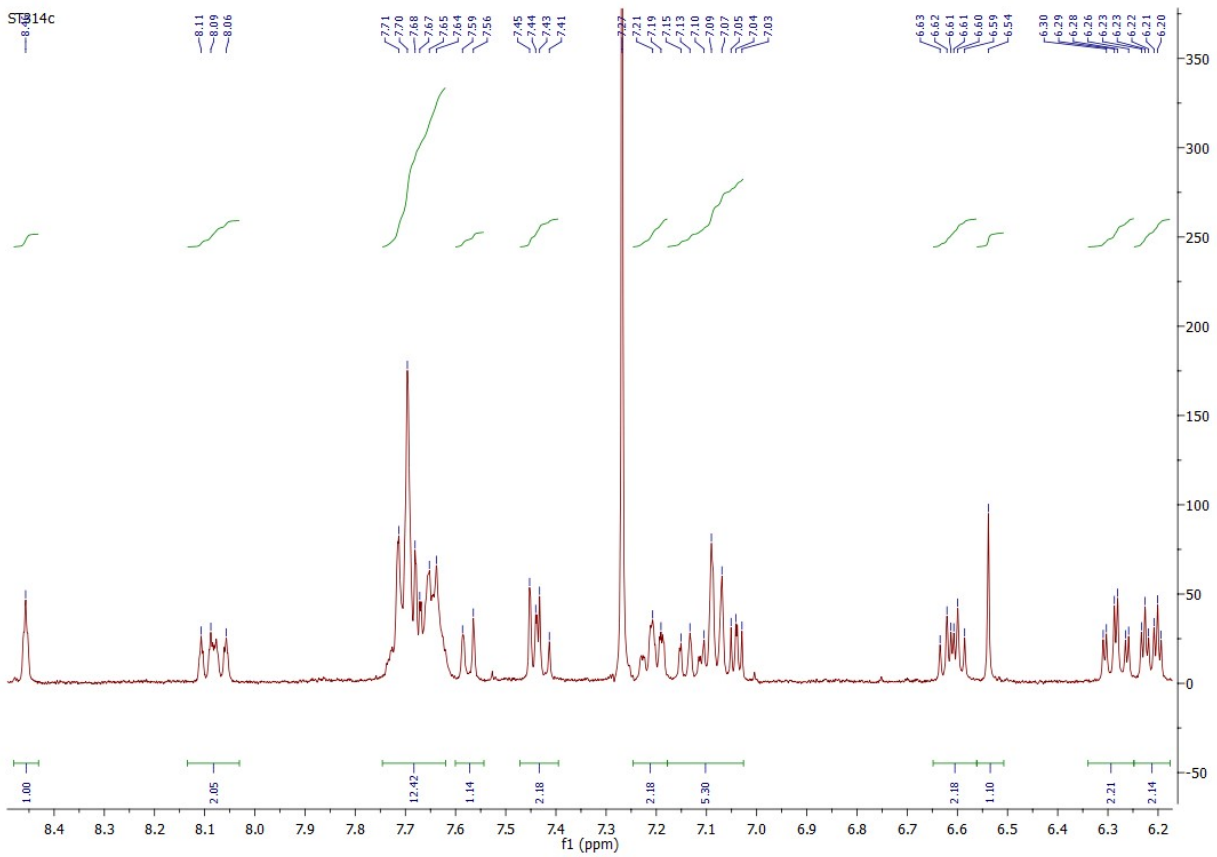

Figure S6. Aromatic region of ^{1}H NMR spectrum of **1** (400 MHz, 298K, $CDCl_3$).

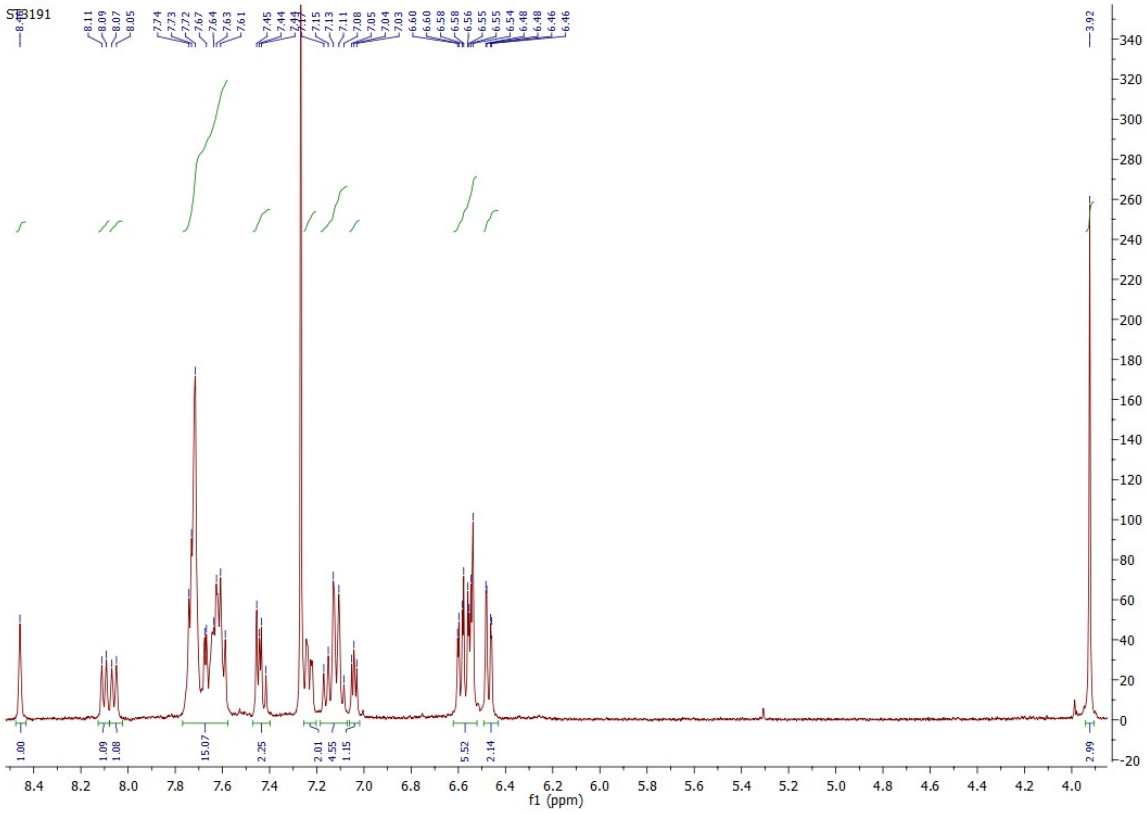

Figure S7. ^{1}H NMR spectrum of **2** (400 MHz, 298K, $CDCl_3$).

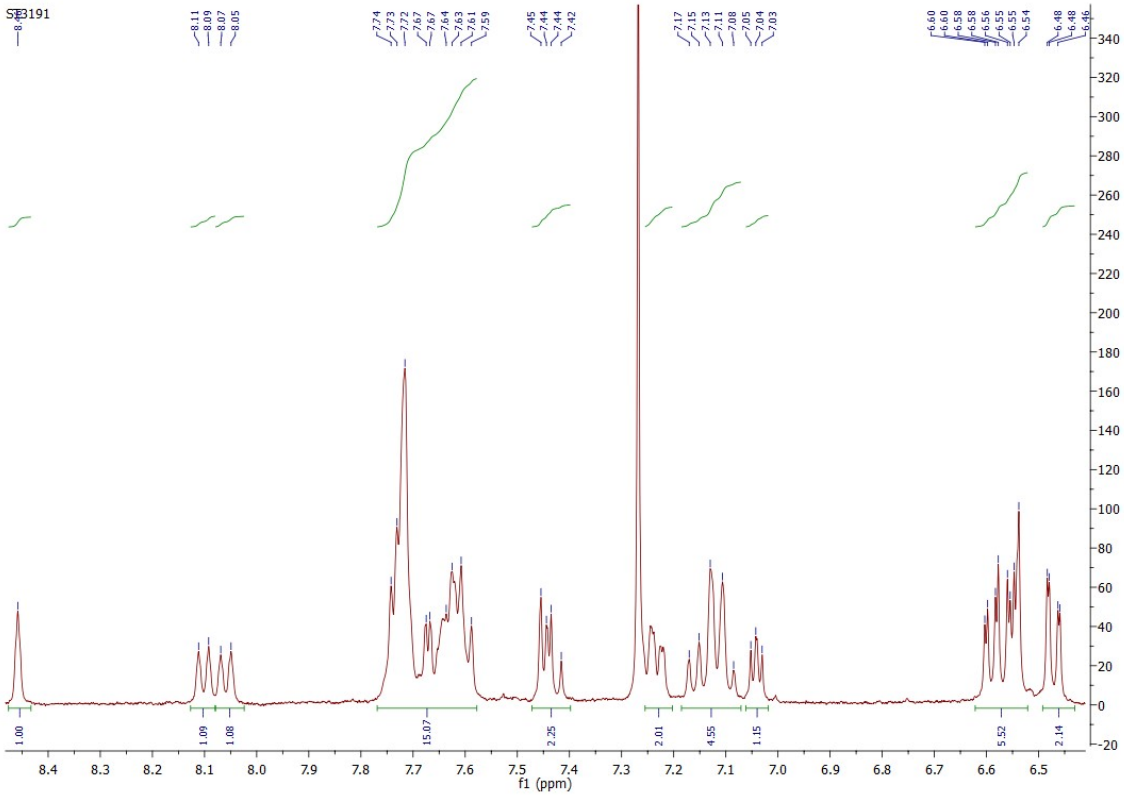

Figure S8. Aromatic region of ^{1}H NMR spectrum of **2** (400 MHz, 298K, $CDCl_3$).

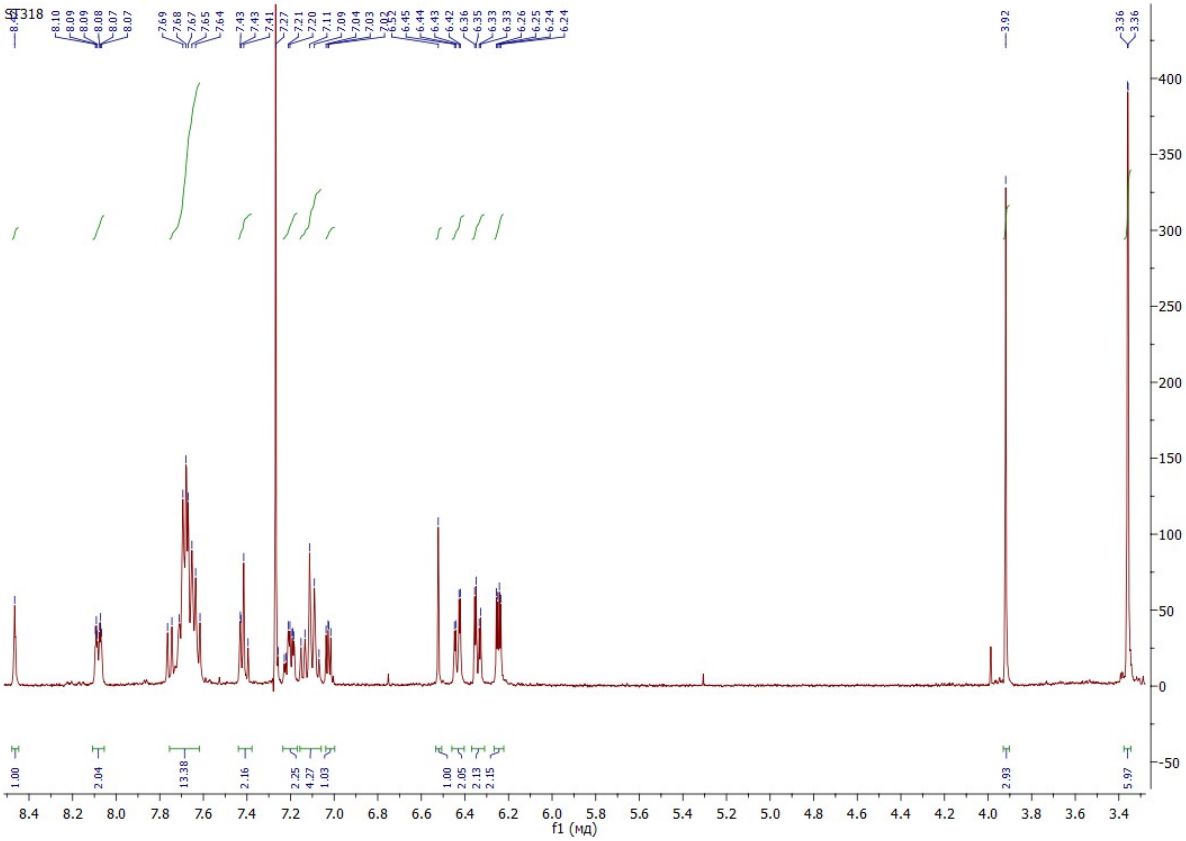

Figure S9. ^{1}H NMR spectrum of **3** (400 MHz, 298K, $CDCl_3$).

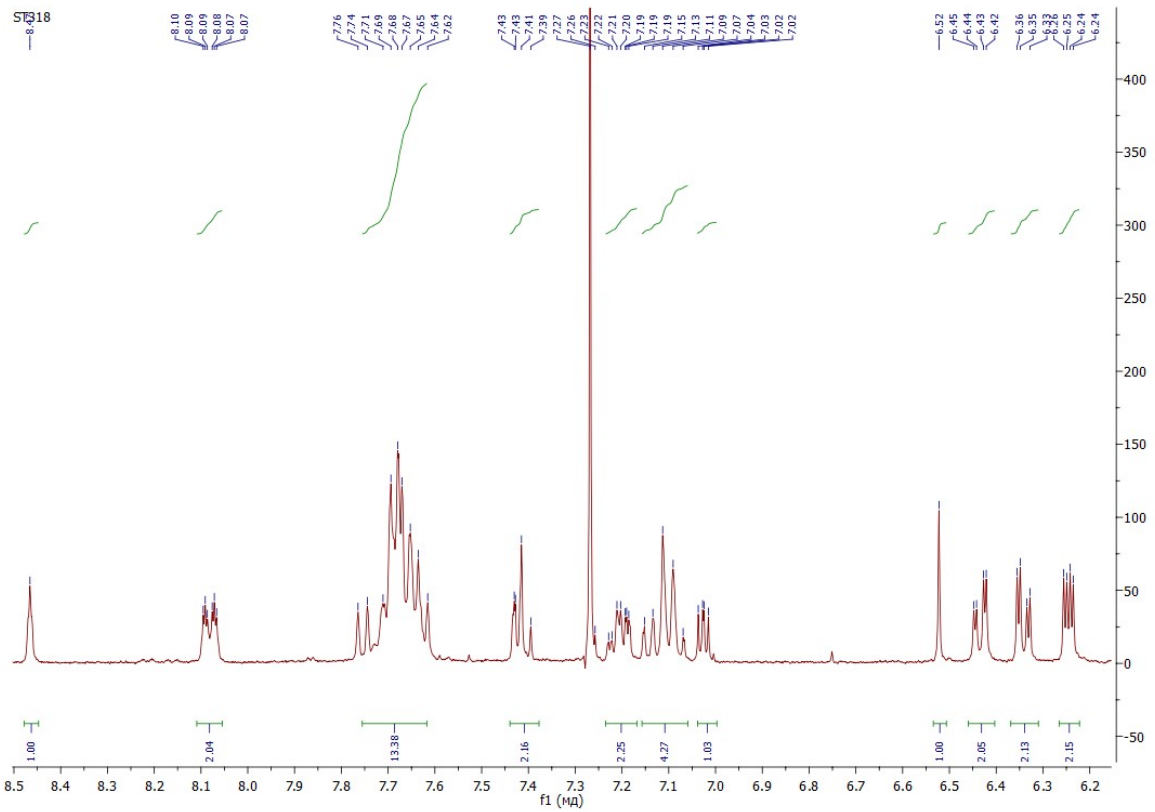

Figure S10. Aromatic region of ^{1}H NMR spectrum of **3** (400 MHz, 298K, $CDCl_3$).

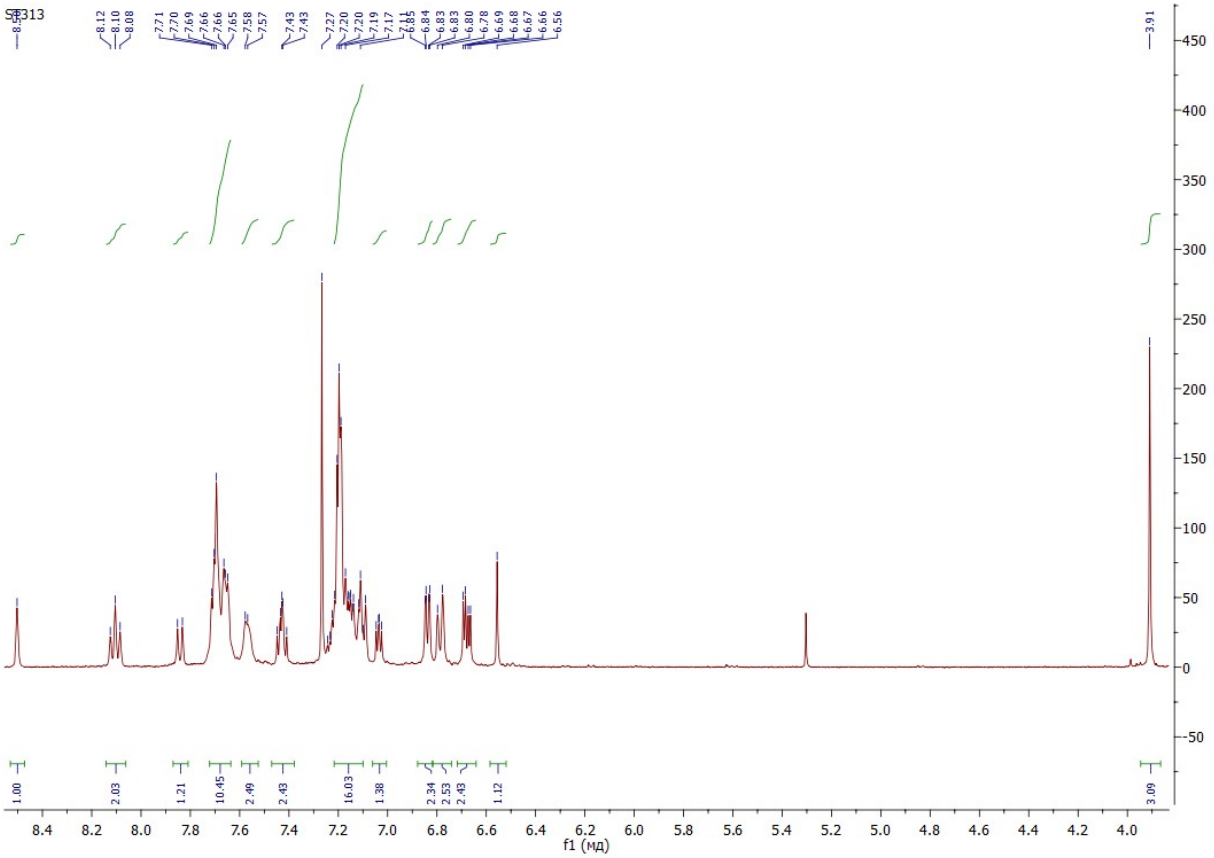

Figure S11. ^{1}H NMR spectrum of **4** (400 MHz, 298K, $CDCl_3$).

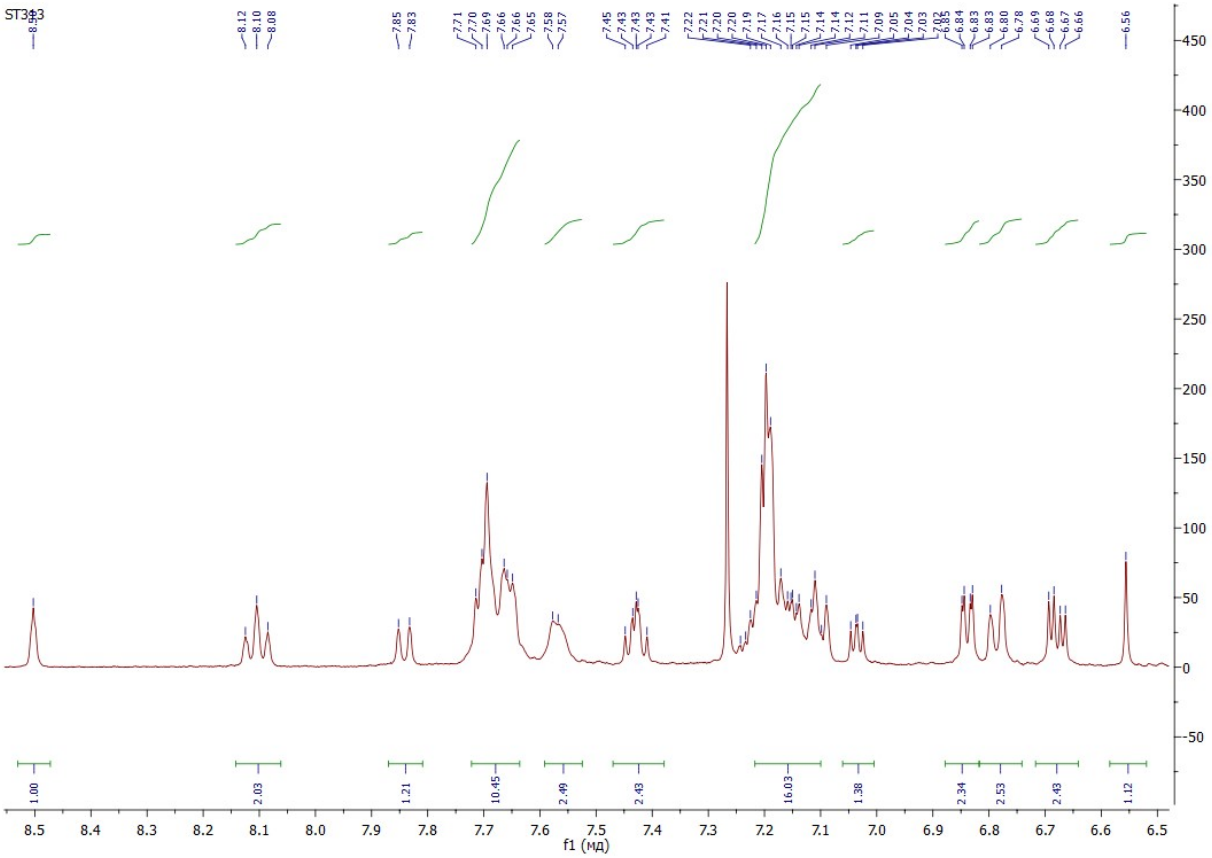

Figure S12. Aromatic region of ^{1}H NMR spectrum of **4** (400 MHz, 298K, $CDCl_3$).

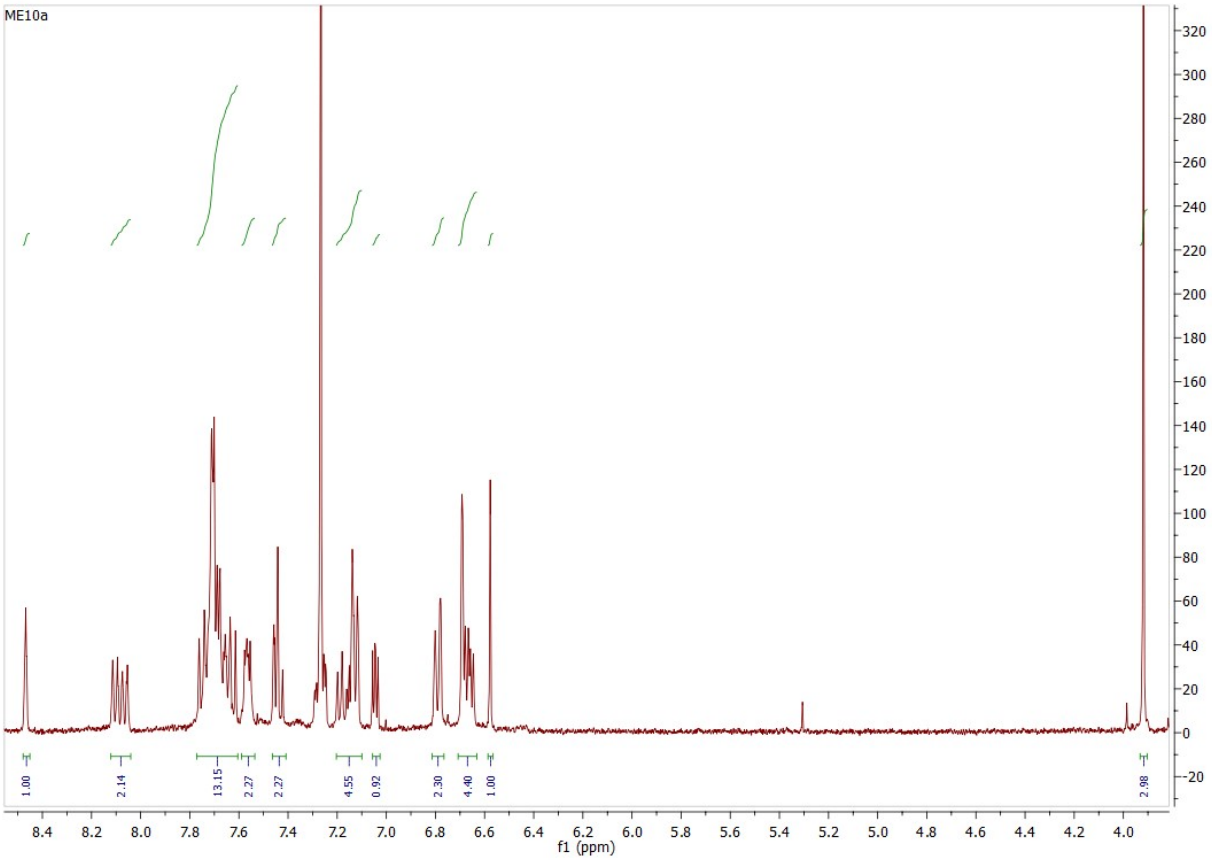

Figure S13. ^{1}H NMR spectrum of **5** (400 MHz, 298K, $CDCl_3$).

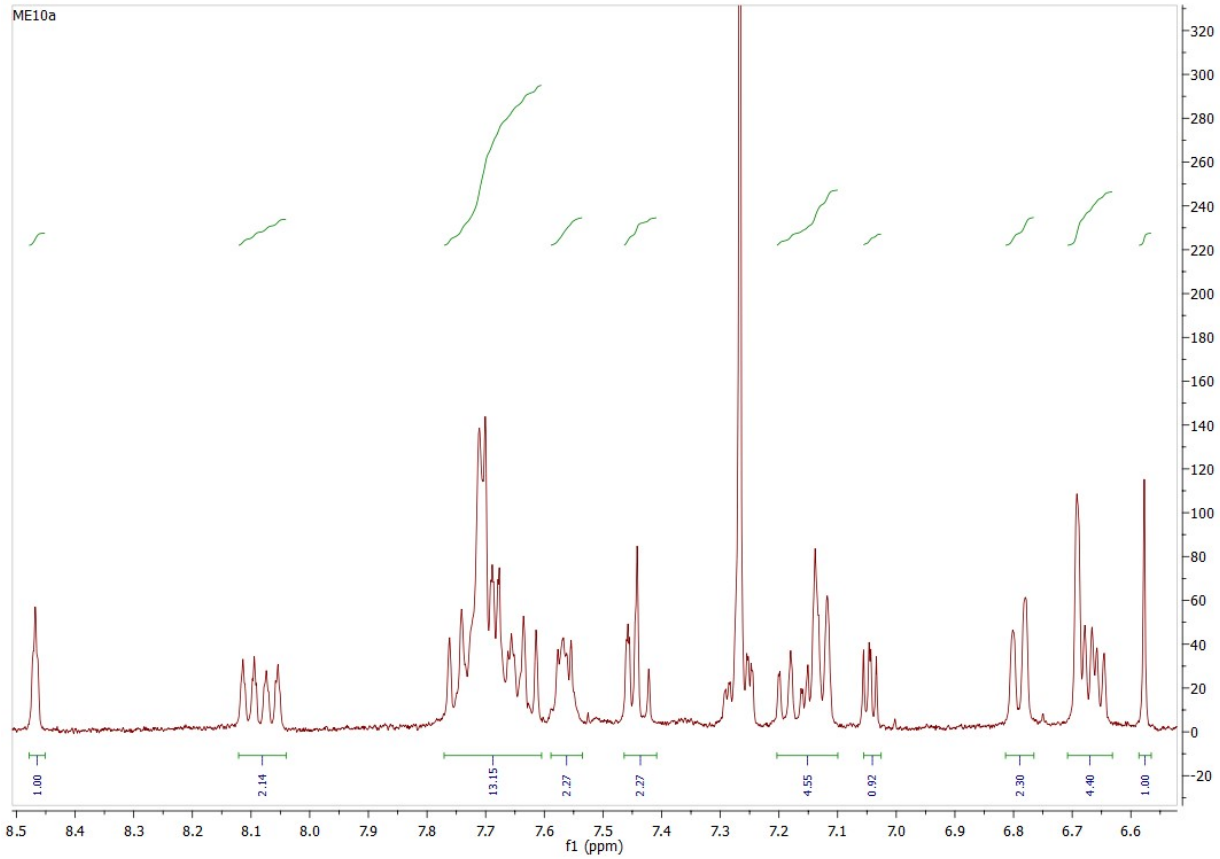

Figure S14. Aromatic region of ^{1}H NMR spectrum of **5** (400 MHz, 298K, $CDCl_3$).

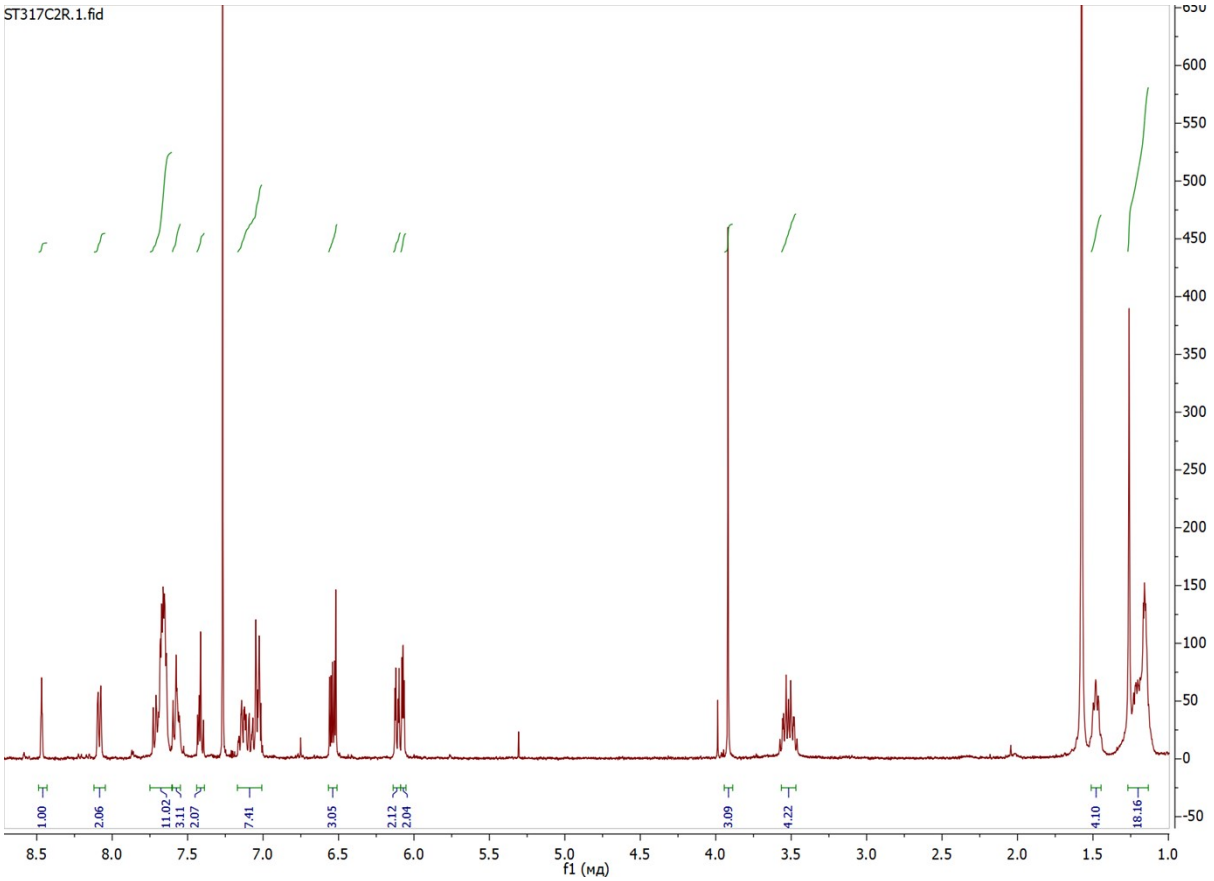

Figure S15. ^{1}H NMR spectrum of **6** (400 MHz, 298K, $CDCl_3$).

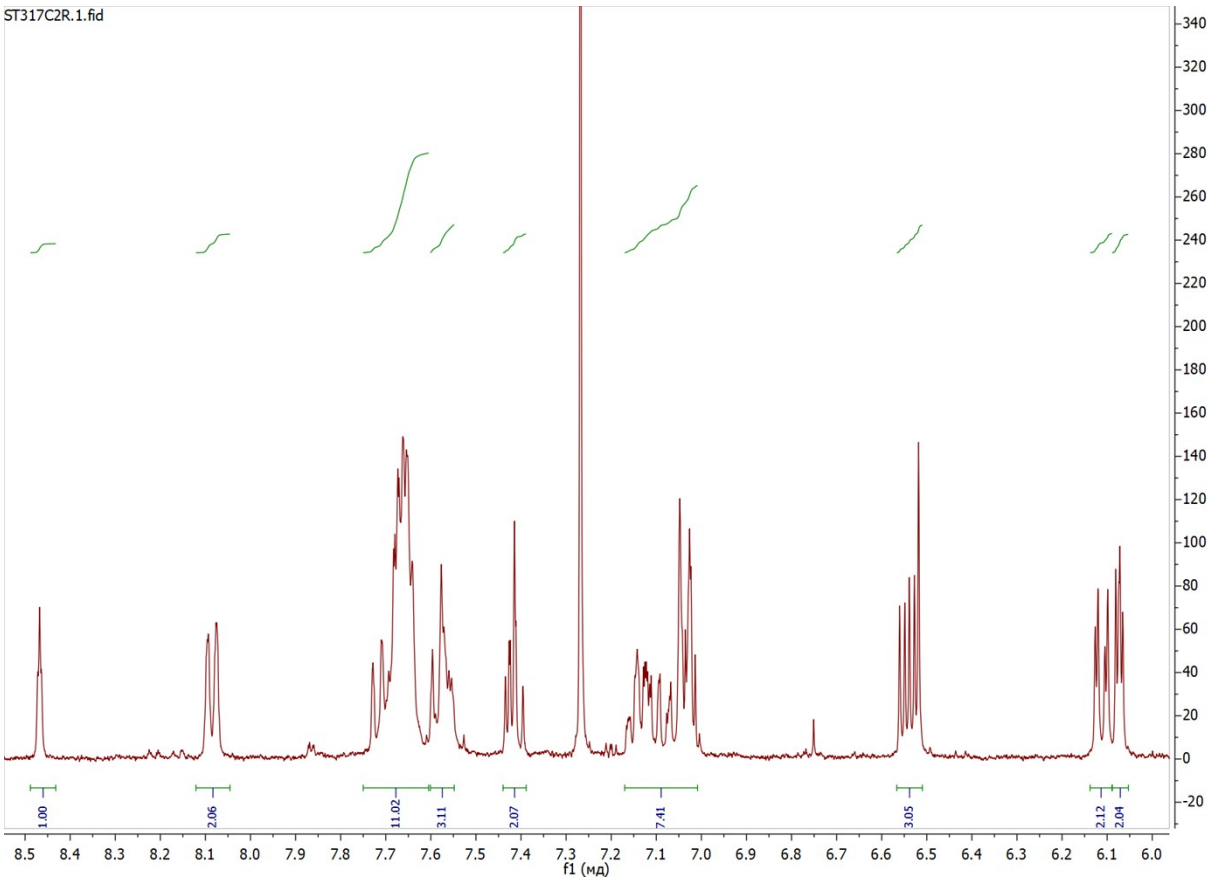

Figure S16. Aromatic region of ^{1}H NMR spectrum of **6** (400 MHz, 298K, $CDCl_3$).

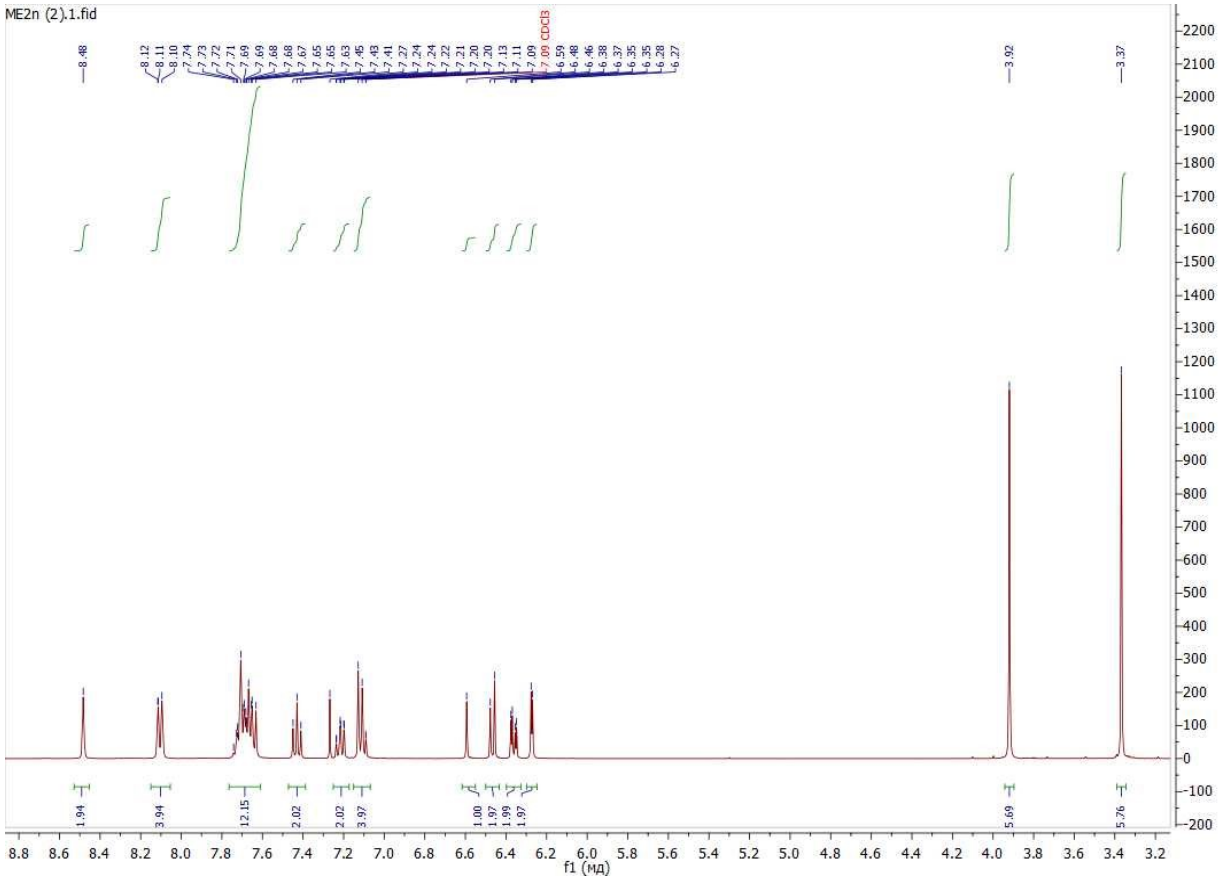

Figure S17. ^{1}H NMR spectrum of **7** (400 MHz, 298K, $CDCl_3$).

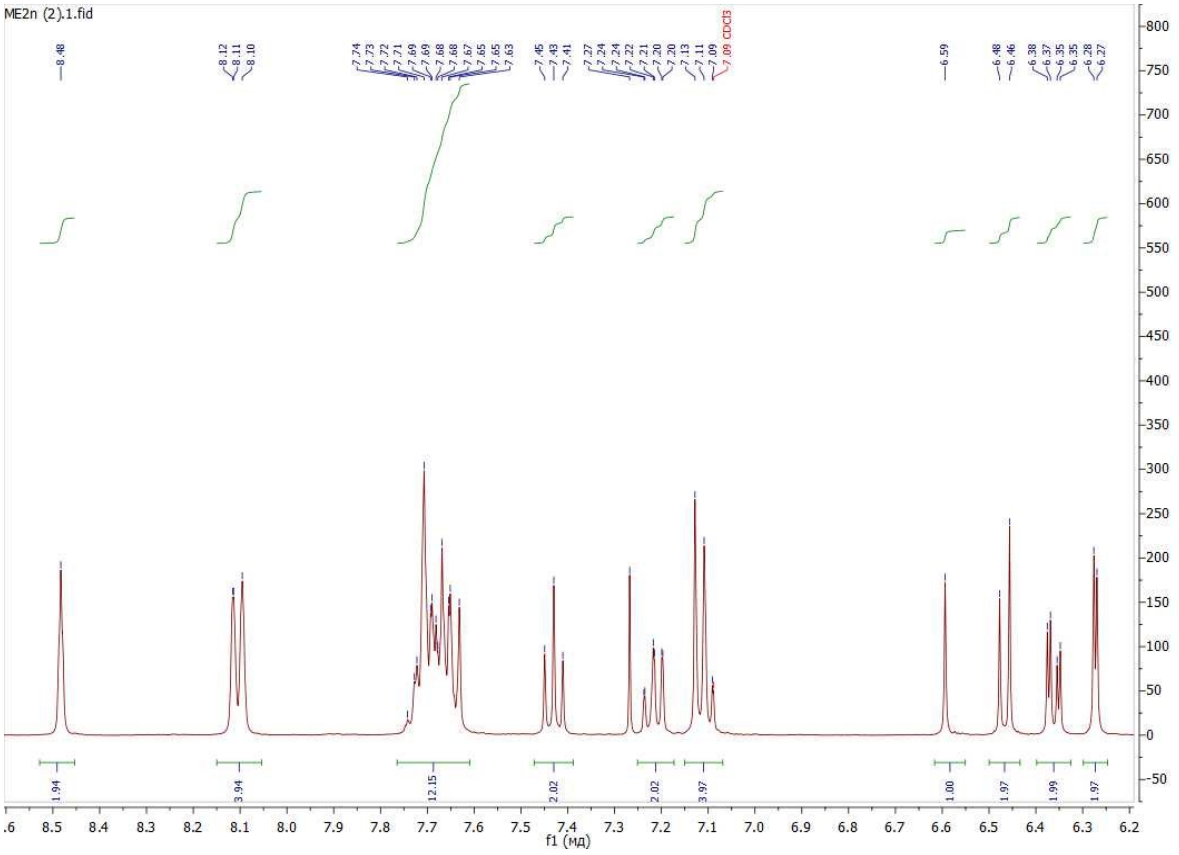

Figure S18. Aromatic region of ^{1}H NMR spectrum of **7** (400 MHz, 298K, $CDCl_3$).

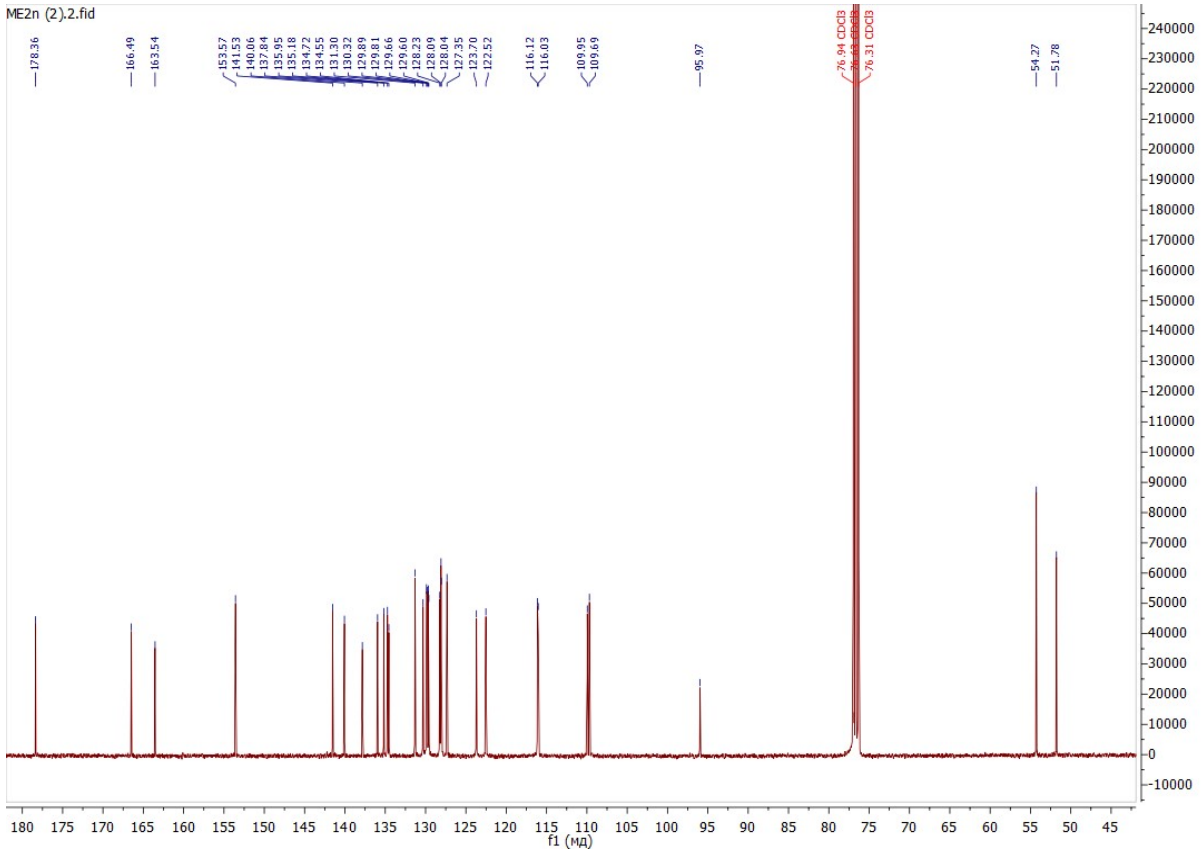

Figure S19. ^{13}C {^{1}H} NMR spectrum of **7** (101 MHz, 298K, $CDCl_3$).

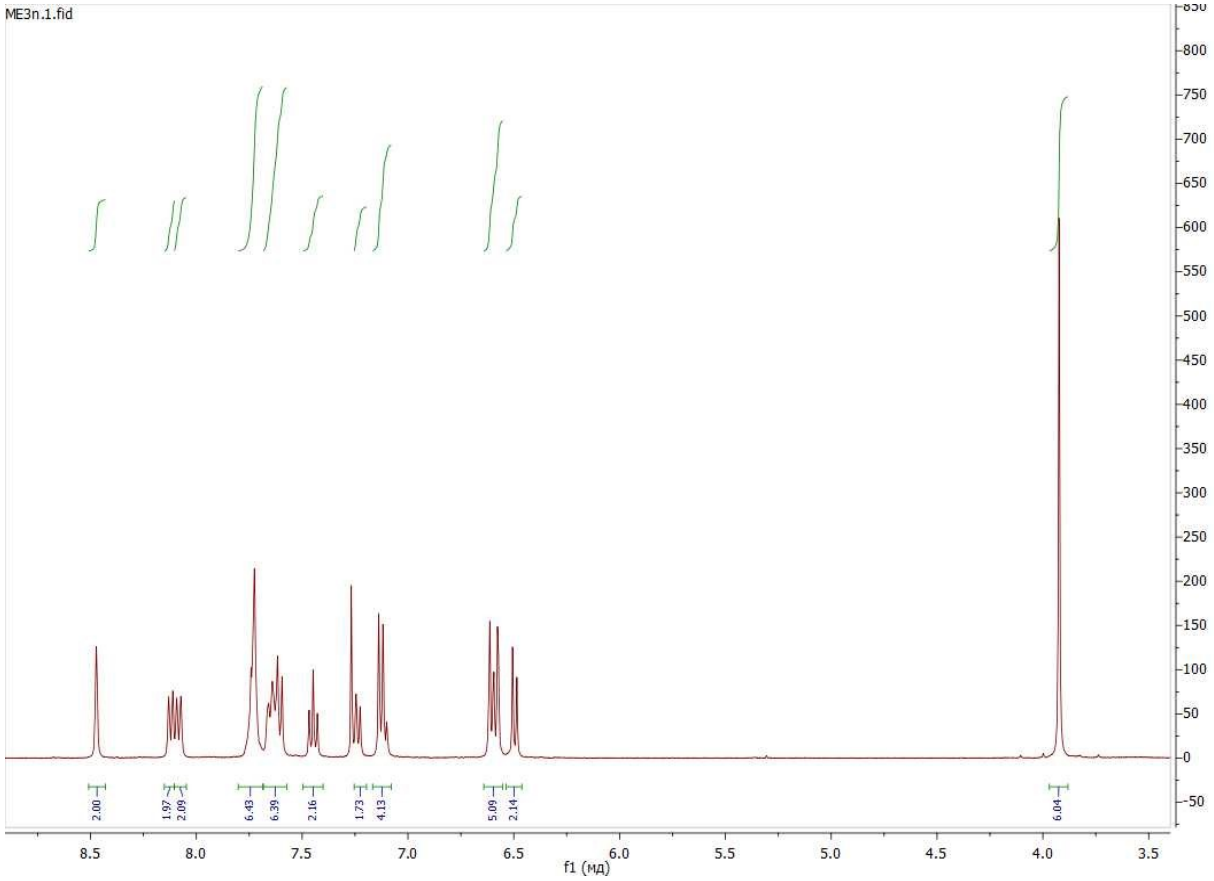

Figure S20. ^{1}H NMR spectrum of **8** (400 MHz, 298K, $CDCl_3$).

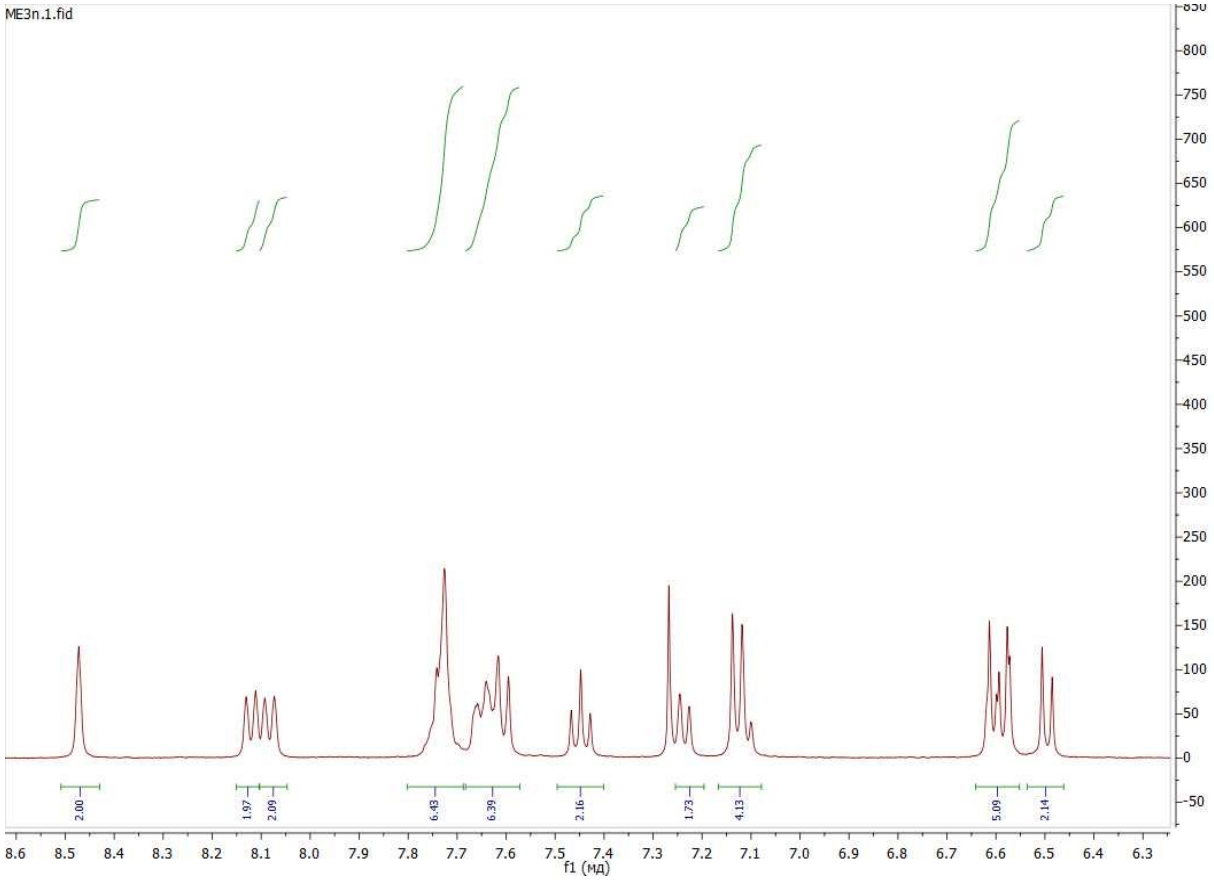

Figure S21. Aromatic region of ^{1}H NMR spectrum of **8** (400 MHz, 298K, $CDCl_3$).

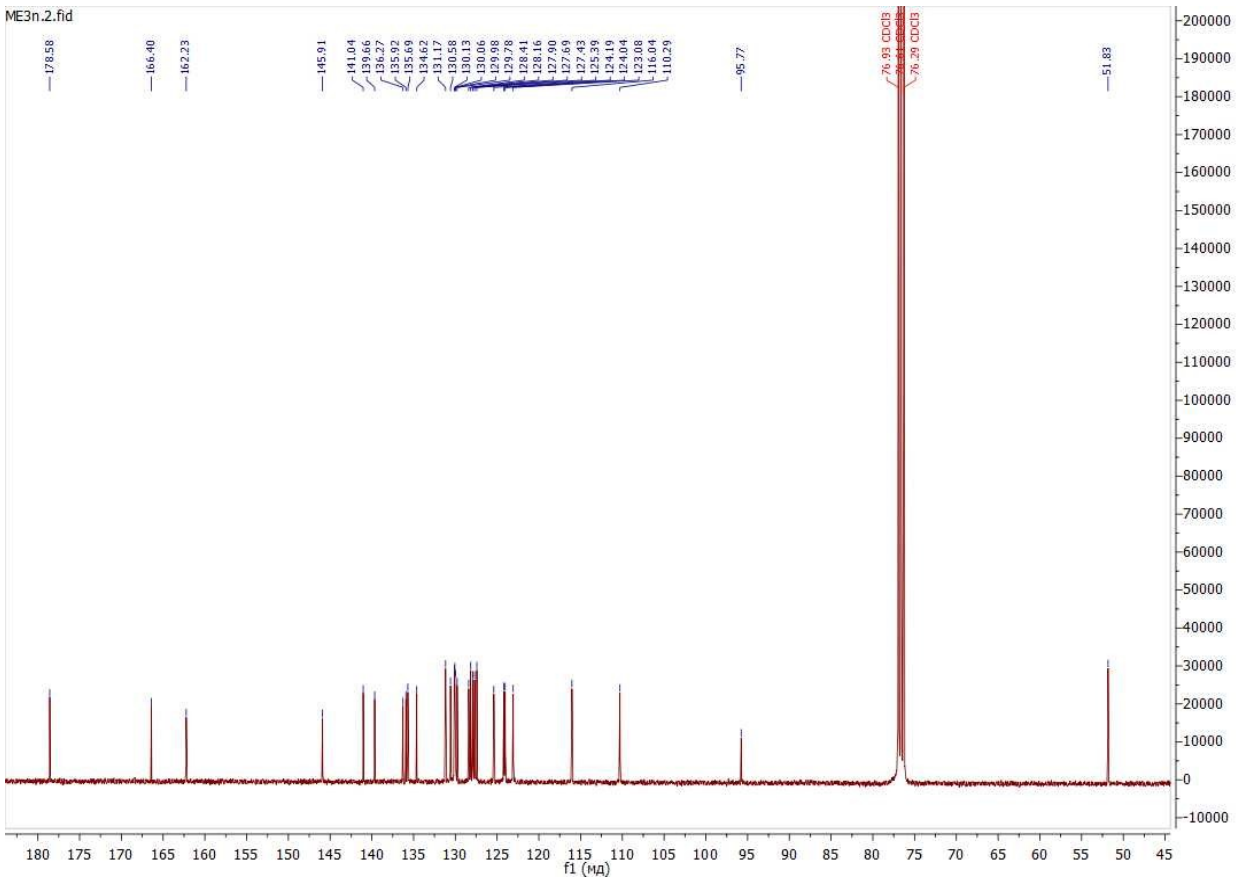

Figure S22. ^{13}C {^{1}H} NMR spectrum of **8** (101 MHz, 298K, $CDCl_3$).

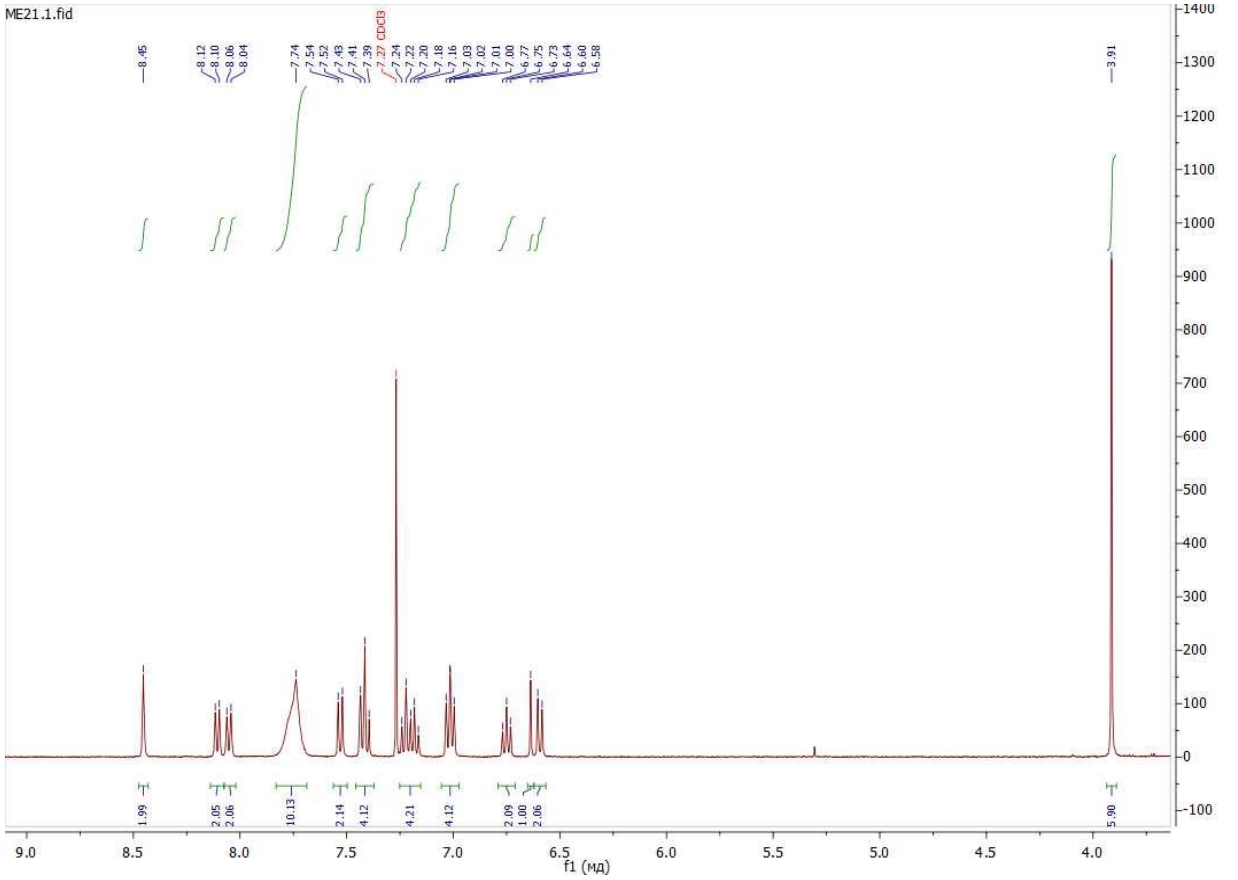

Figure S23. ^{1}H NMR spectrum of **9** (400 MHz, 298K, $CDCl_3$).

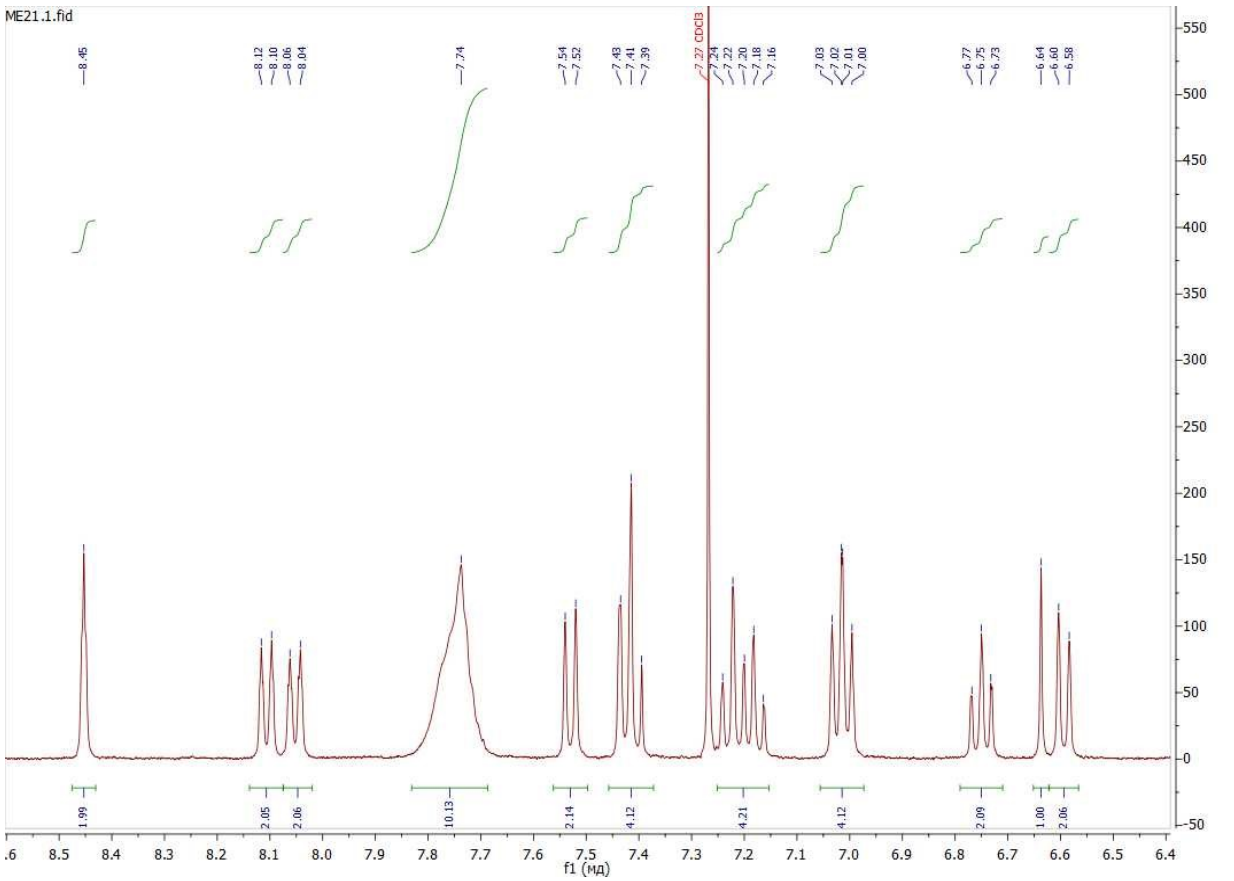

Figure S24. Aromatic region of ^{1}H NMR spectrum of **9** (400 MHz, 298K, $CDCl_3$).

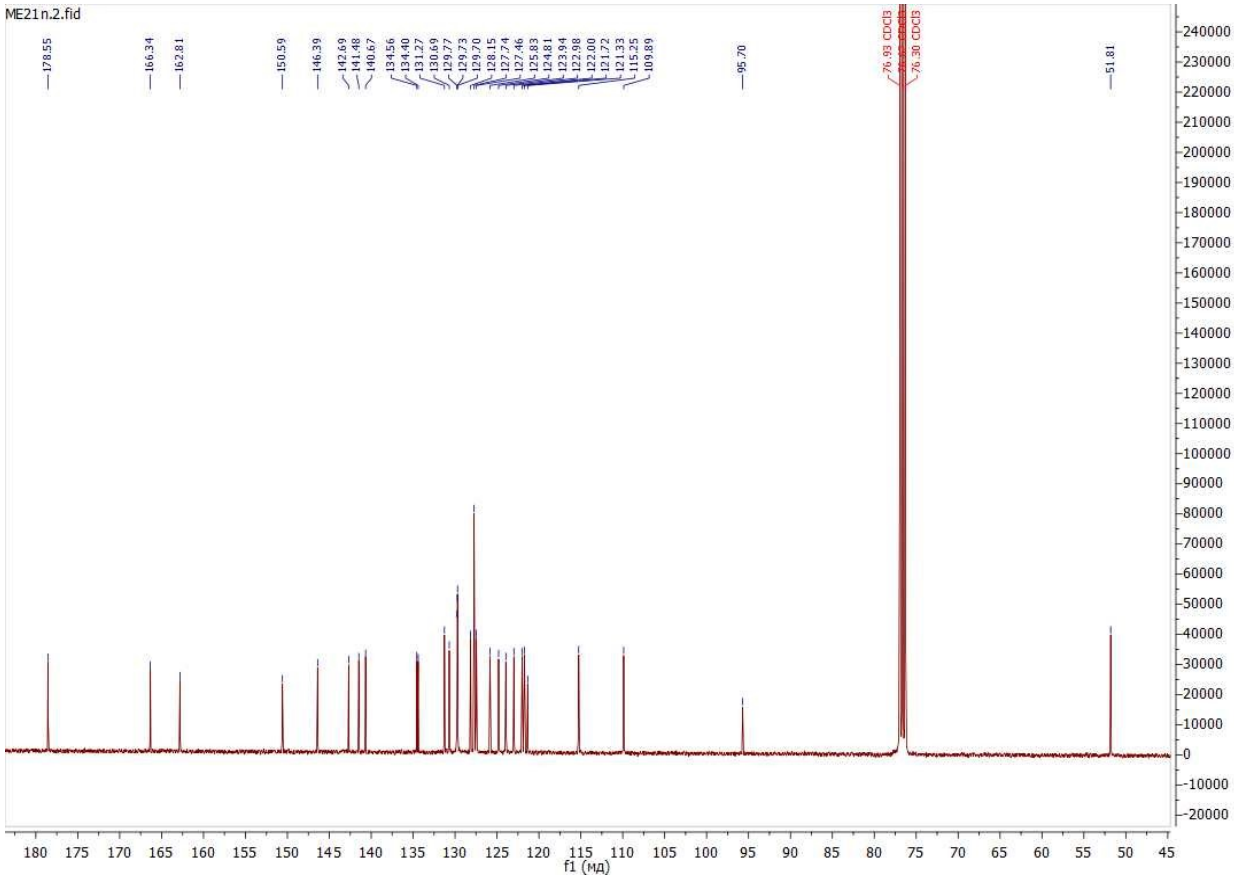

Figure S25. ^{13}C {^{1}H} NMR spectrum of **9** (101 MHz, 298K, $CDCl_3$).

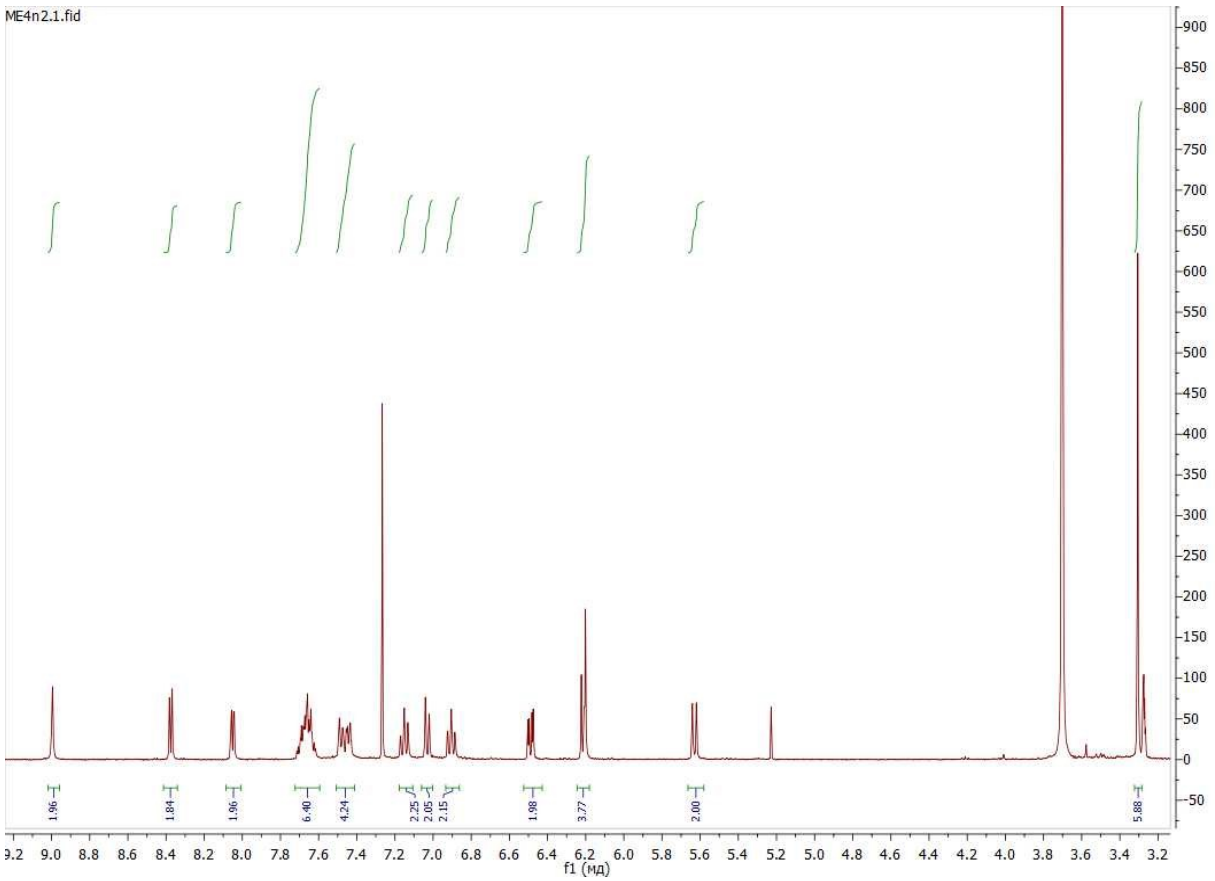

Figure S26. ^{1}H NMR spectrum of **10** (400 MHz, 298K, CDCl3:CD3OD 6:1).

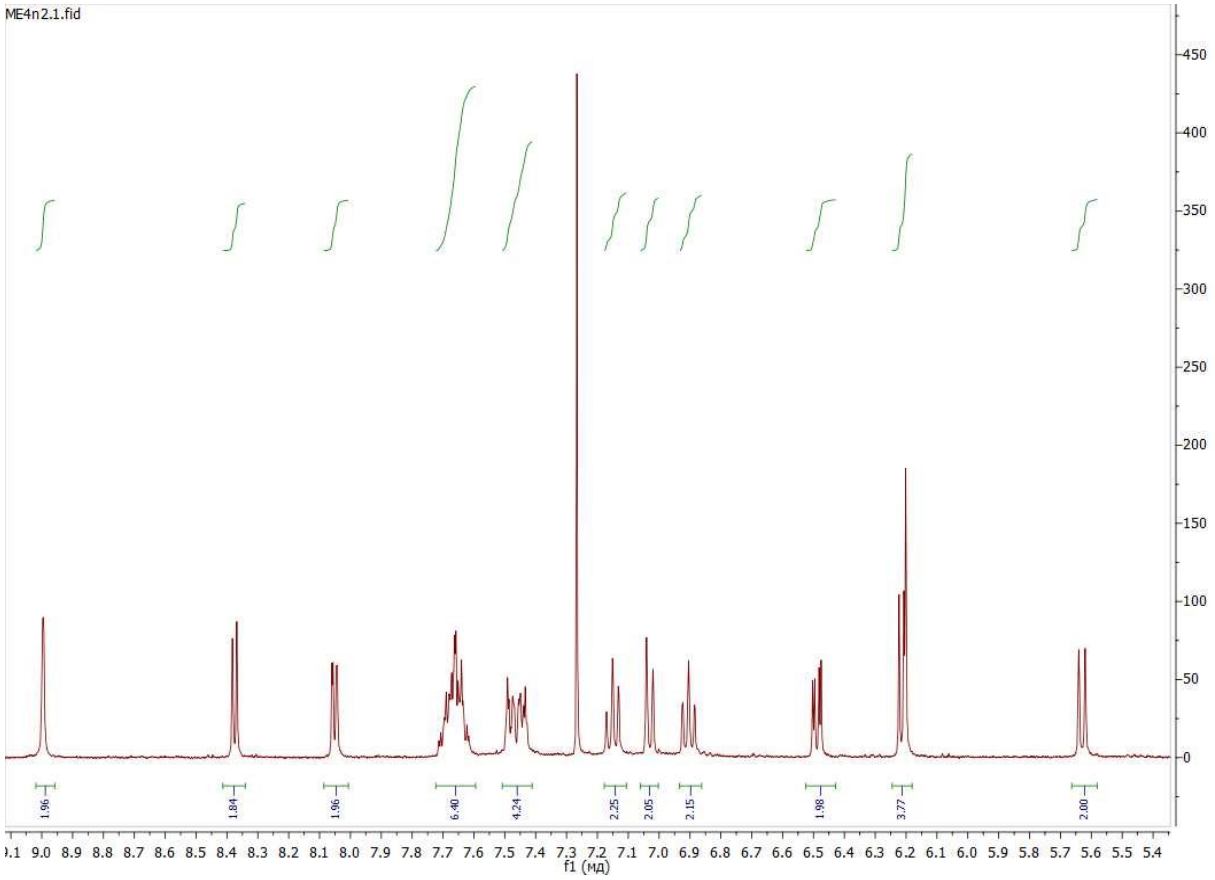

Figure S27. Aromatic region of ^{1}H NMR spectrum of **10** (400 MHz, 298K, CDCl3:CD3OD 6:1).

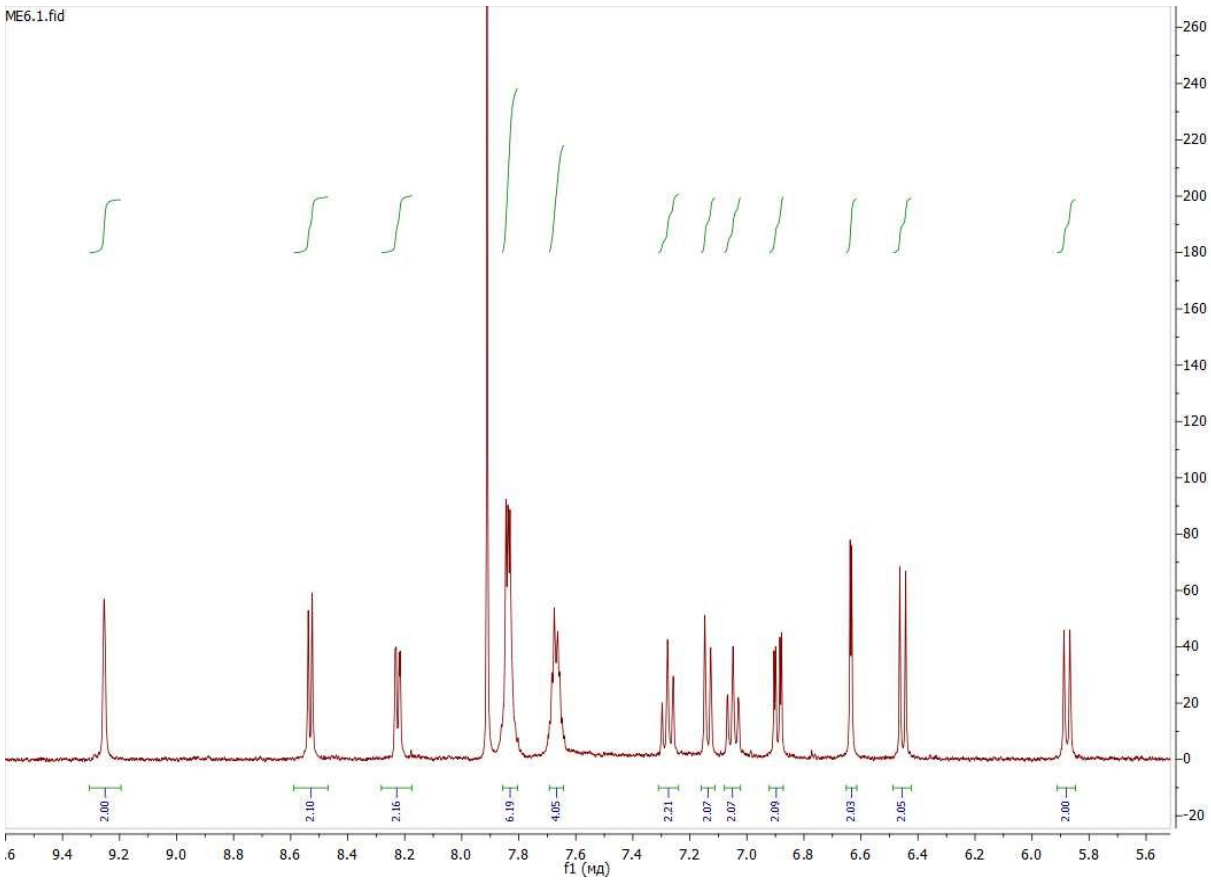

Figure S28. ^{1}H NMR spectrum of **11** (400 MHz, 298K, CD_3OD).

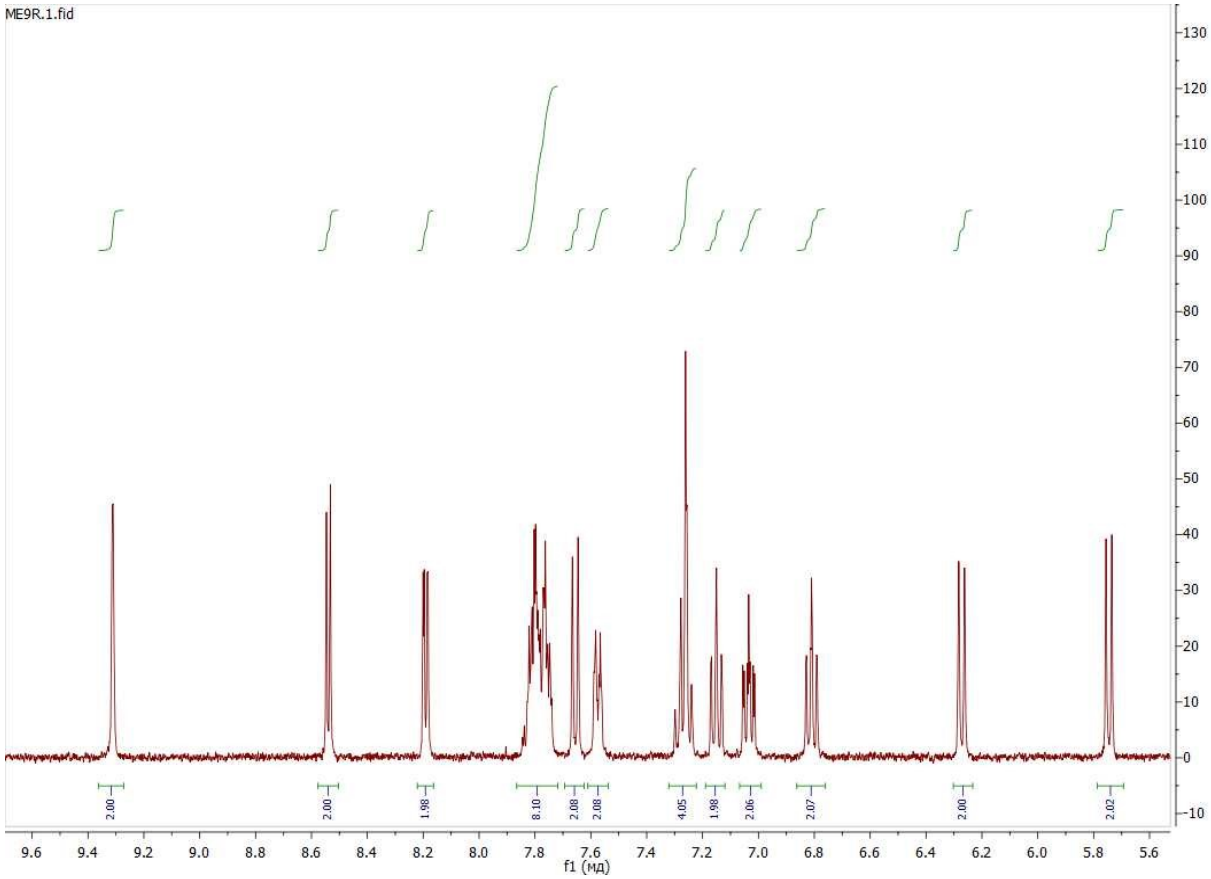

Figure S29. ^{1}H NMR spectrum of **12** (400 MHz, 298K, CD_3OD).

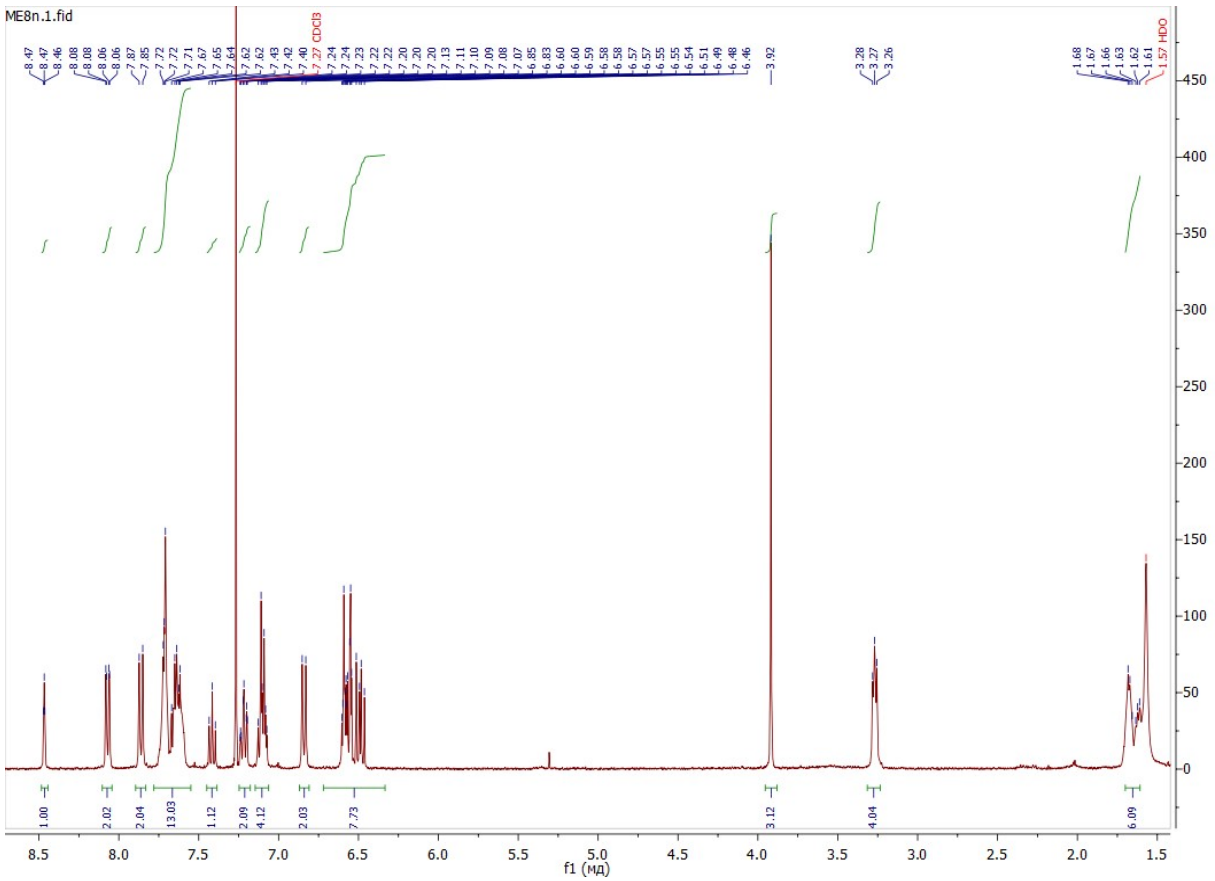

Figure S30. ^{1}H NMR spectrum of **13** (400 MHz, 298K, $CDCl_3$).

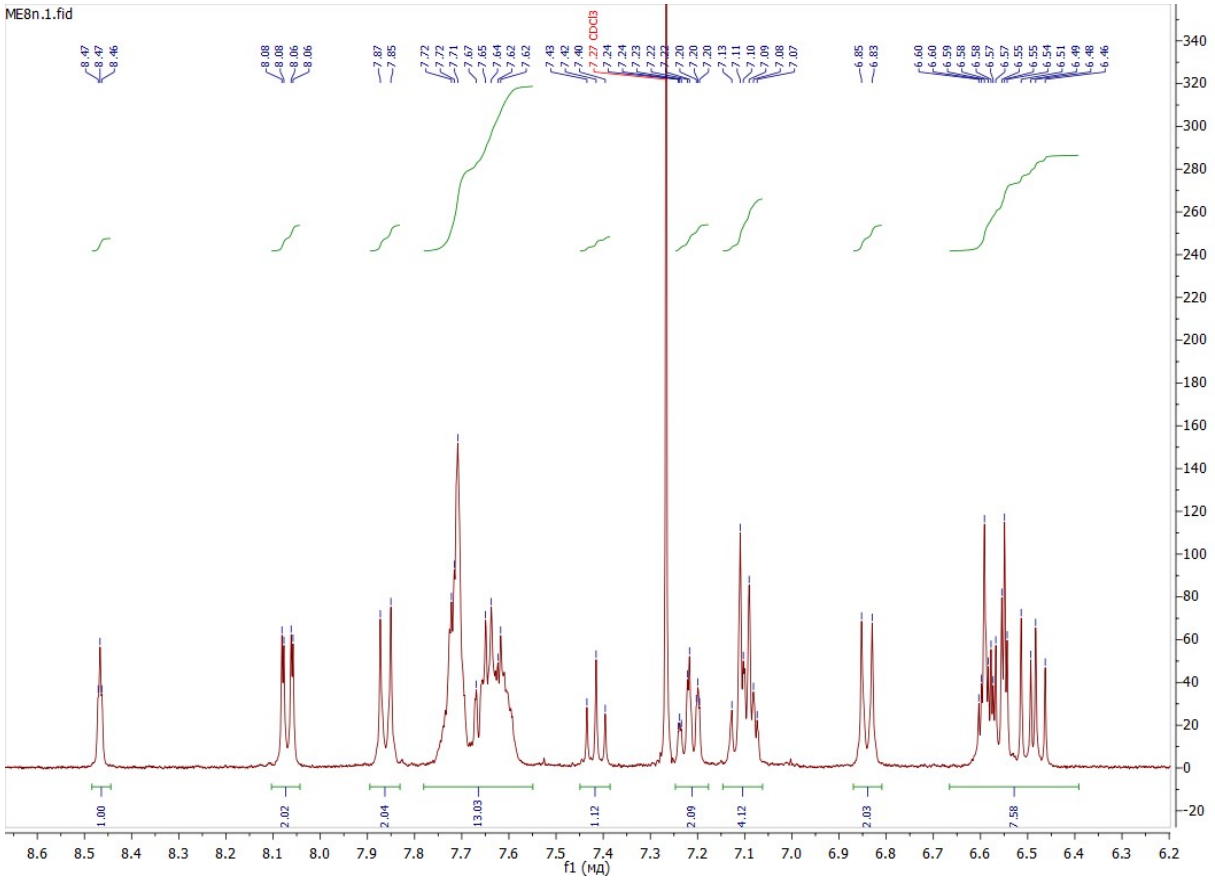

Figure S31. Aromatic region of ^{1}H NMR spectrum of **13** (400 MHz, 298K, $CDCl_3$)

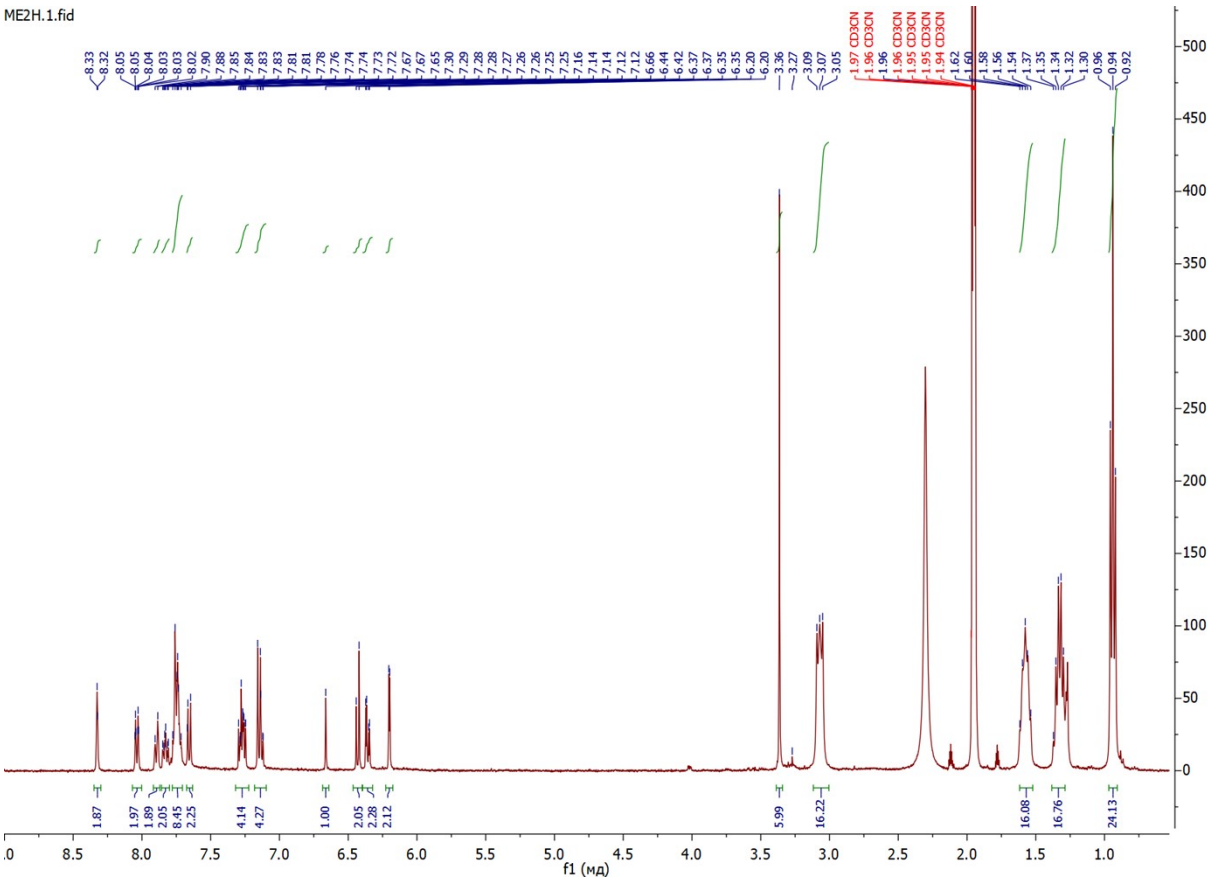

Figure S32. ^{1}H NMR spectrum of hydrolysed complex 2(TBA)$^{+}$(**7H**)$^{2-}$ (400 MHz, 298K, CD_3CN).

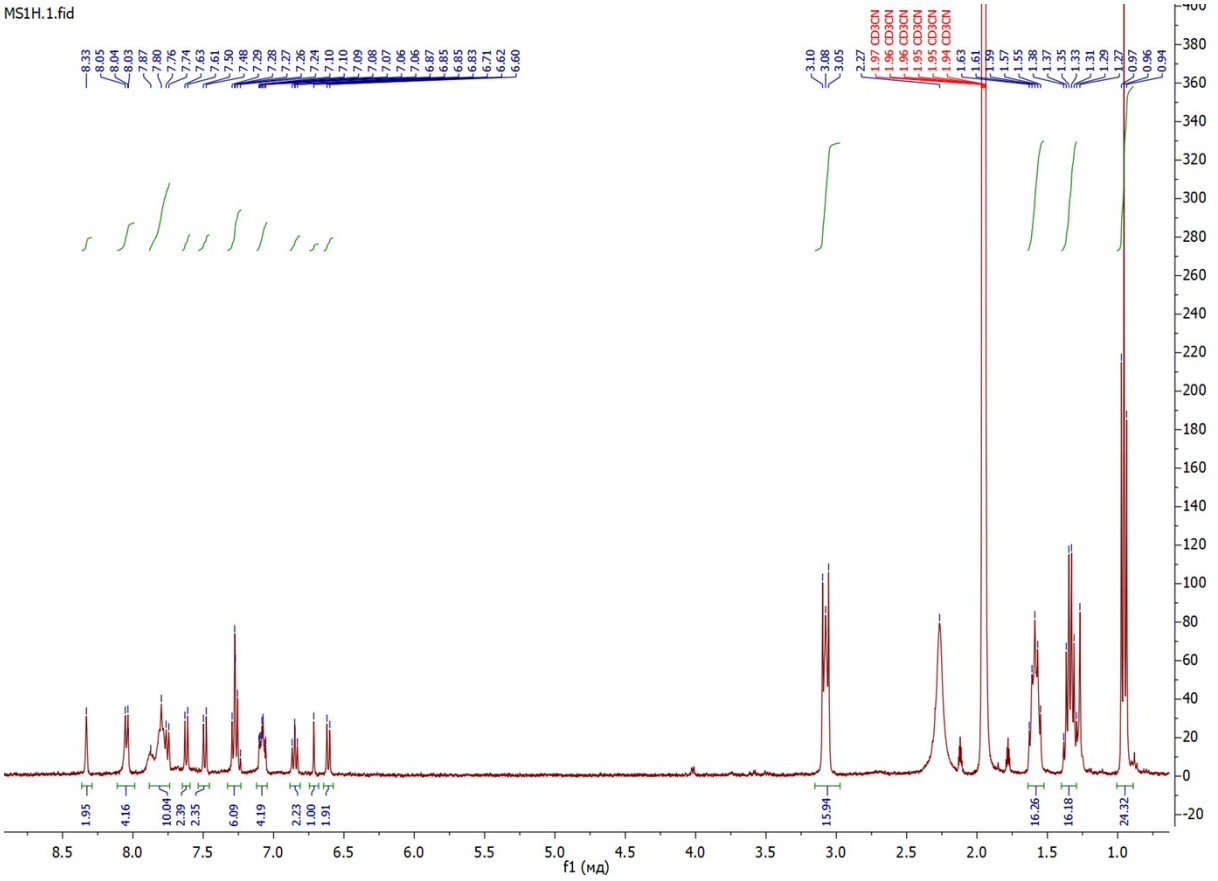

Figure S33. ^{1}H NMR spectrum of hydrolysed complex 2(TBA)$^{+}$(**9H**)$^{2-}$ (400 MHz, 298K, CD_3CN).

Table S1. High resolution mass-spectrum data (m/z) of complexes **1** – **13.**

Complex	$[Ir(C^N)_2(L)]^+$	$[Ir(C^N)_2]^+$
1	1054.1986	767.1591
2	1086.1394	799.0993
3	1078.2371	791.1996
4	1170.2816	883.2417
5	1154.1941	867.1523
6	1218.3963	931.3566
7	1130.2886	832.2258
8	1138.1861	840.1249
9	1182.2107	884.1487
10	1035.2476	
11	1043.1473	797.0998
12	1087.1719	843.1219
12	1164.2613	799.0987

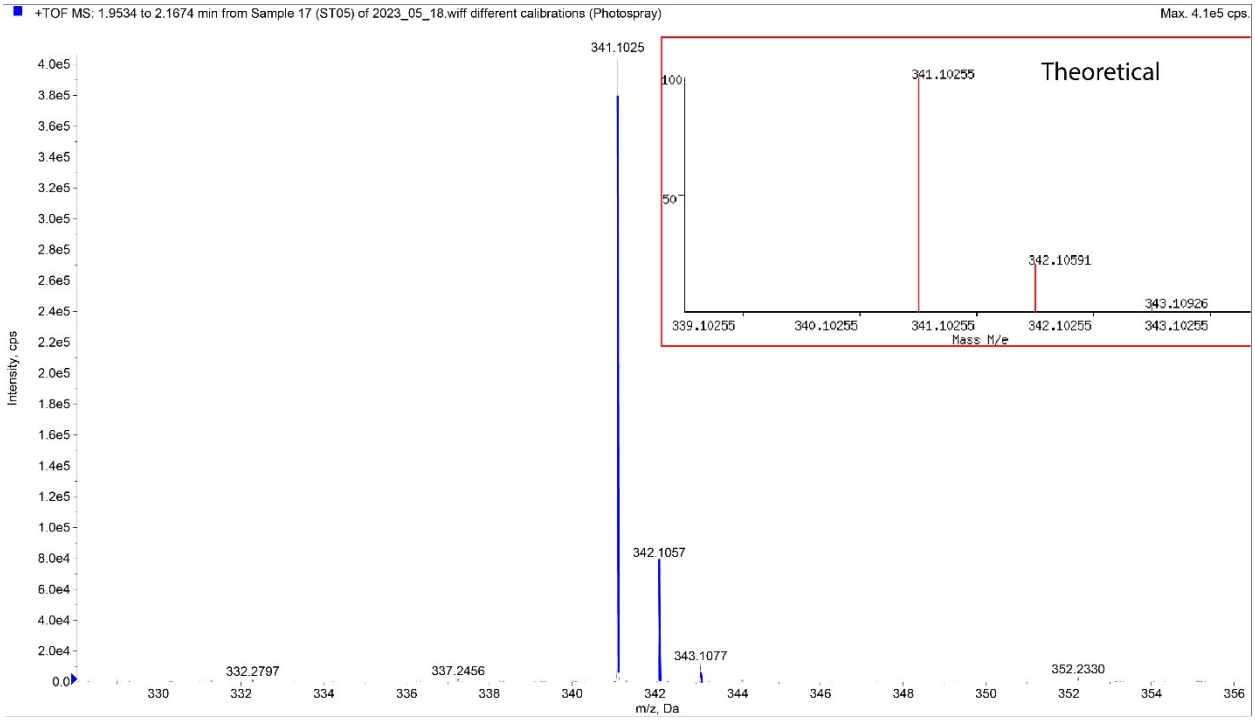

Figure S34. High resolution mass spectrum of $\mathbf{L_2}$.

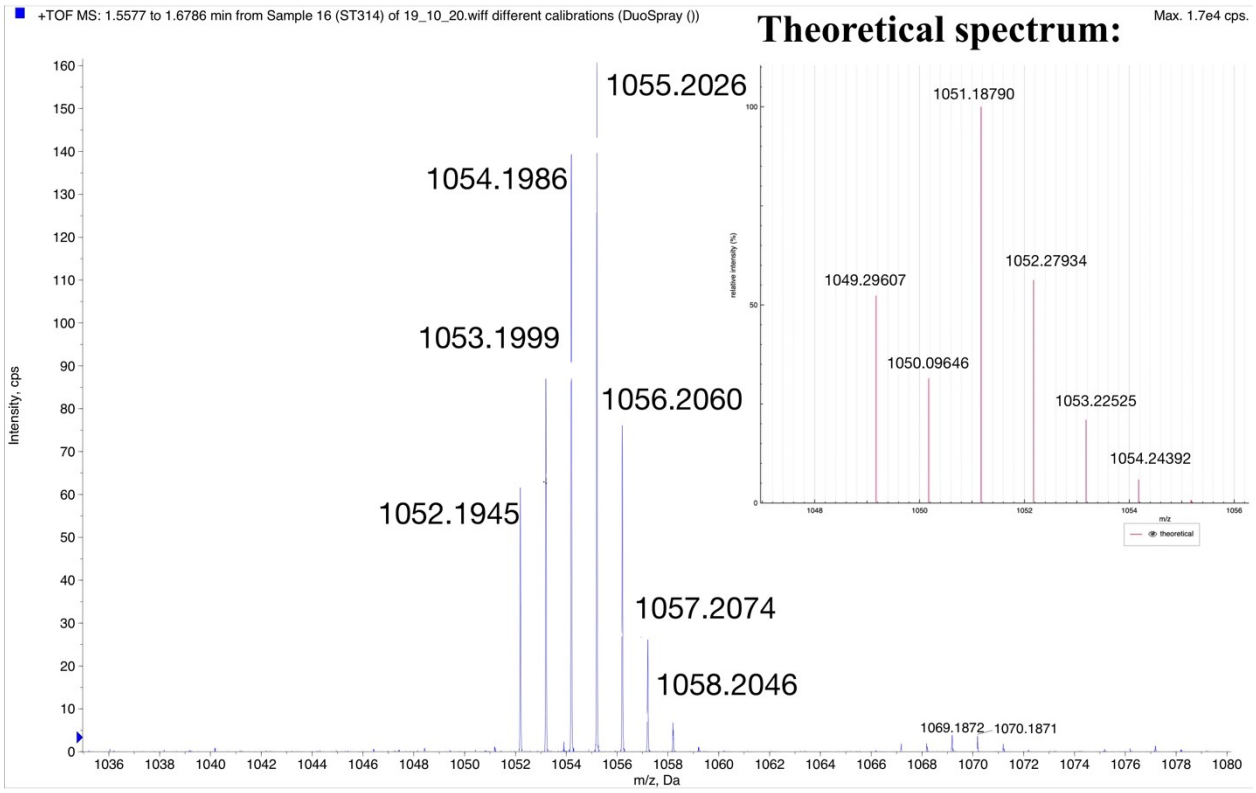

Figure S35. High resolution mass spectrum of **1**.

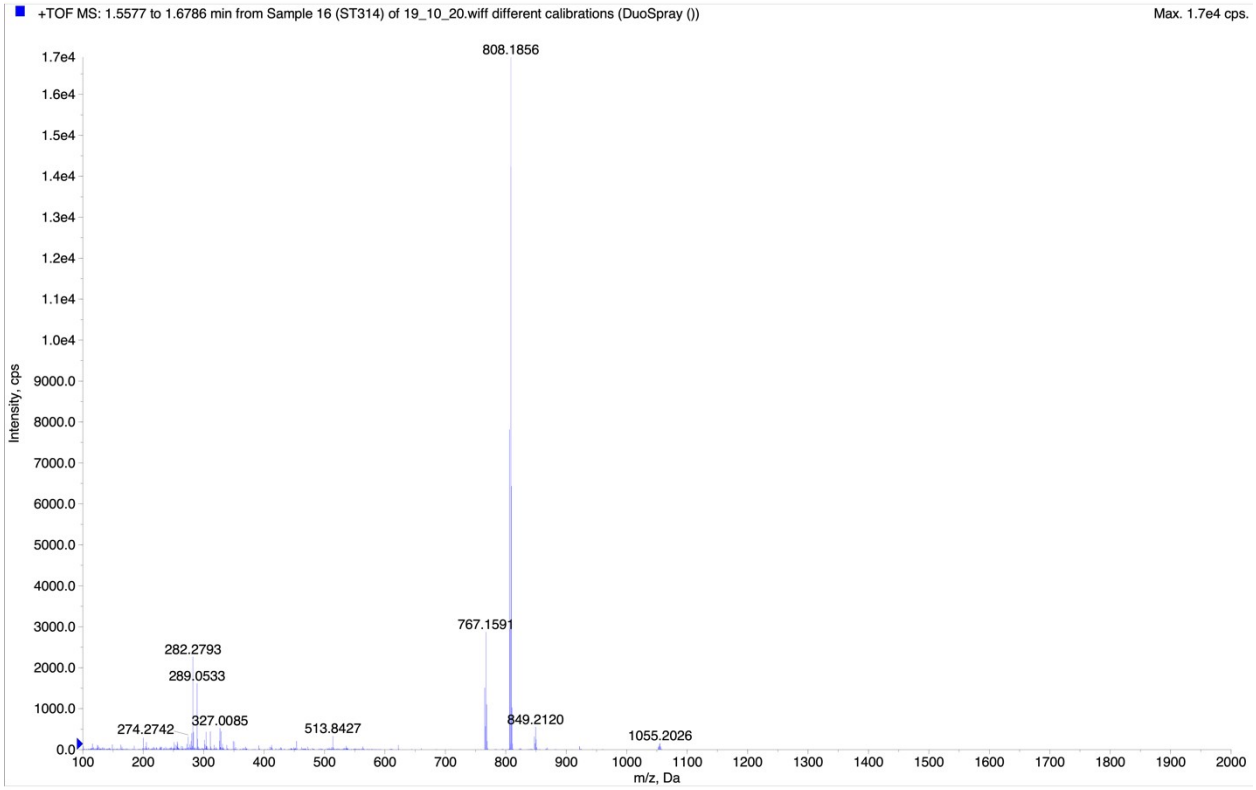

Figure S36. High resolution mass spectrum of **1**.

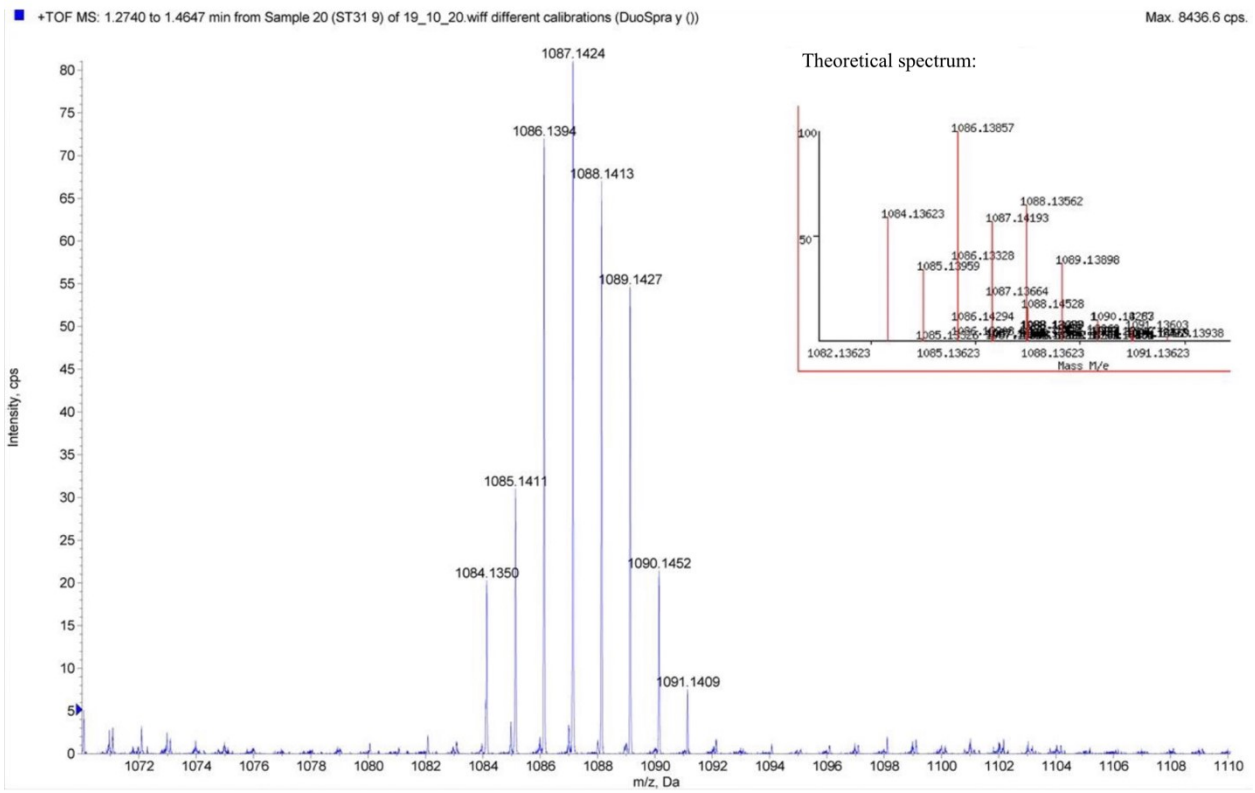

Figure S37. High resolution mass spectrum of **2**.

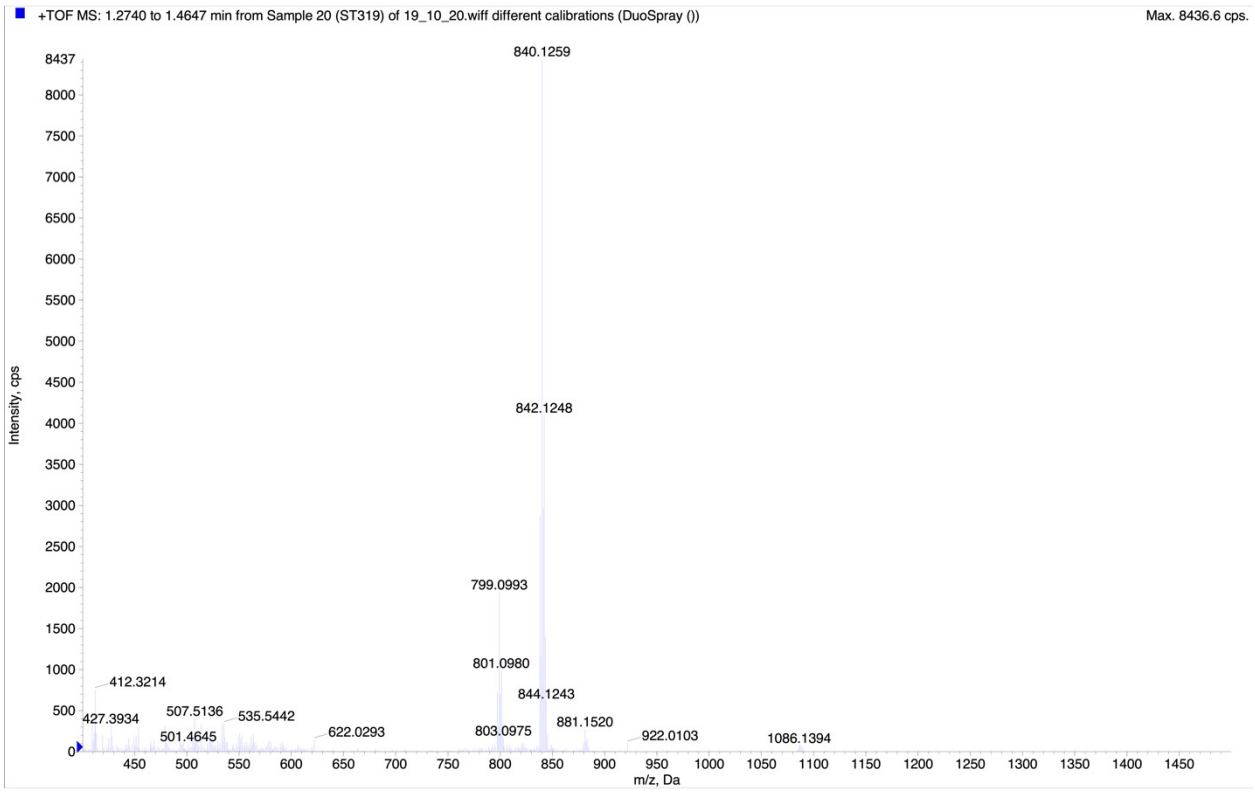

Figure S38. High resolution mass spectrum of **2**.

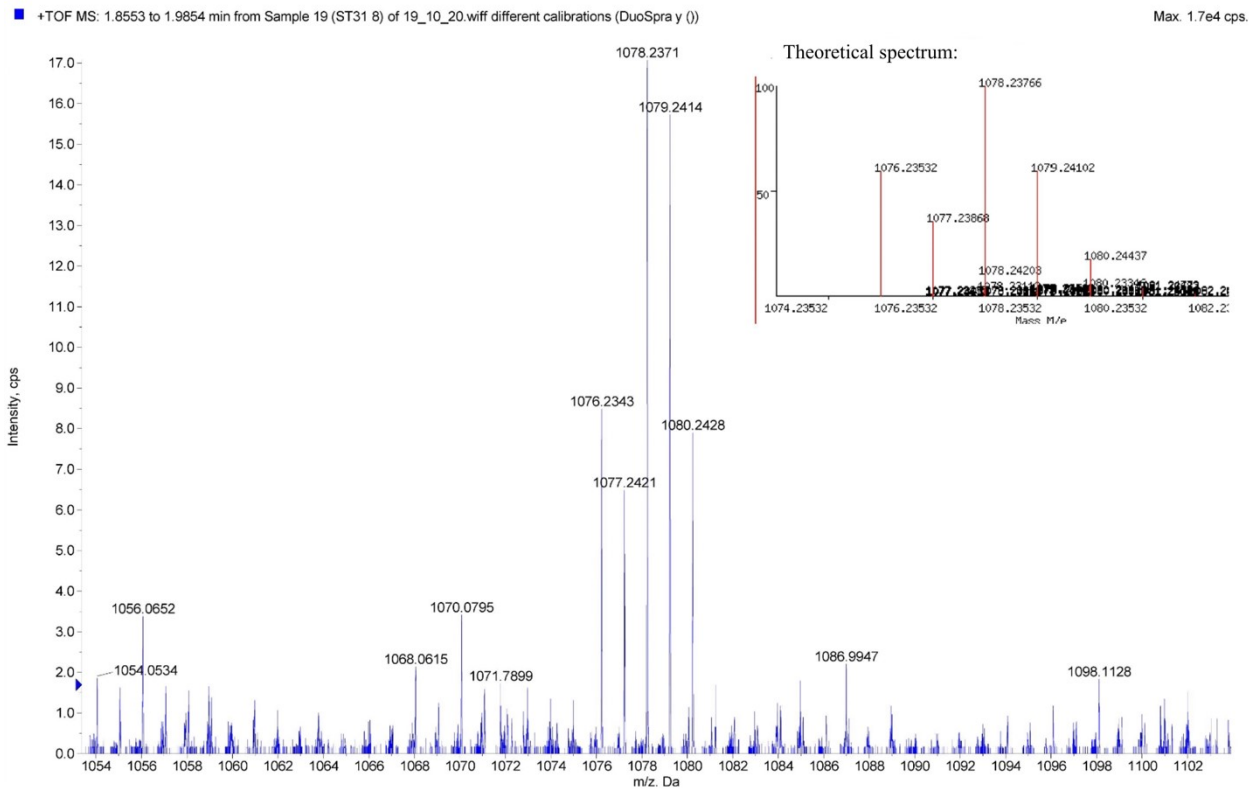

Figure S39. High resolution mass spectrum of **3**.

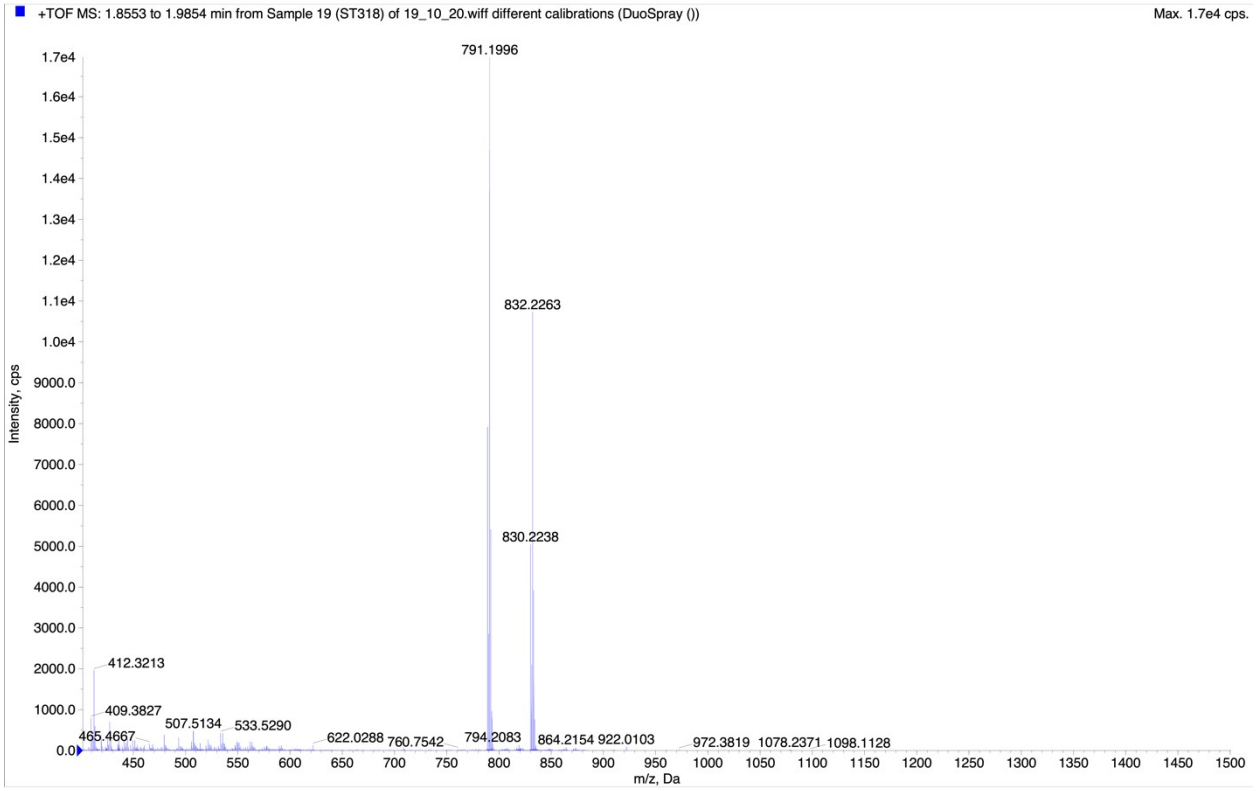

Figure S40. High resolution mass spectrum of **3**.

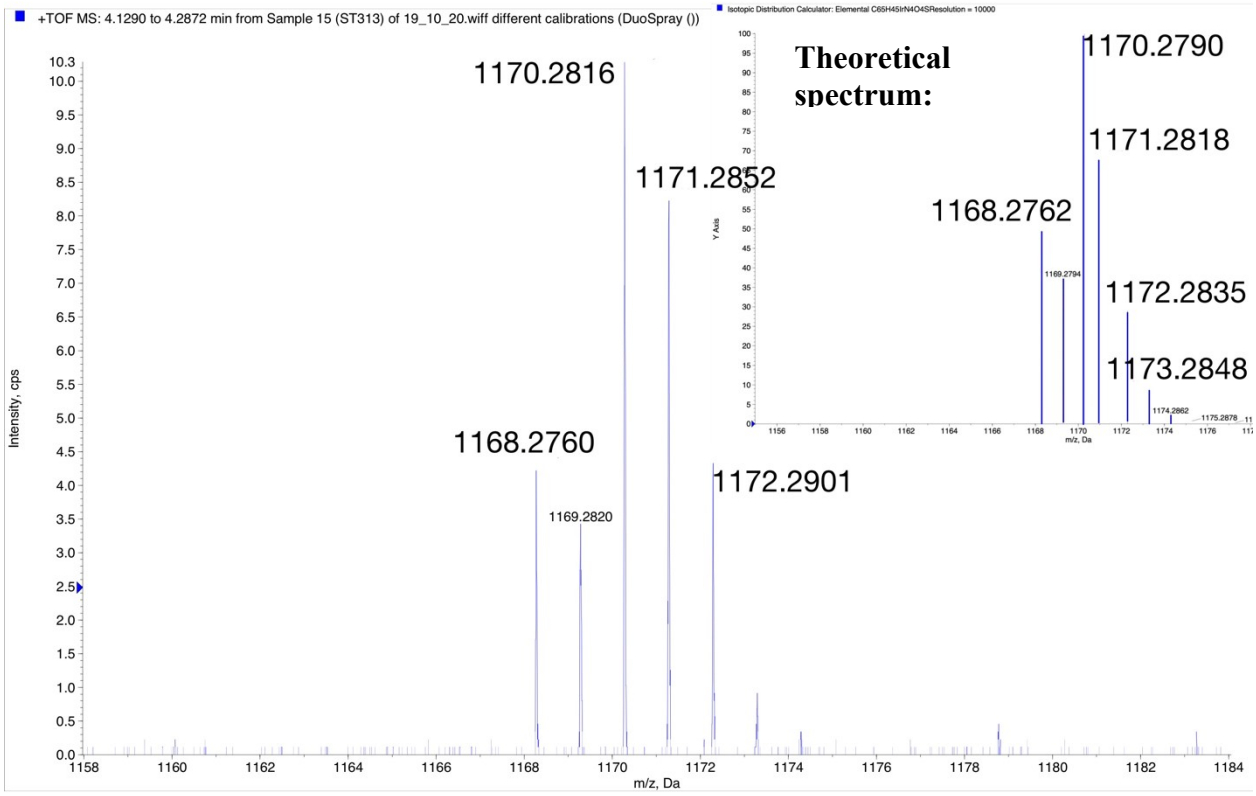

Figure S41. High resolution mass spectrum of **4**.

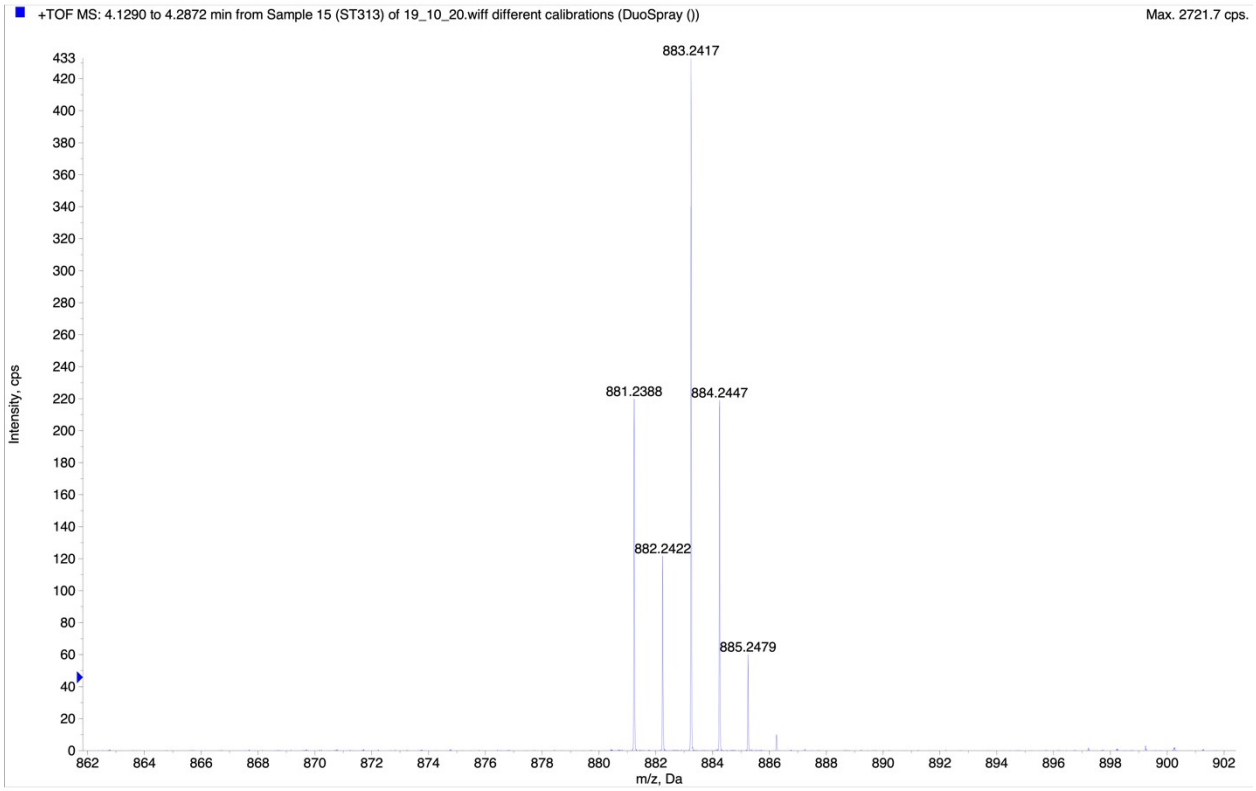

Figure S42. High resolution mass spectrum of **4**.

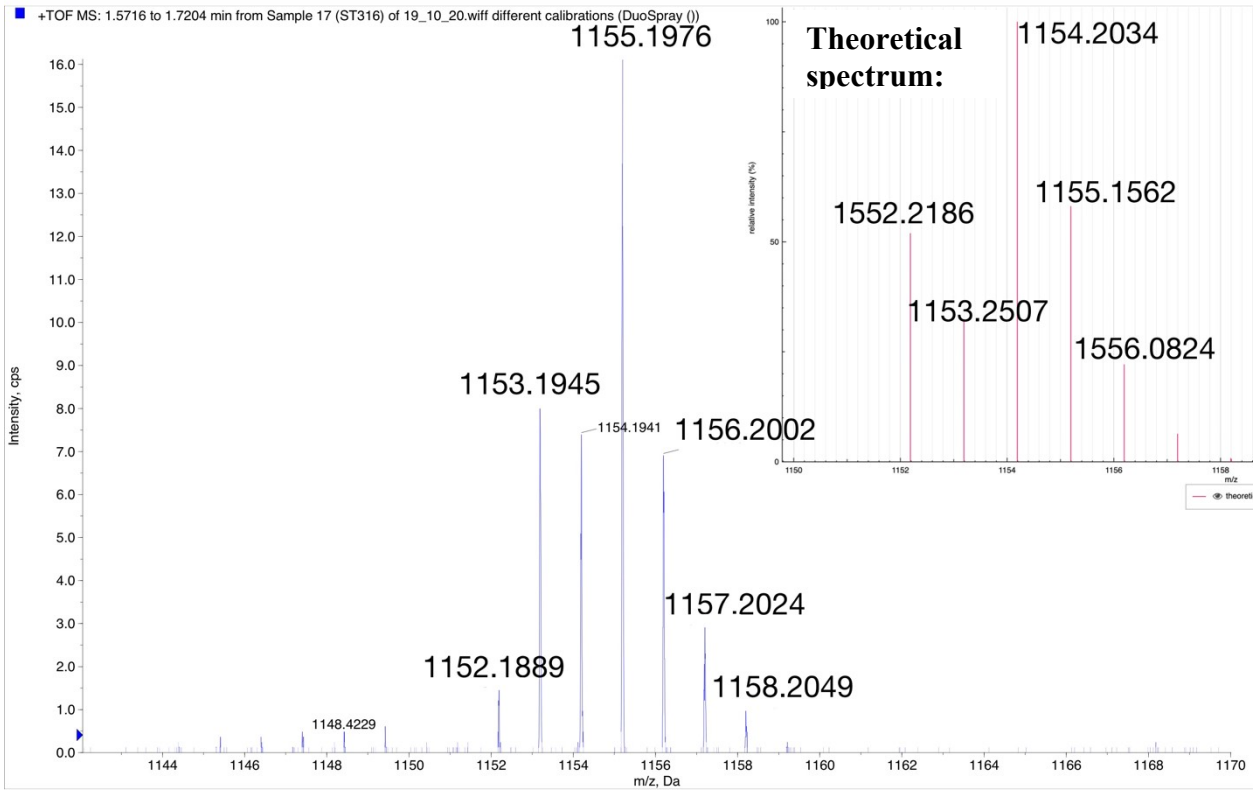

Figure S43. High resolution mass spectrum of **5**.

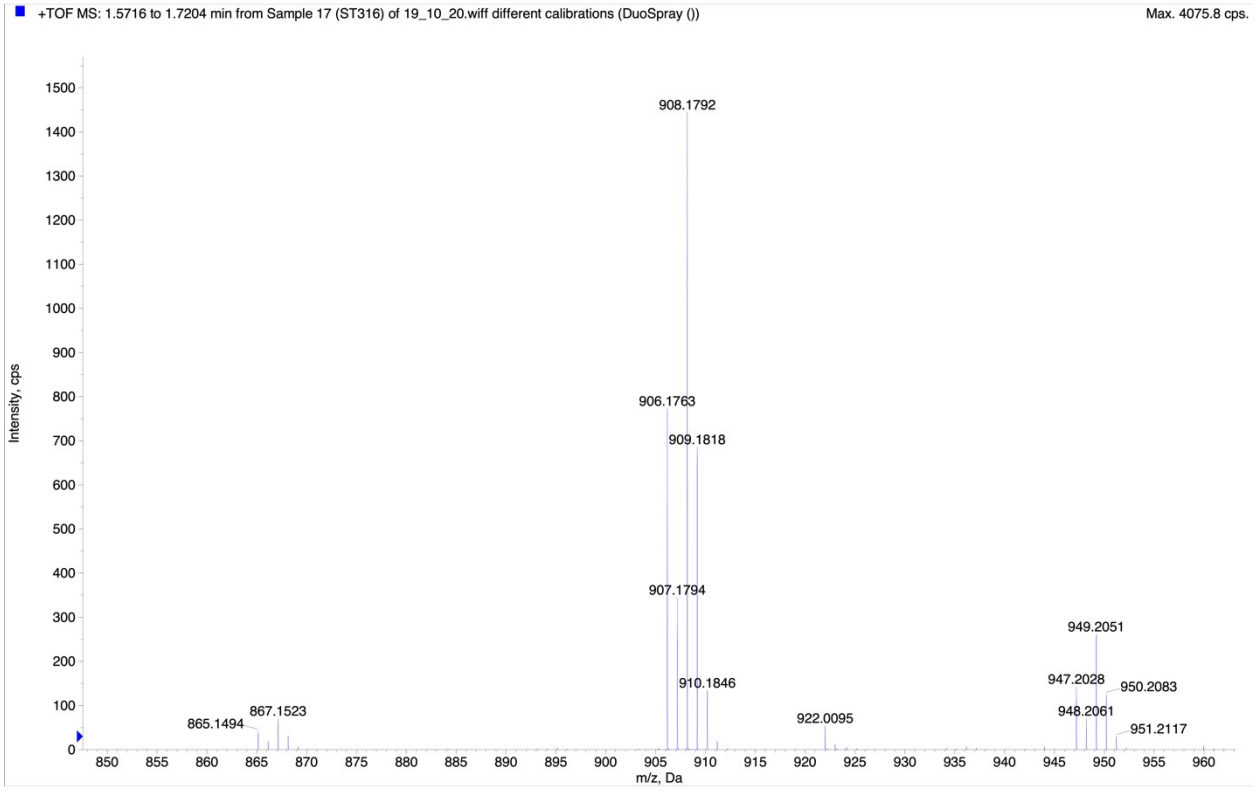

Figure S44. High resolution mass spectrum of **5**.

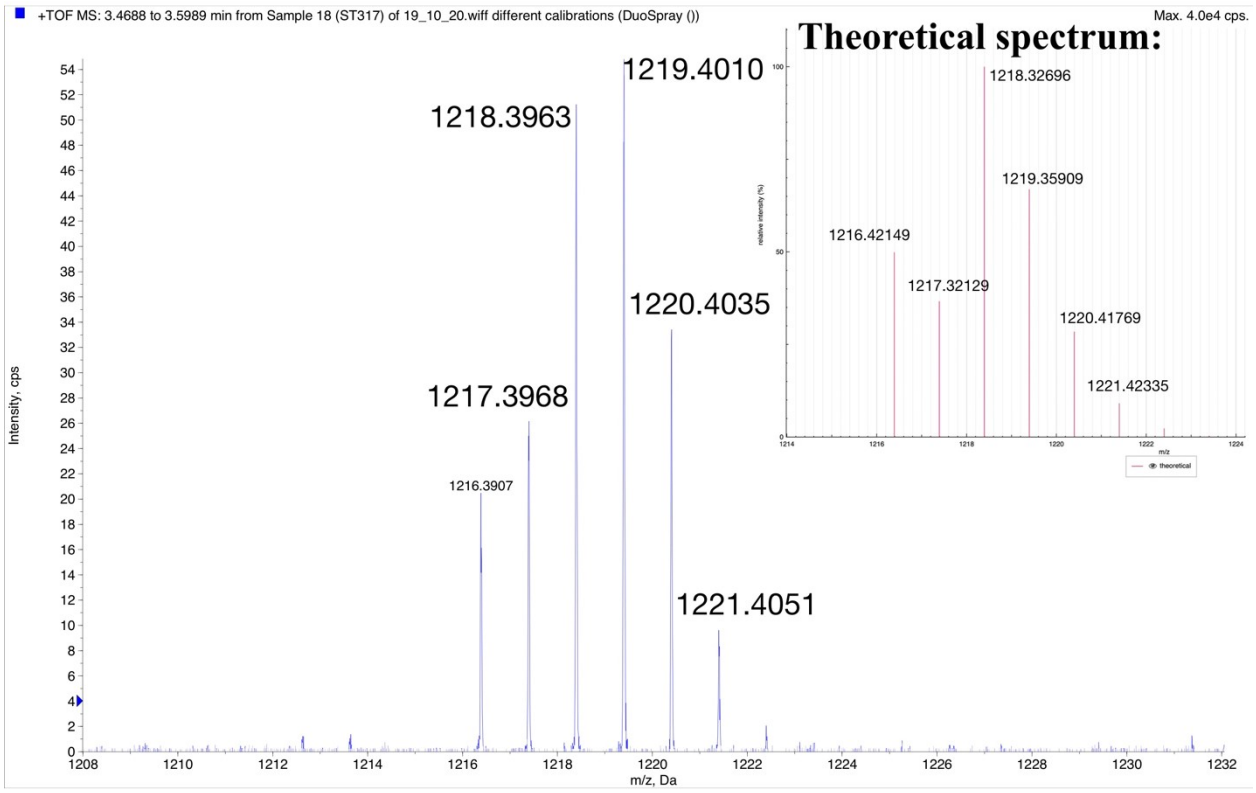

Figure S45. High resolution mass spectrum of **6**.

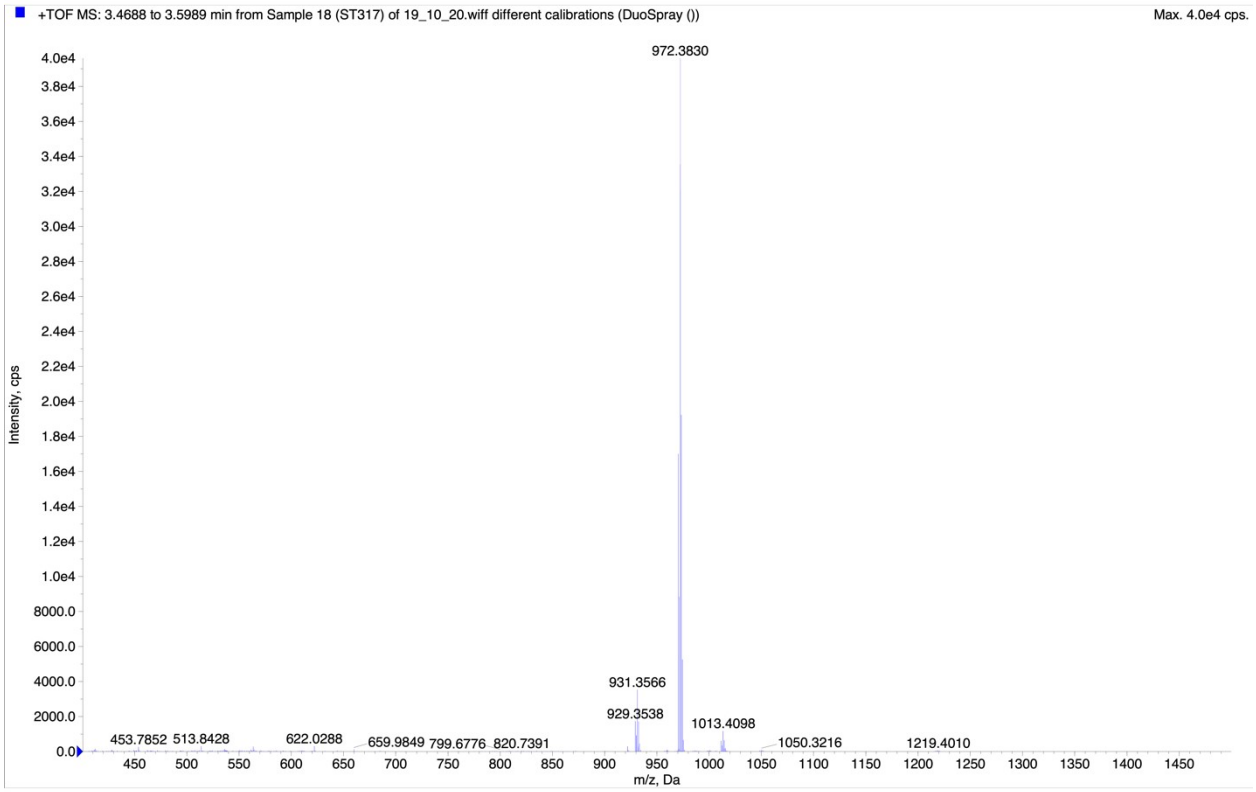

Figure S46. High resolution mass spectrum of **6**.

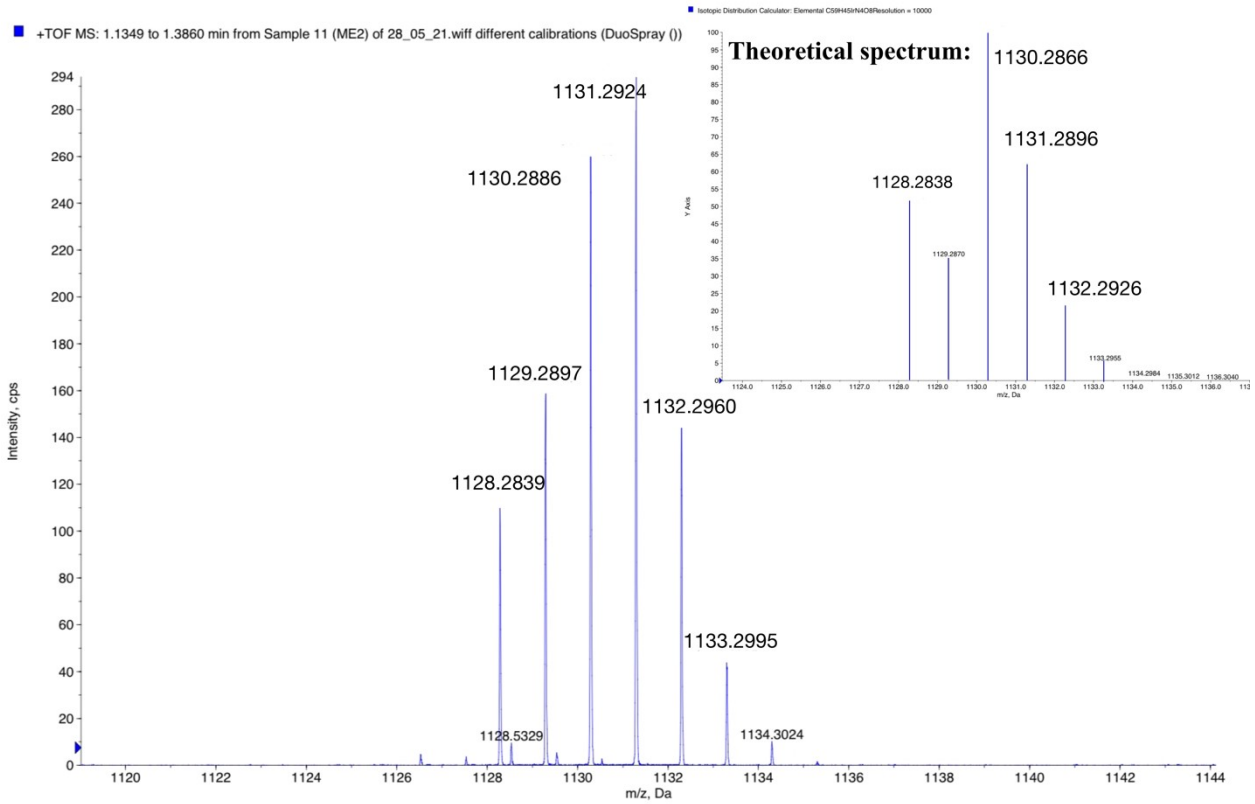

Figure S47. High resolution mass spectrum of **7**.

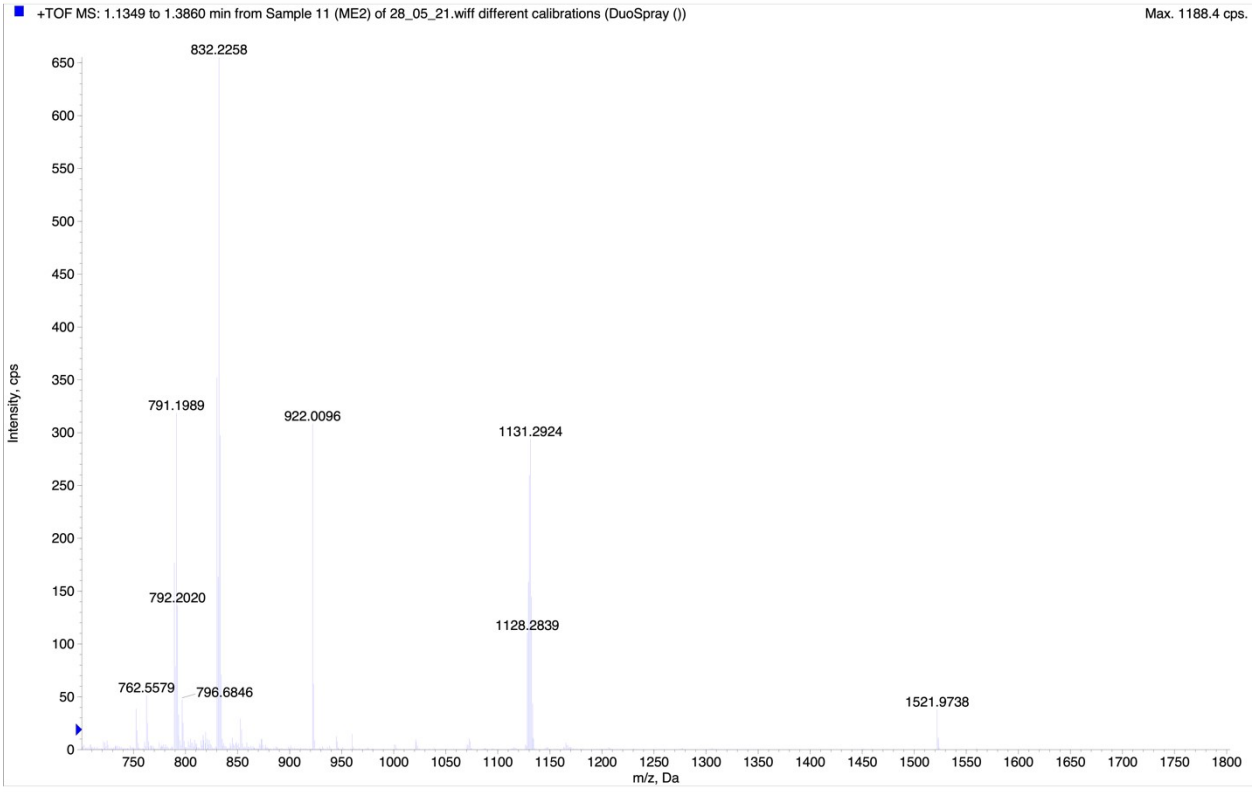

Figure S48. High resolution mass spectrum of **7**.

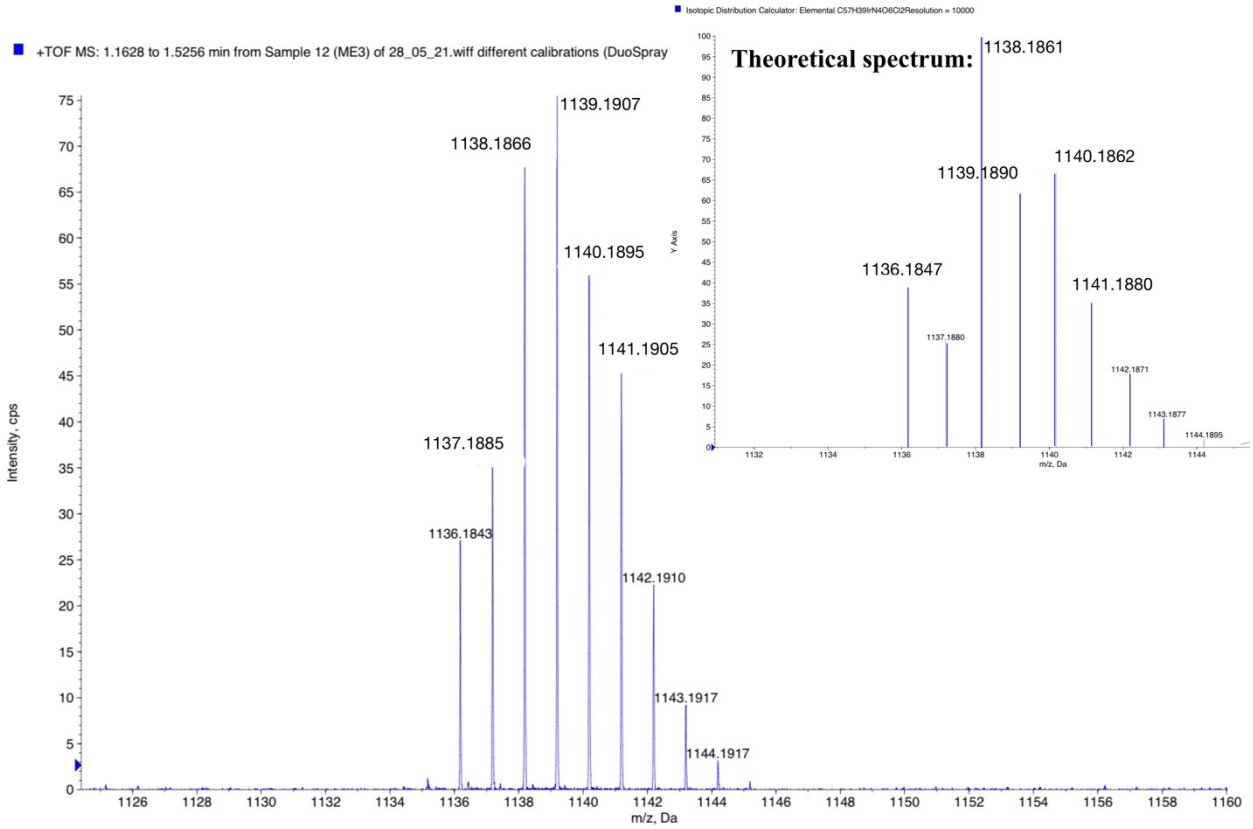

Figure S49. High resolution mass spectrum of **8**.

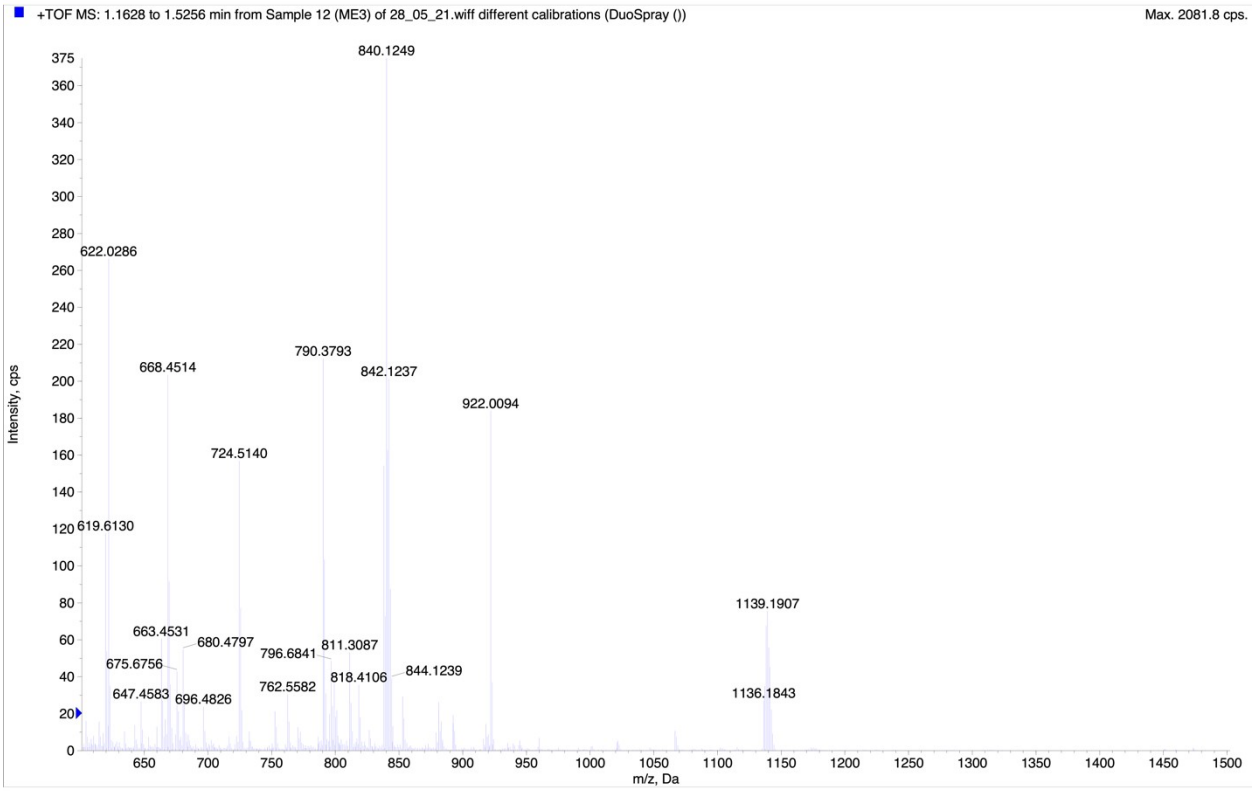

Figure S50. High resolution mass spectrum of **8**.

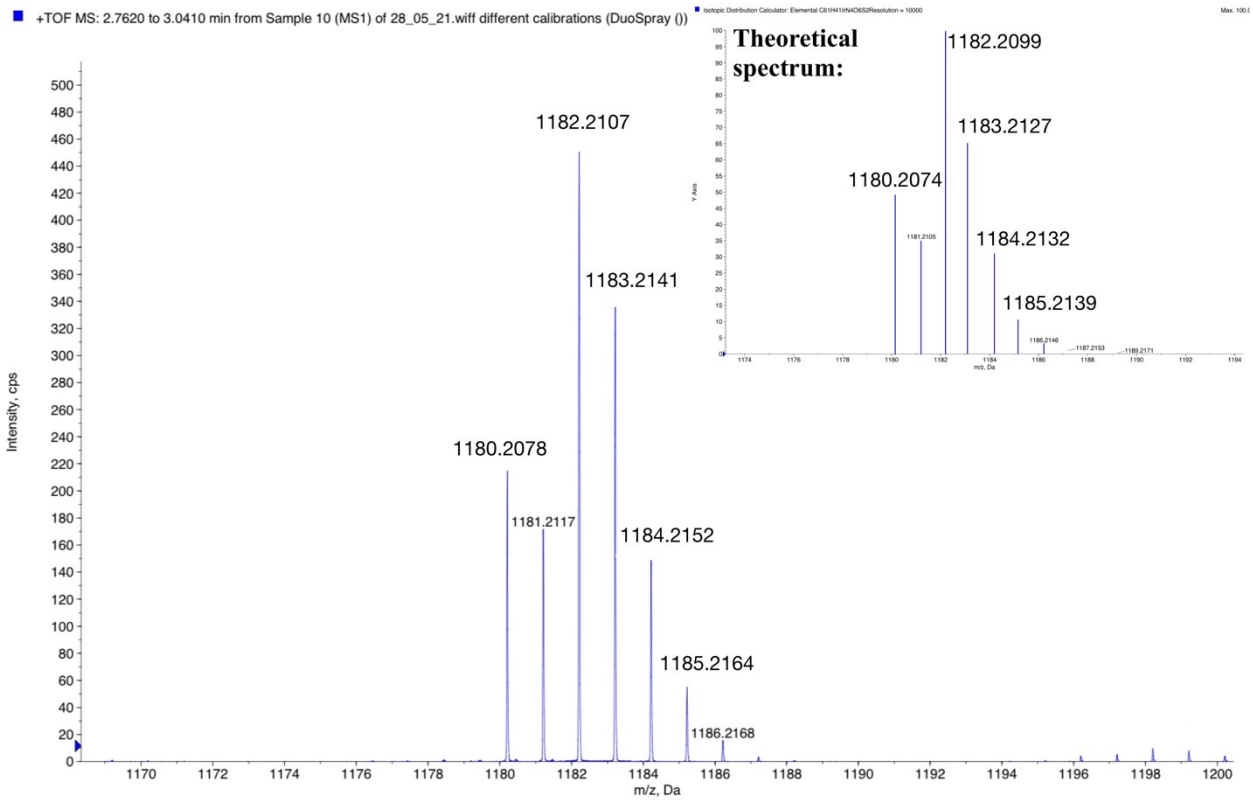

Figure S51. High resolution mass spectrum of **9**.

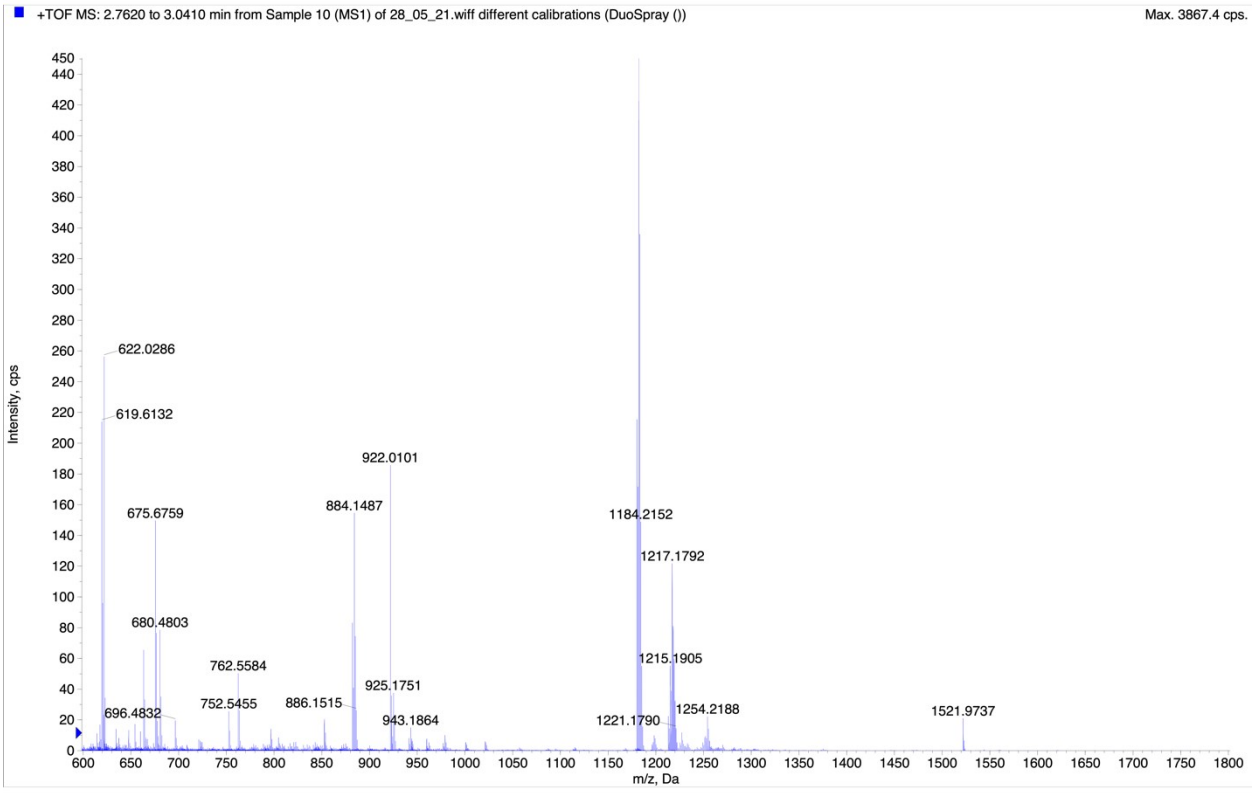

Figure S52. High resolution mass spectrum of **9**.

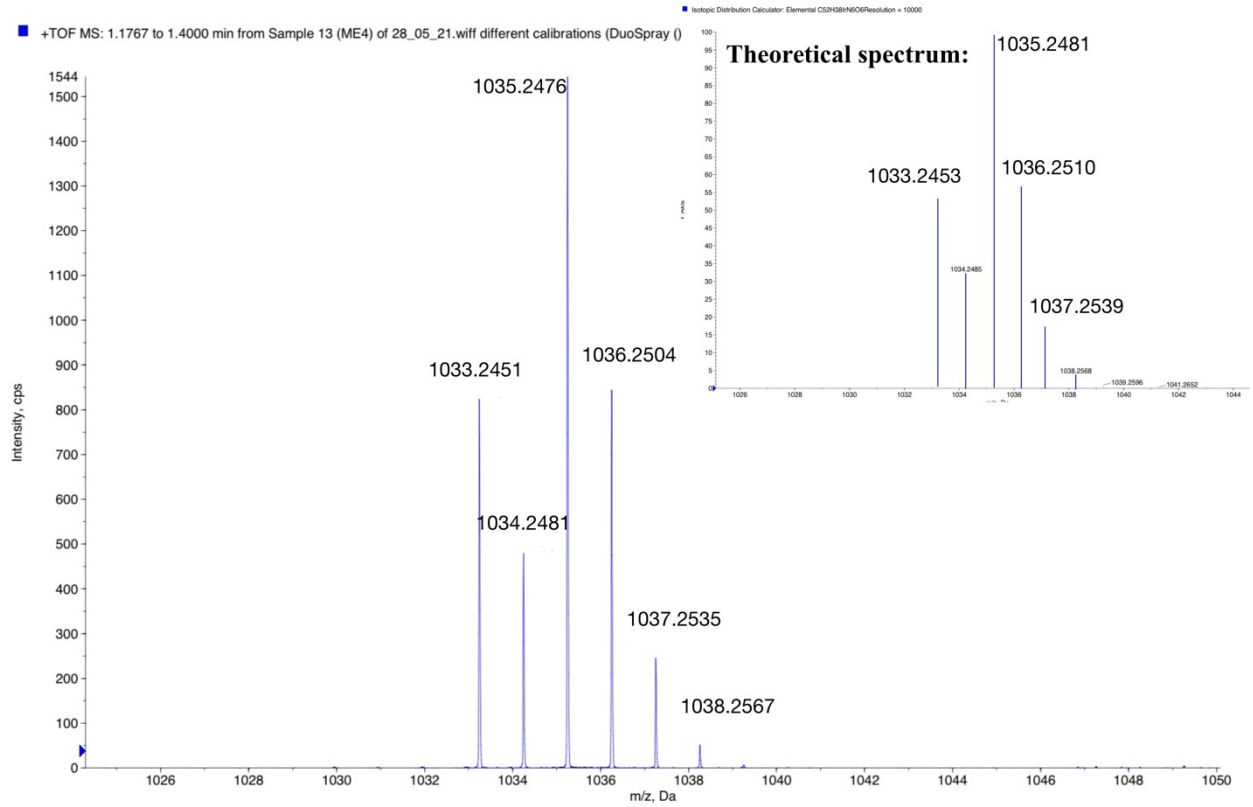

Figure S53. High resolution mass spectrum of **10**.

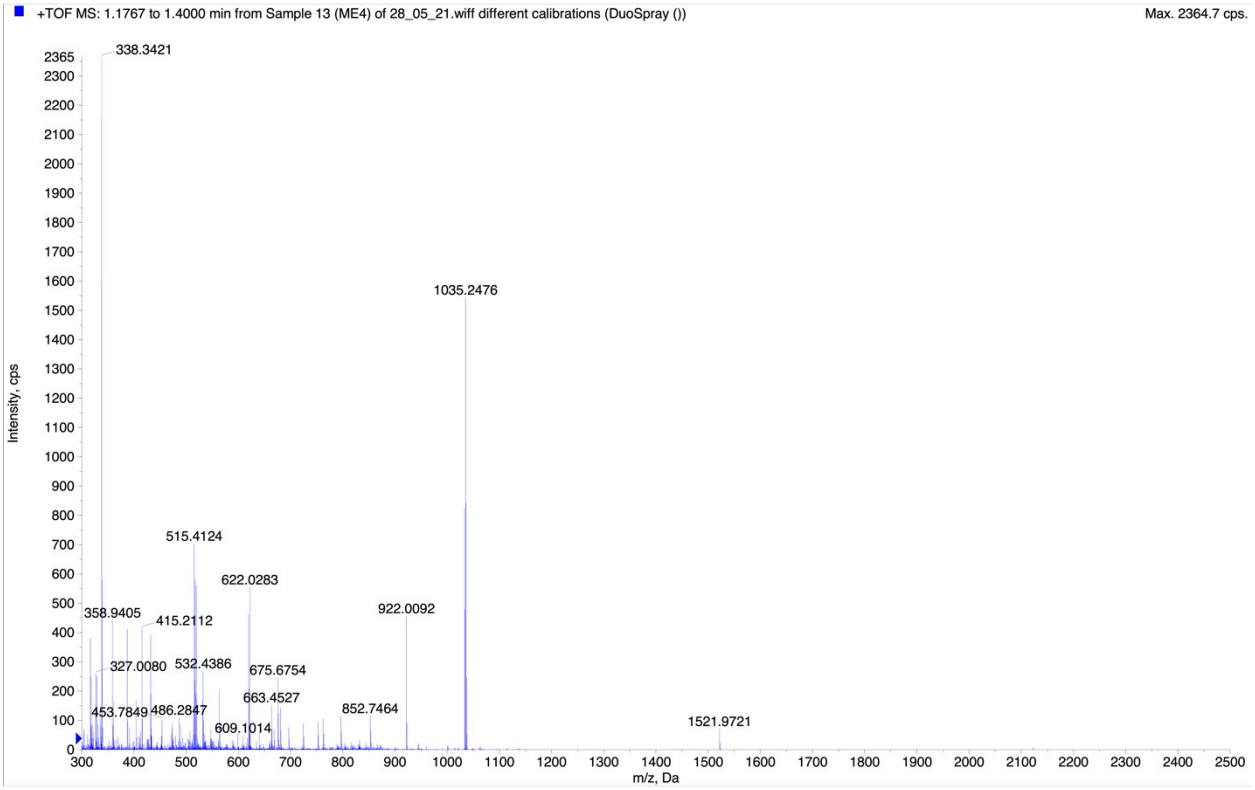

Figure S54. High resolution mass spectrum of **10**.

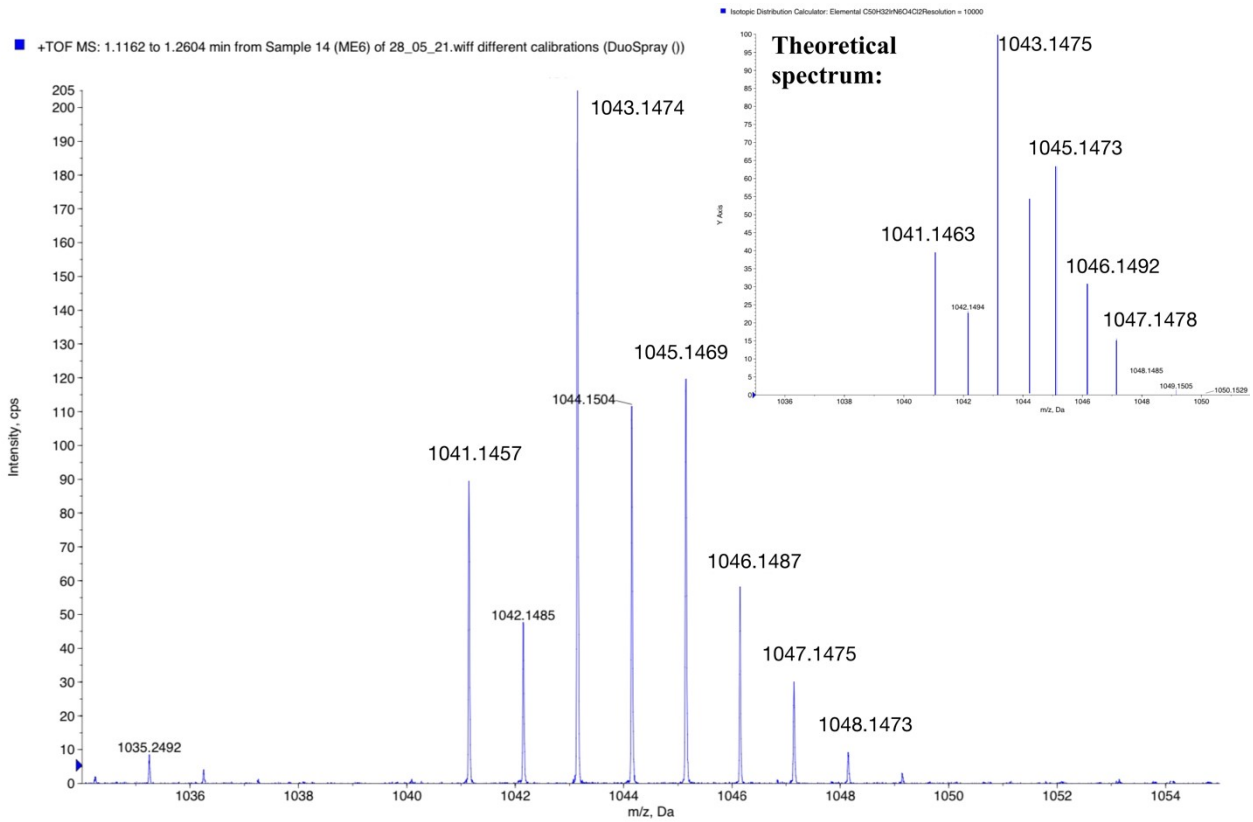

Figure S55. High resolution mass spectrum of **11**.

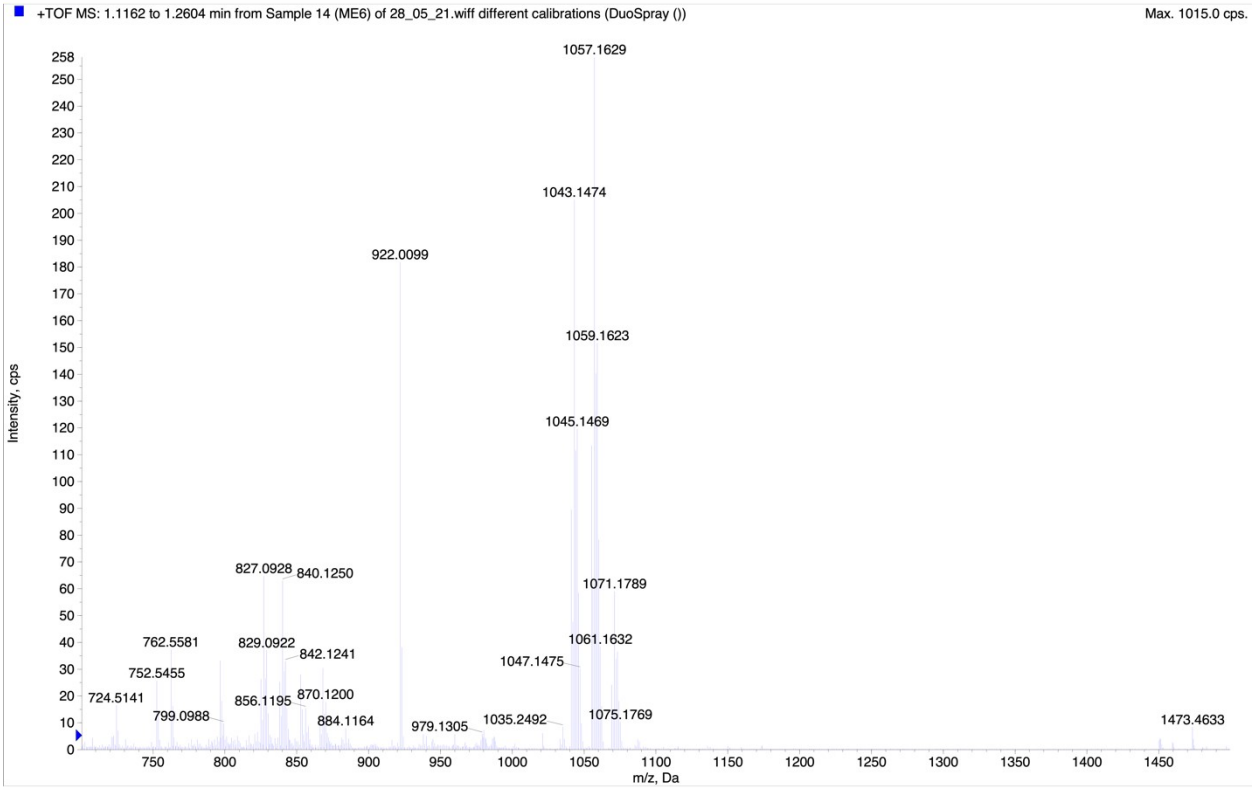

Figure S56. High resolution mass spectrum of **11**.

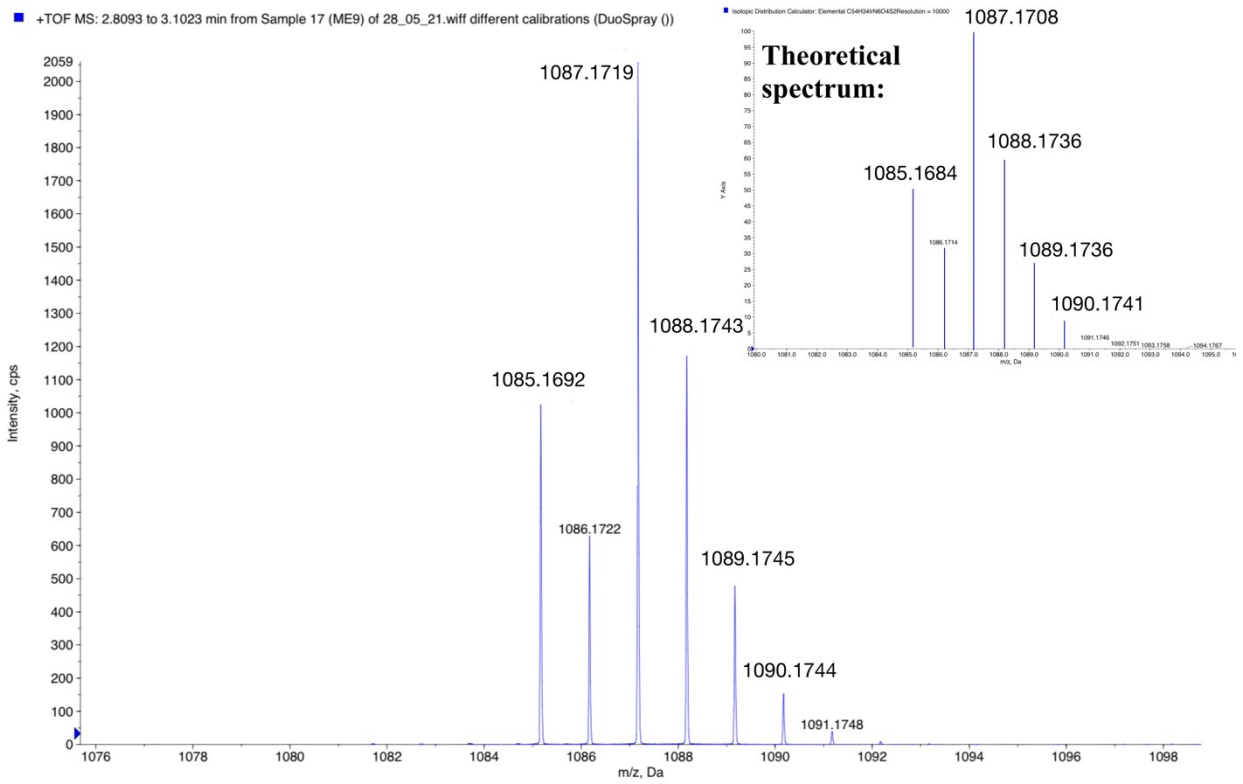

Figure S57. High resolution mass spectrum of **12**.

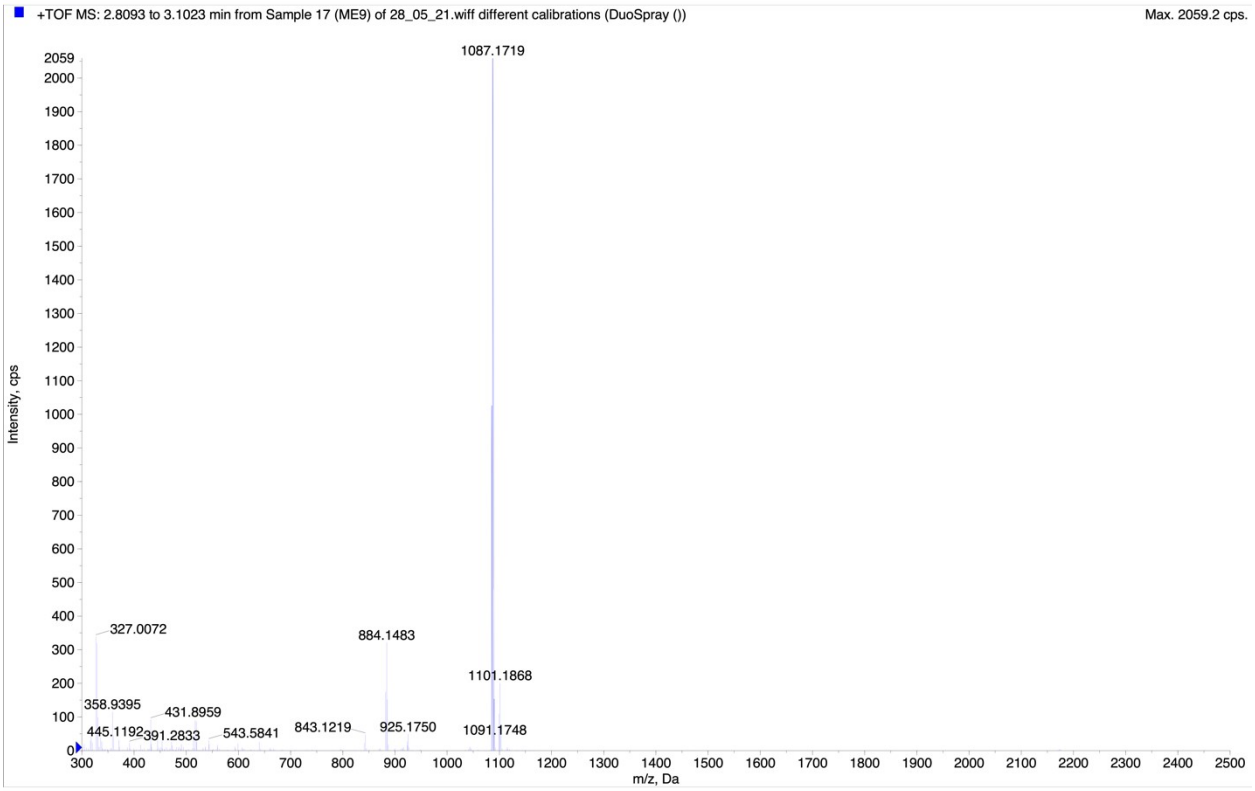

Figure S58. High resolution mass spectrum of **12**.

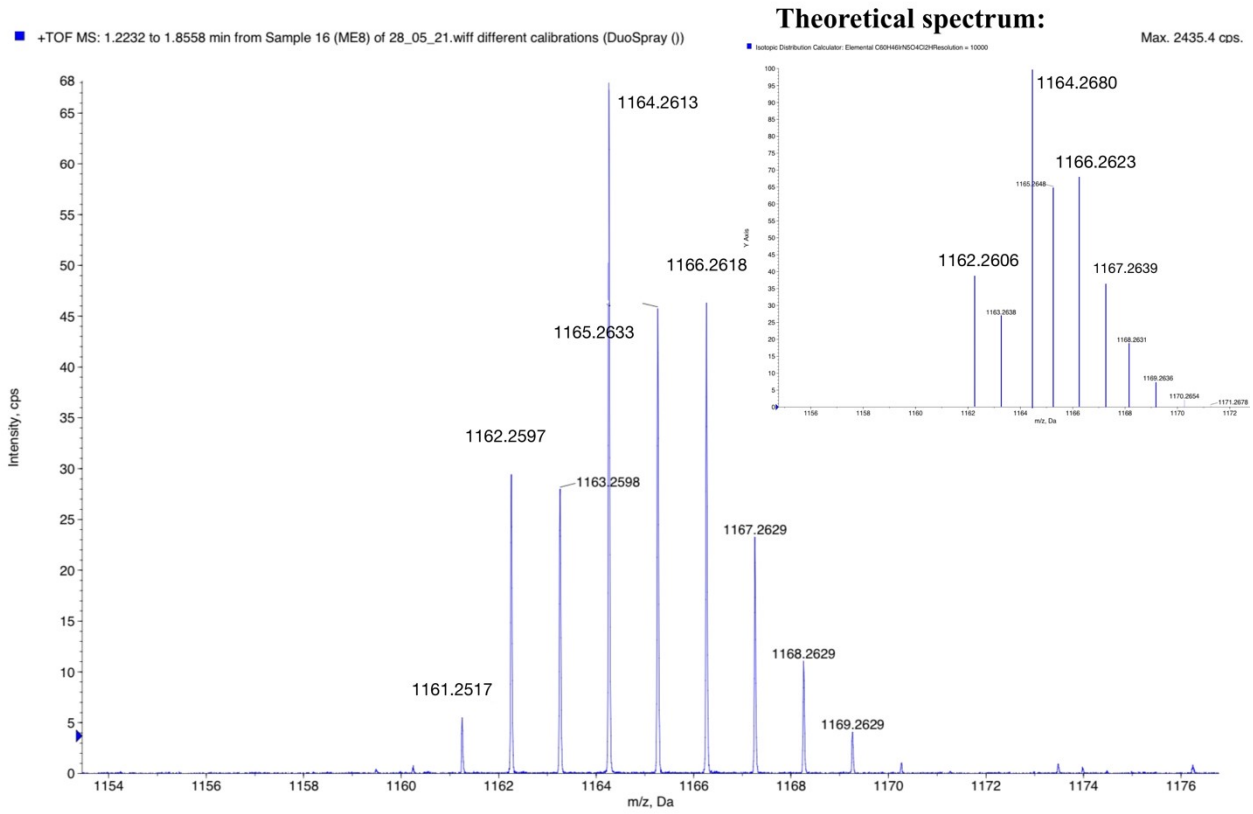

Figure S59. High resolution mass spectrum of **13**.

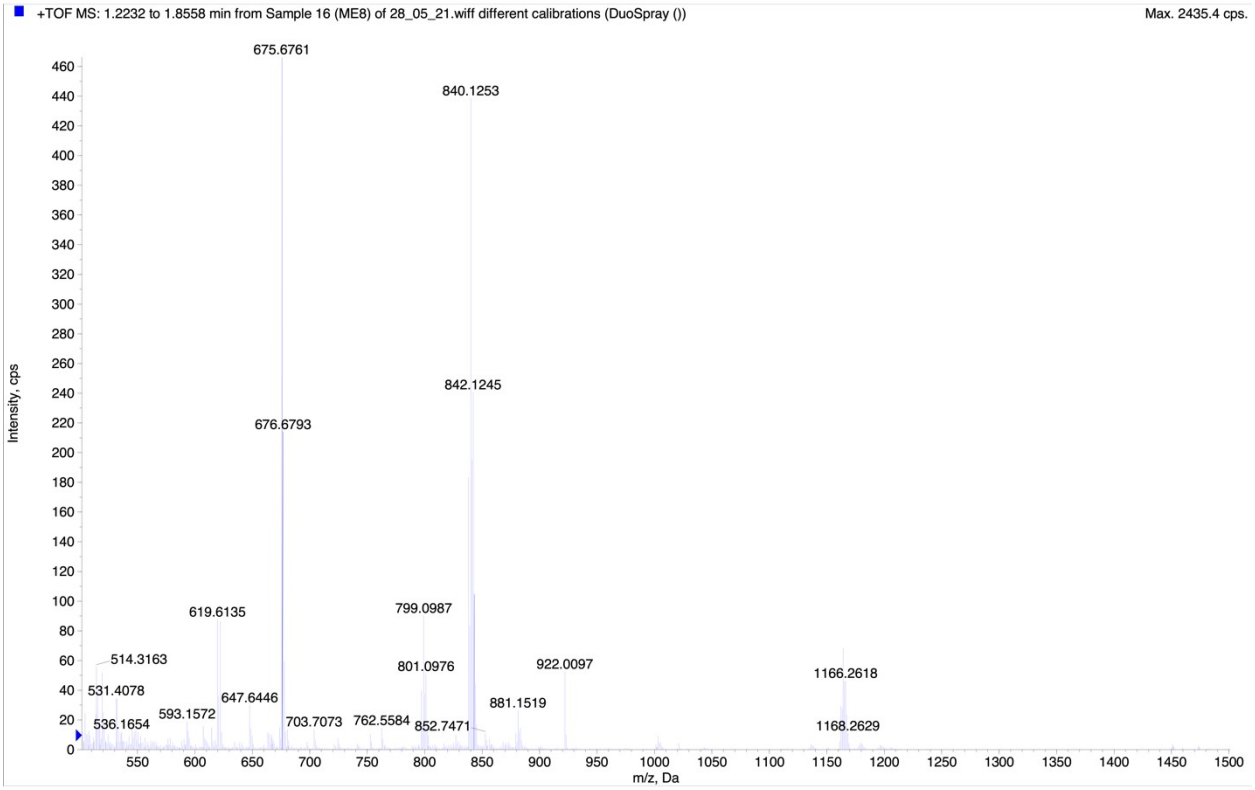

Figure S60. High resolution mass spectrum of **13**.

2. **X-ray data.**

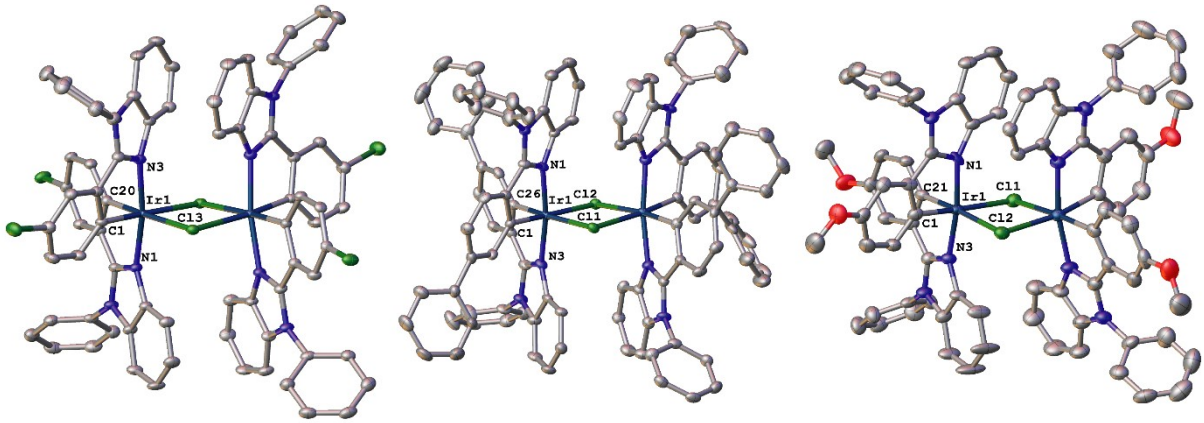

$[Ir(3cbi)_2Cl]_2$ $[Ir(dpbi)_2Cl]_2$ $[Ir(3mbi)_2Cl]_2$

Figure S61. Molecular structures of the chloride dimers. Displacement ellipsoids are shown at 50% probability level. Minor components of disordered groups and hydrogen atoms are not shown.

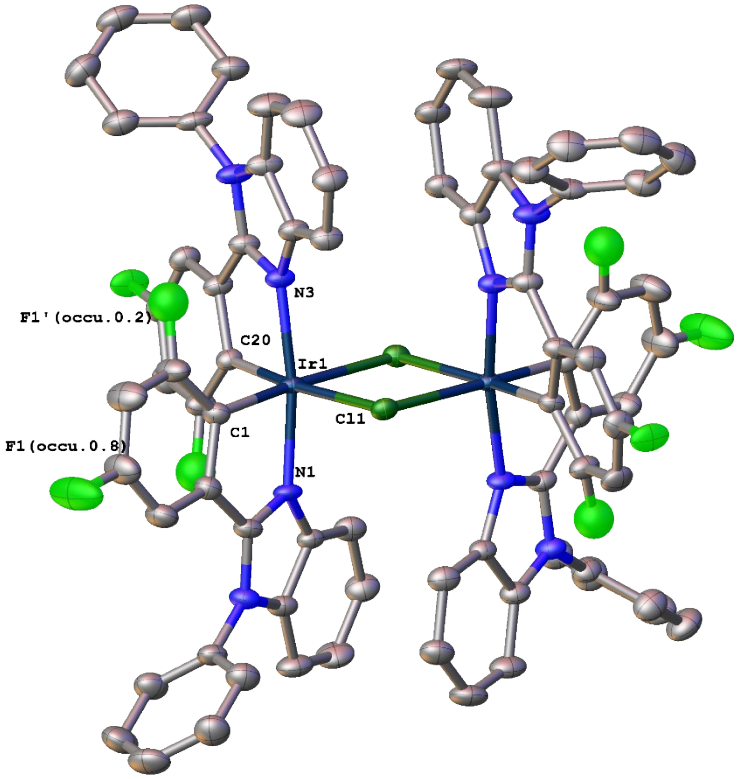

Figure S62. Molecular structure of the $[Ir(3fbi)_2Cl]_2$. Displacement ellipsoids are shown at 50% probability level. The hydrogen atoms are not shown. Both fluorine components are shown with their relative occupancies.

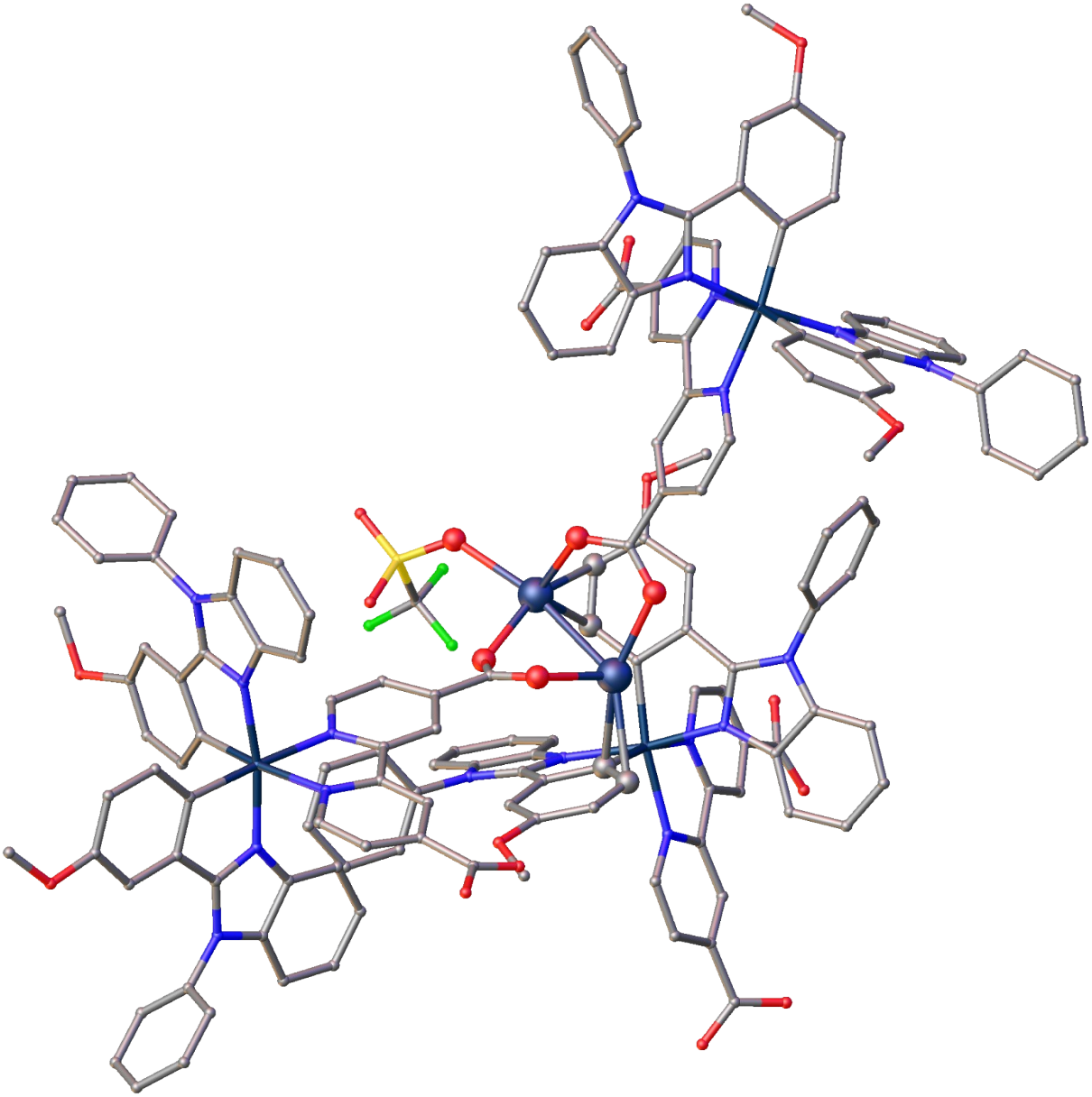

Figure S63. Coordination environment of the silver ions in the Ir_2Ag_2 structure.

Table S2. Details of the X-ray crystal data collection and structure refinement for dimeric compounds

	$[Ir(3cbi)_2Cl]_2$	$[Ir(dpbi)_2Cl]_2$	$[Ir(3mbi)_2Cl]_2$	$[Ir(3fbi)_2Cl]_2$
Empirical formula	$C_{80}H_{56}Cl_{14}Ir_2N_8$ + $4CH_2Cl_2$	$C_{100}H_{68}Cl_2Ir_2N_8$ +solvent	$C_{81}H_{64}Cl_2Ir_2N_8O_5$ +1 CH_3OH	$C_{80}H_{52}Cl_{14}F_4Ir_2N_8$ + 4 $CHCl_3$
M_w	2010.03	1989.79	1684.70	2081.99
Temperature (K)	100	100	296.15	150
Size (mm)	0.30 x 0.27 x 0.04	0.4 × 0.38 × 0.08	0.20 × 0.12 × 0.07	0.15 × 0.15 × 0.10
Cryst. system	monoclinic	triclinic	monoclinic	monoclinic
Space group	C2/c	P-1	$P2_1/n$	C2/c
a (Å)	21.0487(9)	13.0955(3)	20.4452(6)	20.4091(8)
b (Å)	15.2627(6)	19.1698(6)	15.2416(4)	15.0372(5)
c (Å)	23.7169(10)	19.3990(5)	23.5774(7)	25.0183(11)
α(°)	90.00	103.9670(10)	90.00	90.00
β (°)	98.824(2)	93.2770(10)	108.1450(10)	99.107
γ(°)	90.00	101.9530(10)	90.00	90.00
V ($Å^3$)	7529.1(5)	4593.9(2)	6981.8(3)	7581.2(5)
Z	4	2	4	4
ρ_{cald} ($g \cdot cm^{-3}$)	1.773	1.438	1.603	1.824
Abs coeff (mm^{-1})	4.080	3.107	3.944	4.063
F(000)	3936.0	1975.0	3336.0	4064.0
θ range (deg)	4.58< θ < 61.1	3.662< θ <52	3.232< *θ* < 50.1	3.898< *θ* < 57.398
no. of collected/unique rflns	70680/11449	30399/17642	52970/ 12349	40903/ 9781
Completeness to *θ* (%)	99.2	97.7	99.9	100
no. of data/restraints/params	11449/0/469	17642/14/1031	12349/1/903	9781/6/501
Goodness of fit on F^2	1.028	1.022	1.026	1.041
Final *R* indices ($I > 2\sigma(I)$)	R_1 = 0.0308, wR_2 = 0.0645	R_1 = 0.0416, wR_2 = 0.0951	R_1 = 0.0372, wR_2 = 0.0917	R_1 = 0.0406, wR_2 = 0.1014
R indices (all data)	R_1 = 0.0424, wR_2 = 0.0681	R_1 = 0.0607, wR_2 = 0.1013	R_1 = 0.0536, wR_2 = 0.1000	R_1 = 0.0536, wR_2 = 0.1092
Largest diff peak/hole ($e/Å^3$)	1.89/-1.41	1.87/-1.59	1.80/-1.48	1.62/-1.73

Table S3. Details of the X-ray crystal data collection and structure refinement for complexes 1, 2, 5, 7-10, 12, 13

	1	2	5	7	8	9	10	12	13
Empirical formula	$C_{53}H_{35}F_2IrN_4O_4S$ + solvent	$C_{53}H_{35}Cl_2IrN_4O_4S$	$C_{55}H_{35}F_6IrN_4O_4S$ + CH_2Cl_2/ CH_3OH	$C_{59}H_{45}N_4O_8Ir$ + solvent	$C_{57}H_{39}Cl_2IrN_4O_6$ + solvent	$C_{61}H_{41}IrN_4O_6S_2$ + solvent	$[C_{52}H_{37}IrN_6O_6]OTf$	$[C_{54}H_{36}IrN_6O_4S_2]OTf$	$C_{60}H_{46}Cl_2IrN_5O_4$
M_w	1054.11	1087.01	1212.61	1130.19	1139.02	1182.30	1109.11	866.52	1164.12
Temperature (K)	100.00	100.00	100.00	200.00	150.00	100.15	150.00	150.00	100.00
Size (mm)	0.14 × 0.12 × 0.005	0.1 × 0.1 × 0.004	0.22 × 0.20 × 0.11	0.42 × 0.28 × 0.20	0.35 × 0.30 × 0.30	0.2 × 0.03 × 0.003	0.25 × 0.22 × 0.05	0.30 × 0.30 × 0.07	0.45 × 0.40 × 0.25
Cryst. system	monoclinic	monoclinic	triclinic	orthorhombic	orthorhombic	triclinic	triclinic	triclinic	triclinic
Space group	$P2_1/n$	$P2_1/n$	P-1	Pnc2	Pbcn	P-1	P-1	P-1	P-1
a (Å)	11.3870(9)	13.2139(5)	11.6380(3)	29.2455(14)	13.7388(5)	12.7102(7)	15.1677(14)	20.2850(8)	12.8762(11)
b (Å)	22.3107(18)	24.0162(16)	12.0786(4)	13.7868(7)	12.7766(5)	14.9577(8)	17.1131(17)	21.1480(8)	12.9389(11)
c (Å)	18.4099(14)	13.8114(8)	18.5157(5)	12.7980(6)	28.3069(9)	15.6155(8)	20.8414(18)	28.2673(11)	15.9754(15)
α(°)	90.00	90.00	91.2080(10)	90.00	90.00	115.4936(19)	69.915(3)	80.1990(10)	80.087(3)
β (°)	102.871(3)	90.525(2)	96.2940(10)	90.00	90.00	104.484(2)	80.152(3)	71.5230(10)	89.178(3)
γ(°)	90.00	90.00	100.4940(10)	90.00	90.00	100.722(2)	72.408(4)	81.6440(10)	69.118(3)
V (Å^3)	4559.6(6)	4382.8(4)	2541.56(13)	5160.2(4)	4968.9(3)	2443.6(2)	4829.4(8)	11279.1(8)	2446.4(4)
Z	4	4	2	4	4	2	4	8	2
ρ_{cald} (g·cm^{-3})	1.536	1.647	1.585	1.455	1.523	1.607	1.525	1.531	1.580
Abs coeff (mm^{-1})	3.033	3.270	2.794	2.647	2.850	2.878	2.852	2.525	2.894
F(000)	2096.0	2160.0	1204.0	2272.0	2272.0	1184.0	2212.0	5210.0	1168.0

θ range (deg)	2.912 < θ <52.81	3.402< θ <51.406	3.99< θ <52.774	3.266< θ <50.096	4.132< θ <52.79	4.66< θ <53.996	3.312 < θ <50.098	2.676< θ <55.998	3.856< θ <52.762
no. of collected/unique rflns	47812/9340	8346/8297	53682/10384	82138/9157	49989/5089	21603/10623	40635/16932	163620/54411	39476/9973
Completeness to θ (%)	99.9	99.4	99.8	100	99.9	99.9	99.9	99.9	99.6
no. of data/restraints/params	9340/2/590	8297/257/592	10384/61/584	9157/200/643	5089/0/318	10623/193/755	16932/39/1280	54411/62/2900	9973/1/614
Goodness of fit on F^2	1.080	1.141	1.154	1.086	1.063	1.014	1.035	1.020	1.050
Final R indices ($I > 2\sigma(I)$)	R_1 = 0.0469, wR_2 = 0.1074	R_1 = 0.0649, wR_2 = 0.1562	R_1 = 0.0450, wR_2 = 0.1164	R_1 = 0.0308, wR_2 = 0.0747	R_1 = 0.0239, wR_2 = 0.0522	R_1 = 0.0441, wR_2 = 0.0761	R_1 = 0.0556, wR_2 = 0.1134	R_1 = 0.0373, wR_2 = 0.0723	R_1 = 0.0392, wR_2 = 0.0824
R indices (all data)	R_1 = 0.0659, wR_2 = 0.1161	R_1 = 0.0797, wR_2 = 0.1636	R_1 = 0.0477, wR_2 = 0.1179	R_1 = 0.0521, wR_2 = 0.0881	R_1 = 0.0341, wR_2 = 0.0561	R_1 = 0.0659, wR_2 = 0.0837	R_1 = 0.0962, wR_2 = 0.1281	R_1 = 0.0558, wR_2 = 0.0780	R_1 = 0.0529, wR_2 = 0.0883
Largest diff peak/hole (e/Å^3)	2.23/-1.69	3.05/-2.27	2.16/-1.42	1.69/-0.82	0.89/-1.16	0.96/-1.26	1.93/-1.48	1.97/-0.74	0.80/-0.95

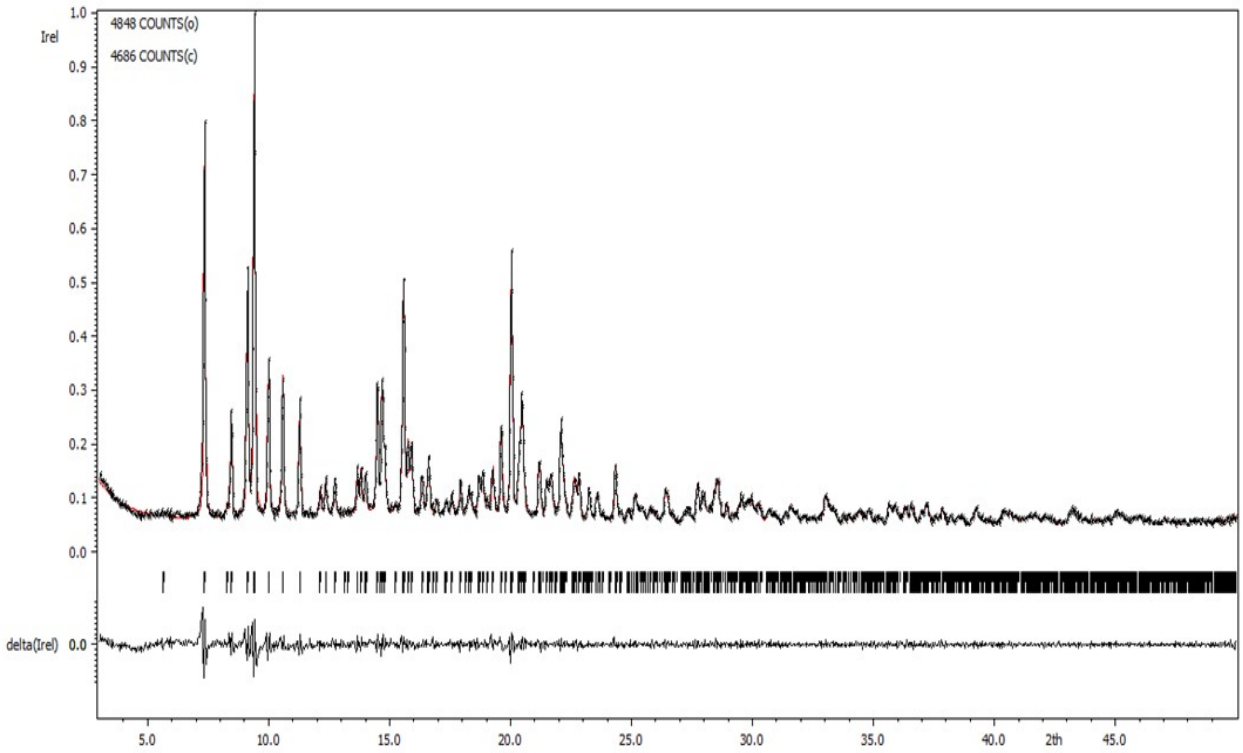

Figure S64. Powder XRD pattern of complex **13** (black line) with the simulated pattern (red line). The differential is presented in the bottom.

3. Redox and optical properties.

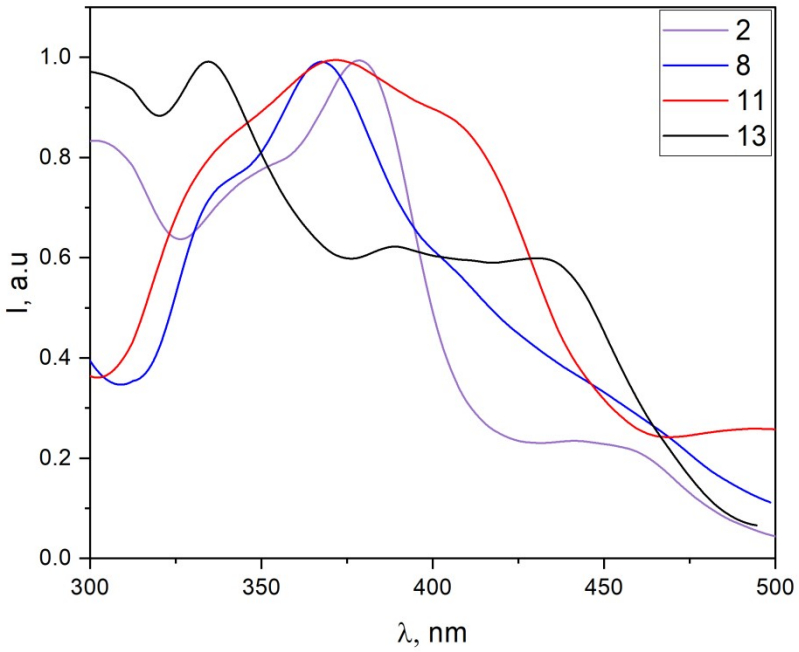

Figure S65. Normalised excitation spectra of complexes **2**, **8**, **11**, **13** with 3cbi as cyclometalated ligand measured under Ar atmosphere in CH_2Cl_2 at 25°C

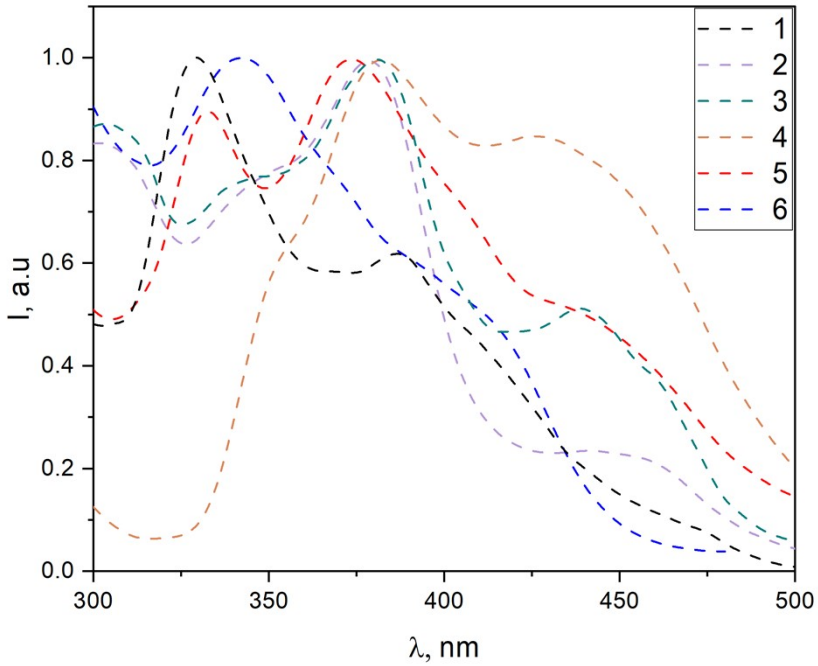

Figure S66. Normalised excitation spectra of complexes **1-6** with L_1 as ancillary ligand measured under Ar atmosphere in CH_2Cl_2 at 25°C

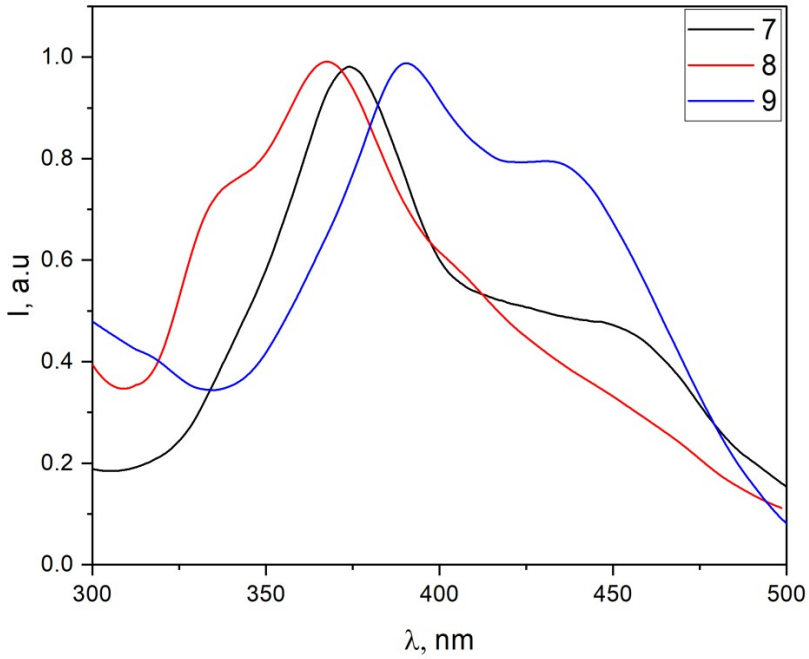

Figure S67. Normalised excitation spectra of complexes **7-9** with L_2 as ancillary ligand measured under Ar atmosphere in CH_2Cl_2 at 25°C

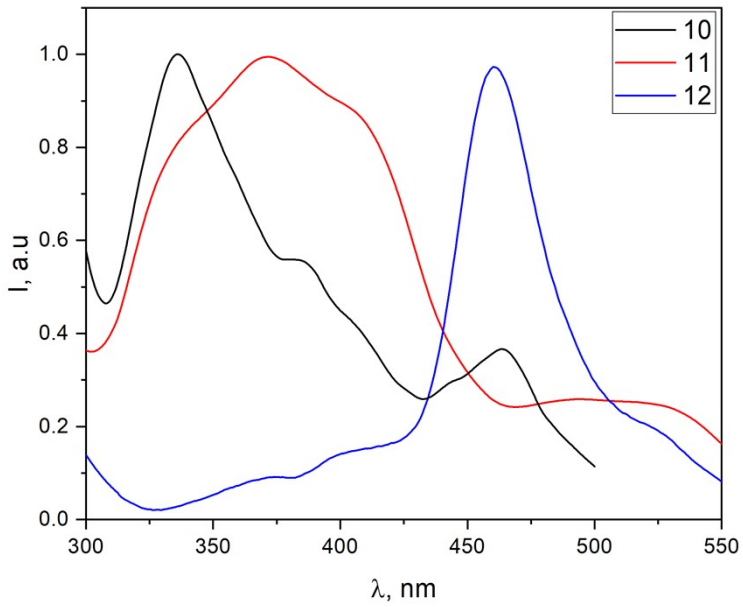

Figure S68. Normalised excitation spectra of complexes **10-12** with L_3 as ancillary ligand measured under Ar atmosphere in CH_2Cl_2 with 0,01M CF_3COOH at 25°C

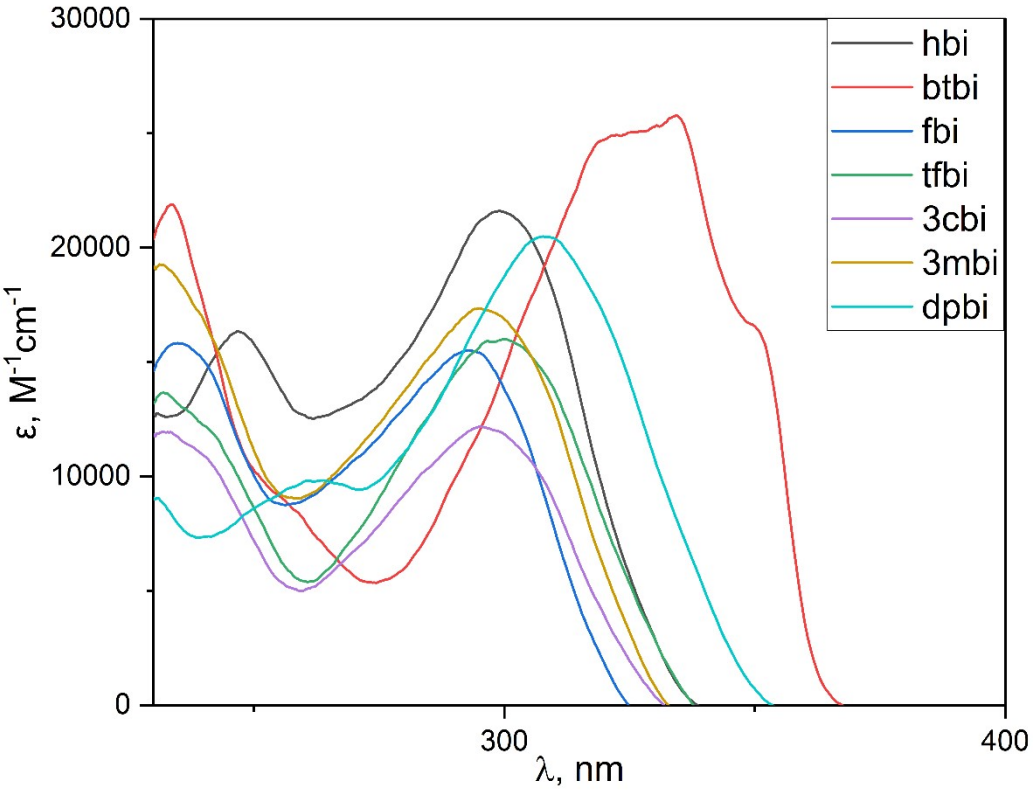

Figure S69. Absorption spectra of cyclometalating benzimidazole ligands (CH_2Cl_2).

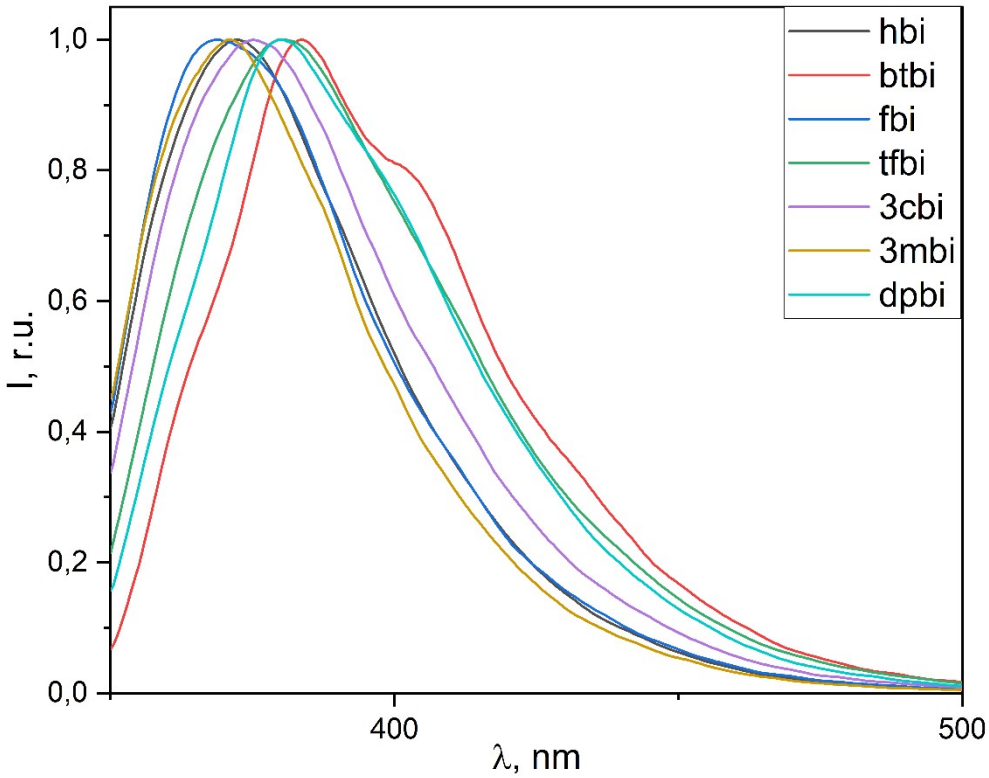

Figure S70. Normalised luminescence spectra of cyclometalating benzimidazole ligands (CH_2Cl_2).

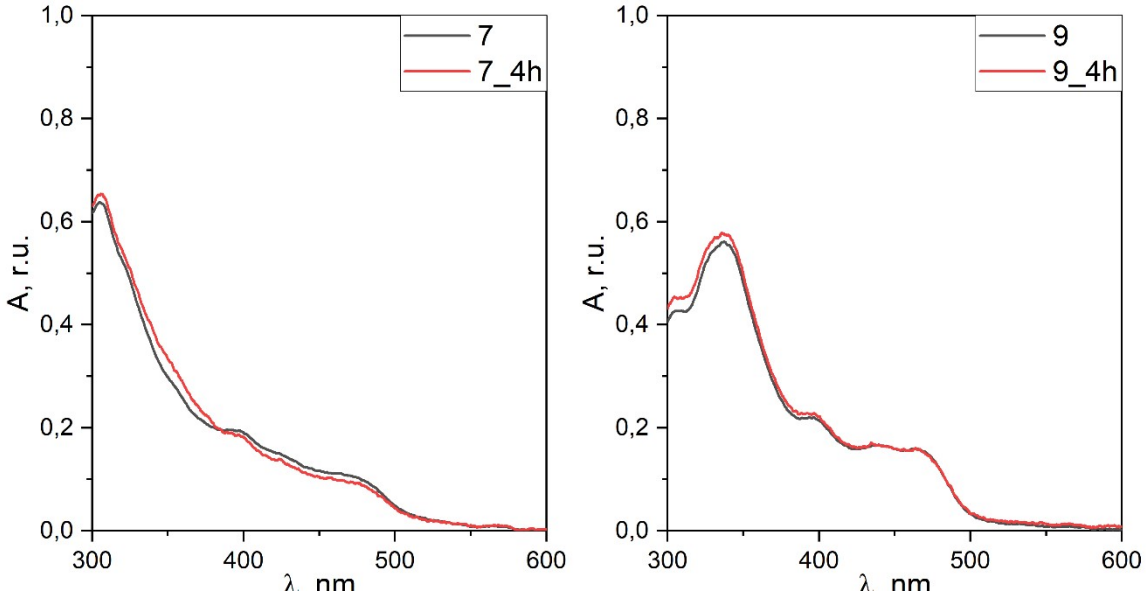

Figure S71. Absorbtion spectra of complexes 7 and 9 before(grey) and after (red) 4 hours of UV irradiation.

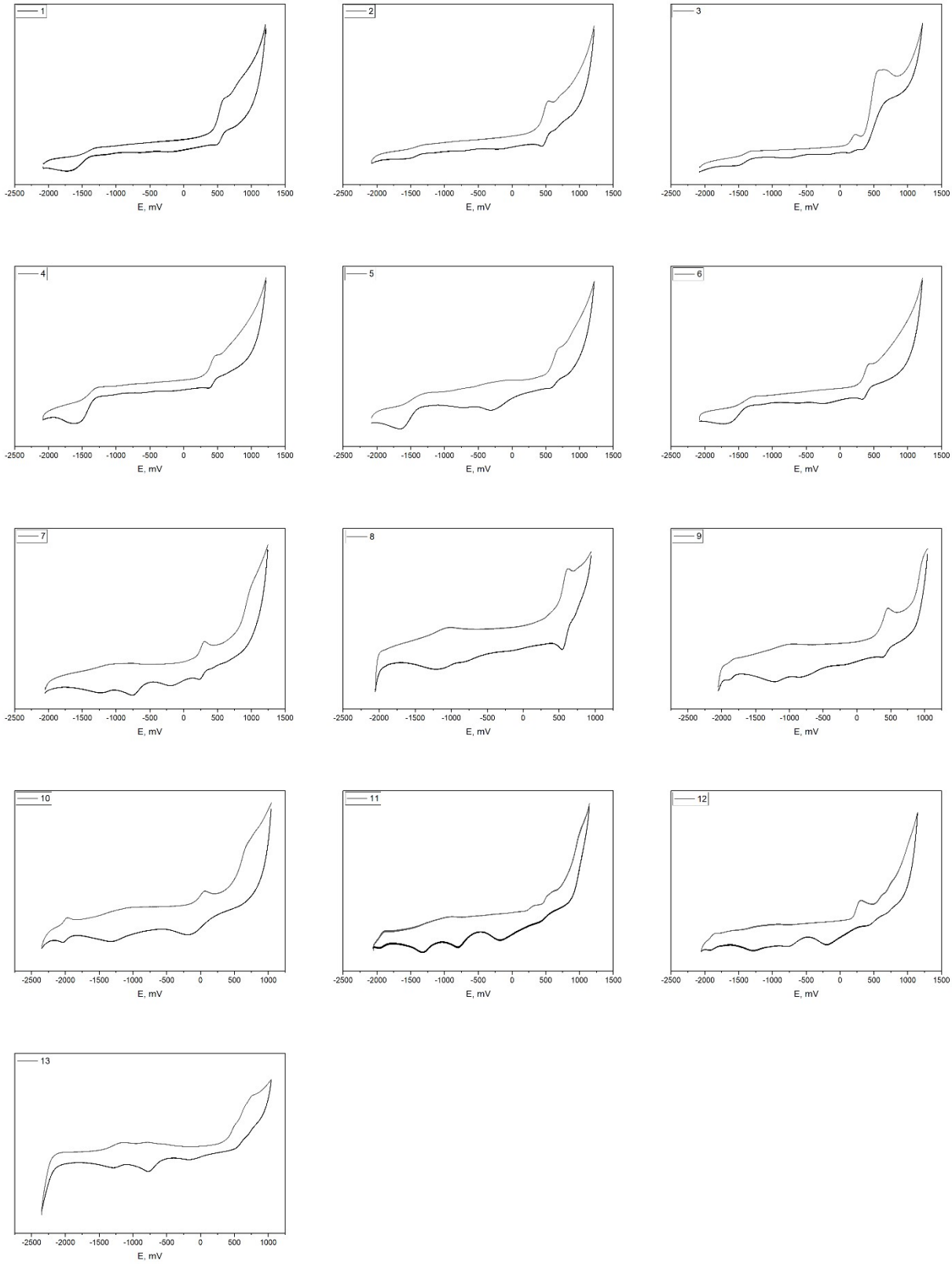

Figure S72. Cyclic voltammetry curves of complexes **1** – **13**. E is presented vs Fc^{+}/Fc couple.

4. **Computational details**

Table S4. Comparison of the bond lengths from the crystal structures and the calculations (structure/calculation)

	1	**2**	**5**	**7**	**8**	**9**	**13**
Ir – C1	1.997 / 2.0173	1.986 / 2.0144	1.989 / 2.0188	1.971 / 2.0163	1.998 / 2.0115	2.001/2.0231	1.993 / 2.0182
Ir – C2	2.003 / 2.0109	1.990 / 2.0145	2.000 / 2.0120	1.971 / 2.0164	1.998 / 2.0115	1.997/2.0207	1.998 / 2.0140
Ir – N1	2.028 / 2.0810	2.042 / 2.0722	2.023 / 2.0714	2.040 / 2.0677	2.045 / 2.0630	2.028/2.0818	2.039 / 2.0802
Ir – N2	2.043 / 2.0619	2.046 / 2.0732	2.033 / 2.0660	2.040 / 2.0675	2.045 / 2.0632	2.054/2.0858	2.030 / 2.0738
Ir – O1	2.152 / 2.2175	2.140 / 2.1866	2.112 / 2.1824	2.133 / 2.1940	2.145 / 2.1745	2.108/2.1731	2.119 / 2.1925
Ir – O2	2.121 / 2.1732	2.152 / 2.1915	2.130 / 2.1889	2.133 / 2.1925	2.145 / 2.1745	2.154/2.1750	2.133 / 2.1774

Table S5. Comparison of the bond lengths from the crystal structures and the calculations (structure/calculation)

*for the complexes **10** and **12** data for one on the molecules in the independent unit is shown.

	10*	**12***
Ir – C1	2.001/2.0359	2.027 / 2.0496
Ir – C2	2.031/2.0390	2.042 / 2.0463
Ir – N1	2.043/2.0893	2.044 / 2.1042
Ir – N2	2.046/2.0874	2.065 / 2.0990
Ir – N3	2.113/2.2078	2.121 / 2.1980
Ir – N4	2.141/2.2095	2.102 / 2.1988

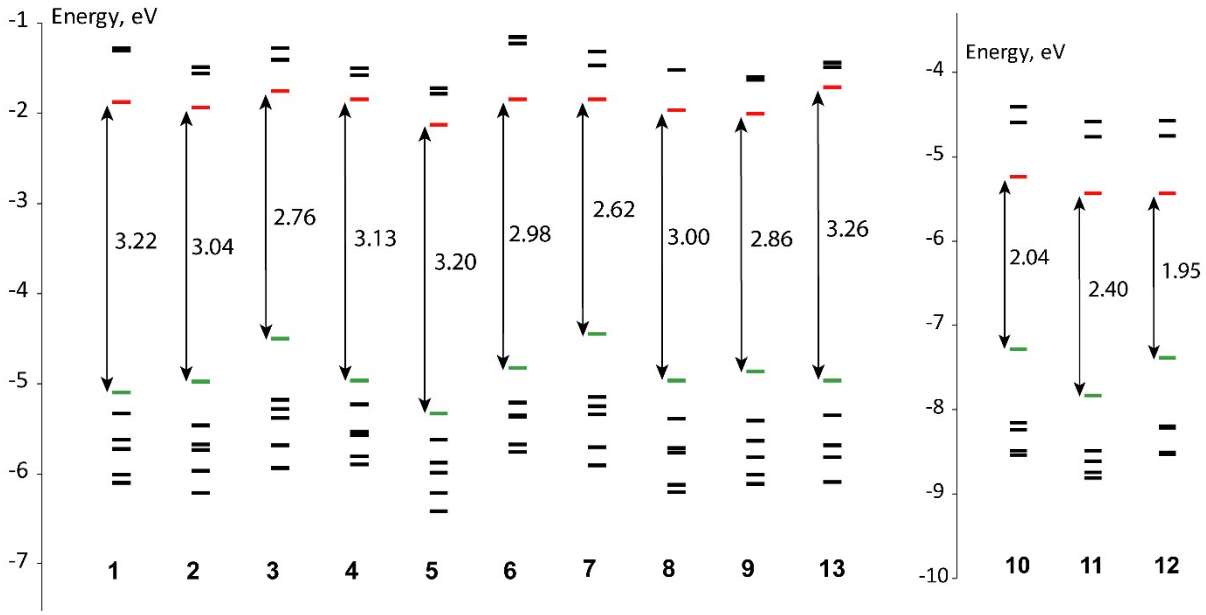

Figure S73. Energy of frontier molecular orbitals of complexes **1 – 9, 13** (left) and **10** – **12** (right) and HOMO-LUMO gaps calculated by DFT (HOMO – highest occupied molecular orbital, LUMO – lowest unoccupied molecular orbital, DFT – Density Functional Theory).

Table S6. Composition of frontier molecular orbitals for **1** – **13**.

complex		**1**	**2**	**3**	**4**	**5**	**6**	**7**	**8**	**9**	**10**	**11**	**12**	**13**
HOMO-1	Ir	0,46	0,50	0,51	0,42	0,42	0,36	0,57	0,52	0,13	0,35	0,14	0,01	0,17
	C^N	0,22	0,19	0,23	0,27	0,14	0,51	0,32	0,23	0,84	0,51	0,86	0,79	0,04
	O^O	0,32	0,31	0,26	0,30	0,44	0,13	0,11	0,25	0,03	0,17	0,00	0,20	0,79
HOMO	Ir	0,46	0,42	0,39	0,45	0,46	0,40	0,40	0,42	0,11	0,33	0,31	0,17	0,44
	C^N	0,50	0,55	0,55	0,51	0,51	0,53	0,58	0,55	0,72	0,68	0,69	0,65	0,49
	O^O	0,04	0,03	0,06	0,04	0,03	0,07	0,02	0,03	0,17	0,03	0,00	0,18	0,07
LUMO	Ir	0,01	0,01	0,01	0,01	0,02	0,01	0,02	0,02	0,02	0,02	0,03	0,03	0,01
	C^N	0,01	0,11	0,02	0,02	0,04	0,46	0,15	0,01	0,90	0,63	0,09	0,63	0,06
	O^O	0,98	0,88	0,97	0,97	0,94	0,53	0,84	0,97	0,08	0,35	0,88	0,34	0,93
LUMO+1	Ir	0,02	0,01	0,00	0,02	0,03	0,00	0,00	0,00	0,54	0,02	0,01	0,01	0,02
	C^N	0,96	0,41	0,17	0,98	0,96	0,37	0,02	0,00	0,43	0,50	0,02	0,64	0,96
	O^O	0,02	0,58	0,82	0,00	0,00	0,63	0,98	1	0,03	0,48	0,97	0,36	0,03

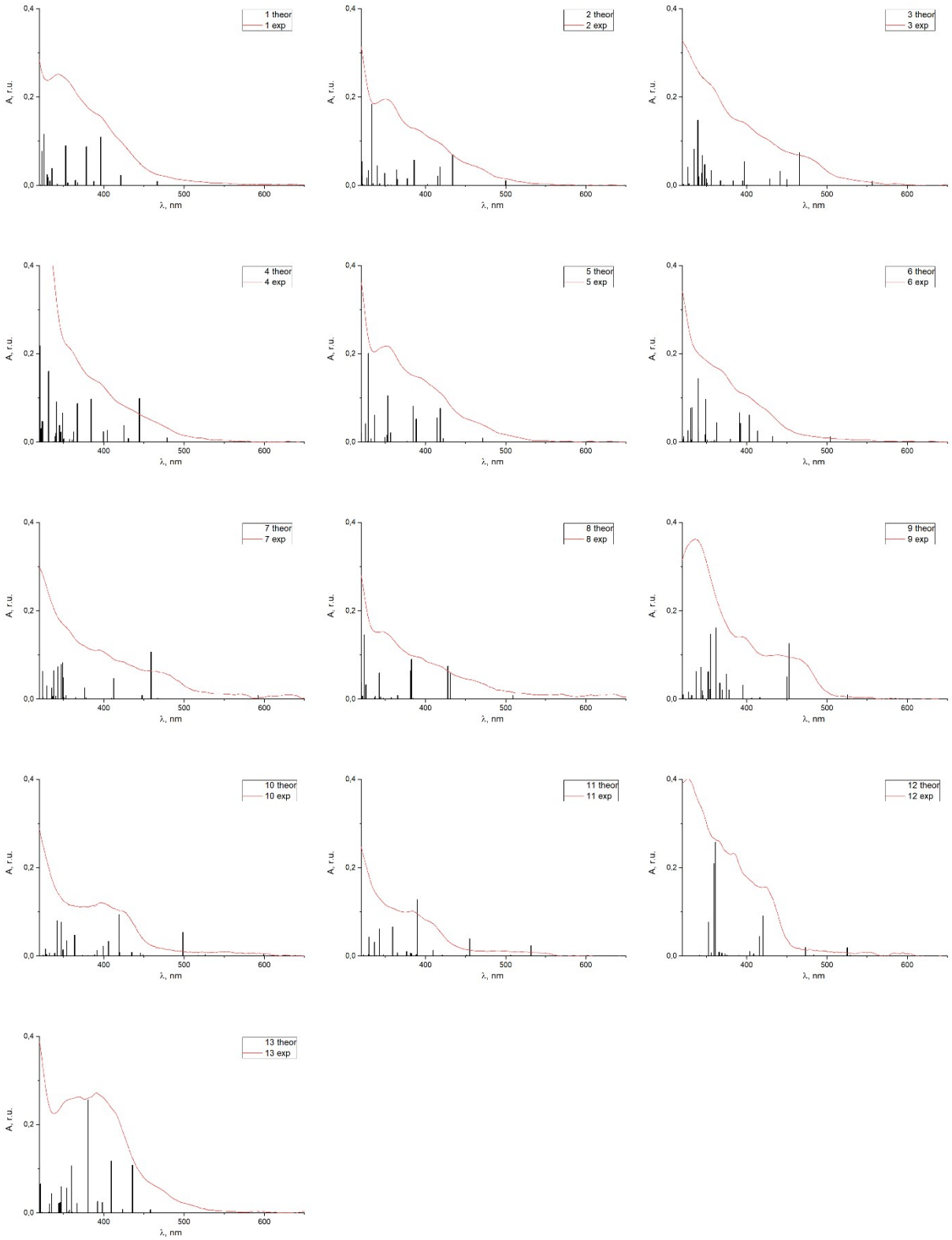

Figure S74. TDDFT (black) and experimental (red) electronic spectra of complexes **1** – **13**.

5. **Photovoltaic measurements**

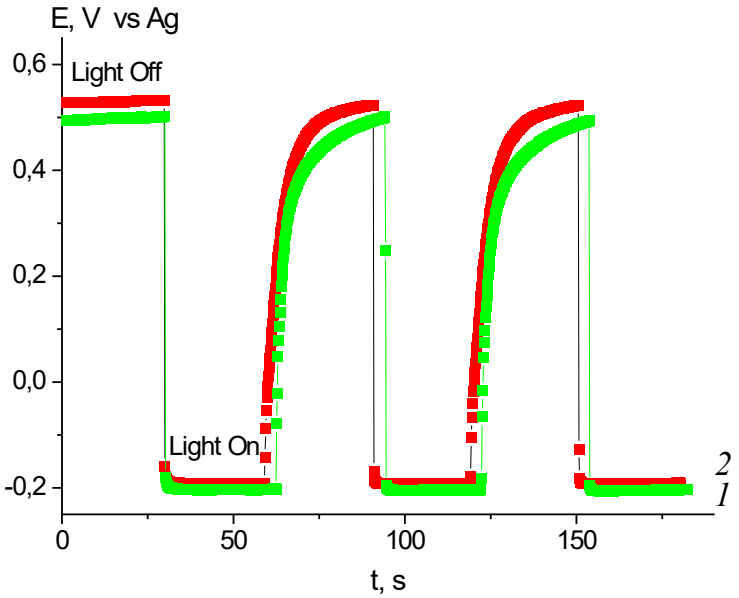

Figure S75. Time dependence of photopotential for TiO_2 photoanodes sensitized by complexes **7H** (1) and **9H** (2) in the dark and on exposure to AM 1.5 G simulated solar light (100 mW cm^{-2}).

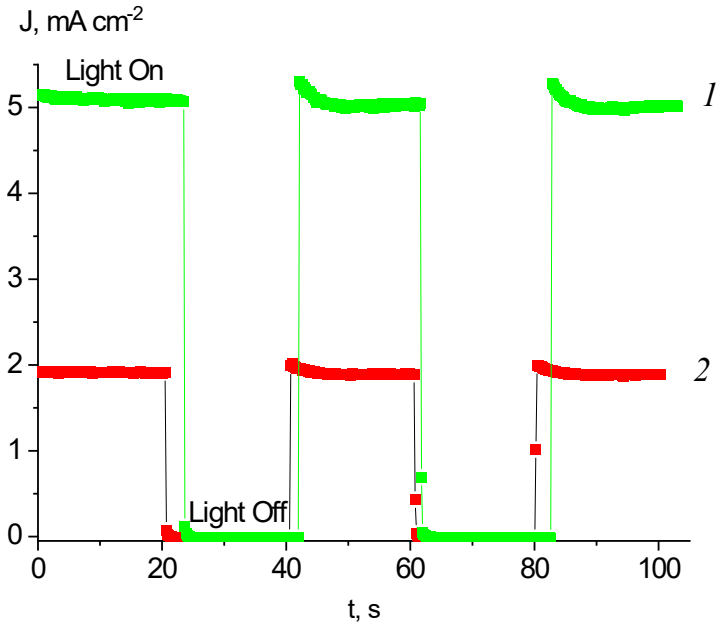

Figure S76. Time dependence of photocurrent at short-circuit for TiO_2 photoanodes sensitized by complexes **7H** (1) and **9H** (2) in the dark, and on exposure to AM 1.5 G simulated solar light (100 mW cm^{-2}).